

**COATING OF PARTICULATES BY  
BOTTOM-SPRAY AIR SUSPENSION PROCESSES**

**TANG SOOK KHAY ELAINE**

*B.Sc.(Pharm.)Hons, NUS*

**A THESIS SUBMITTED  
FOR THE DEGREE OF DOCTOR OF PHILOSOPHY  
DEPARTMENT OF PHARMACY  
NATIONAL UNIVERSITY OF SINGAPORE**

**2008**

## **ACKNOWLEDGEMENT**

I would like to express my heartfelt thanks to my supervisors, A/P Chan Lai Wah and A/P Paul Heng, for their guidance and help during the course of my research. I wish to also thank Dr Celine Liew for being helpful and approachable. This thesis would not have been possible without all their support.

I am indebted to NUS for the research scholarship given to fund this higher degree.

Too many to name, I appreciate all my friends from GEA-NUS who have helped me in various ways and made the laboratory a very enjoyable working environment.

Special thanks go to laboratory technologists, Mrs Teresa Ang, Mr Peter Leong and Ms Wong Mei Yin, for their invaluable technical assistance.

I would like to thank my parents and Chin Kwang for their support and concern for me throughout my candidature.

Last but not least, I am grateful to God for making everything possible.

Elaine, 2008

*For my son, Julian*

# TABLE OF CONTENTS

<b>ACKNOWLEDGEMENT</b> .....	<b>i</b>
<b>TABLE OF CONTENTS</b> .....	<b>iii</b>
<b>SUMMARY</b> .....	<b>viii</b>
<b>LIST OF TABLES</b> .....	<b>x</b>
<b>LIST OF FIGURES</b> .....	<b>xi</b>
<b>LIST OF SYMBOLS</b> .....	<b>xvi</b>
<b>I INTRODUCTION</b> .....	<b>2</b>
A Background.....	2
A.1 Coating of pharmaceutical products .....	2
A.2 Multiparticulates as coated dosage forms .....	4
A.3 Methods of preparing coated multiparticulates.....	6
A.3.1 Chemical processes .....	7
A.3.2 Mechanical processes.....	8
B Coating of fine particles using air suspension coating .....	12
C Factors affecting air suspension coating of multiparticulates.....	15
C.1 Processing equipment .....	15
C.1.1 Types of air suspension coaters.....	15
C.1.2 Types of bottom-spray air suspension coaters .....	18
C.2 Processing conditions.....	22
C.2.1 Temperature .....	22
C.2.2 Humidity.....	23
C.2.3 Conveying airflow rate.....	24
C.2.4 Atomizing air pressure .....	24
C.2.5 Spray rate.....	25



C.2.6	Partition gap .....	25
C.3	Characteristics of core materials.....	26
C.3.1	Size .....	26
C.3.2	Shape.....	26
C.3.3	Surface roughness .....	27
C.3.4	Porosity.....	27
C.3.5	Properties of drug.....	27
C.3.6	Properties of excipient.....	28
C.4	Components of coating formulation .....	29
C.4.1	Solvent.....	29
C.4.2	Polymer .....	29
C.4.3	Plasticizers.....	30
C.4.4	Colorants .....	31
C.4.5	Anti-tack agents.....	32
<b>II</b>	<b>HYPOTHESES AND OBJECTIVES .....</b>	<b>35</b>
<b>III</b>	<b>EXPERIMENTAL.....</b>	<b>38</b>
A	Materials .....	38
A.1	Core particles .....	38
A.1.1	Sugar pellets .....	38
A.1.2	Lactose particles.....	38
A.2	Coating materials .....	38
B	Method.....	41
B.1	Coating.....	41
B.1.1	Preparation of coating materials.....	41
B.1.2	Equipment for coating.....	42

B.1.3	Standard procedure for coating .....	42
B.1.4	Conditions used for pellet coating.....	44
B.2	Evaluation of process characteristics.....	44
B.2.1	Determination of mass flow rate .....	44
B.2.2	Determination of pellet velocity.....	48
B.2.3	Determination of air velocity .....	48
B.2.4	Determination of process conditions.....	49
B.2.5	Determination of drying efficiency .....	49
B.3	Evaluation of product characteristics.....	51
B.3.1	Characterization of pellets.....	51
B.3.2	Characterization of lactose particles .....	55
B.3.3	Characterization of coating formulations.....	58
B.3.4	Characterization of cast films.....	60
B.4	Experimental designs used.....	62
B.4.1	Comparison of bottom-spray air suspension coaters on pellet coating.....	62
B.4.2	Influence of processing conditions for Precision coating.....	68
B.4.3	Influence of calcium carbonate nanoparticles as a surface modifying agent on Precision coating of lactose particles.....	71
B.4.4	Influence of calcium carbonate nanoparticles as an anti-tack additive on Precision coating of lactose particles.....	72
B.5	Statistical analysis.....	72

<b>IV RESULTS AND DISCUSSION.....</b>	<b>74</b>
A Study of conditions suitable for coating .....	74
A.1 Comparison of bottom-spray air suspension coaters on pellet coating.....	74
A.1.1 Study of the fluid dynamics in Wurster and Precision coaters .....	75
A.1.2 Study of drying efficiency and pellet movement in Wurster and Precision coaters.....	97
A.1.3 Study of the coated products of Wurster and Precision coaters .....	103
A.2 Influence of processing conditions for Precision coating .....	111
A.2.1 Effects of inlet air temperature and airflow rate .....	111
A.2.2 Effect of change in accelerator insert diameter.....	115
A.2.3 Effects of airflow rate and partition gap on the coated pellets.....	121
A.2.4 Effects of airflow rate and partition gap on pellets of different sizes.....	129
B Coating of fine lactose particles .....	134
B.1 Influence of calcium carbonate nanoparticles as a surface modifying agent on Precision coating of lactose particles.....	136
B.1.1 Effects of nano-CaCO <sub>3</sub> concentrations on the coated lactose particles .....	136
B.1.2 Effects of nano-CaCO <sub>3</sub> concentration on core lactose particles.....	139

B.2	Influence of calcium carbonate nanoparticles as an anti-tack additive on Precision coating of lactose particles .....	149
B.2.1	Effects of nano-CaCO <sub>3</sub> concentration on coated lactose particles.....	149
B.2.2	Effects of nano-CaCO <sub>3</sub> concentration on the coating formulations .....	149
B.2.3	Effects of nano-CaCO <sub>3</sub> concentration on the cast films .....	158
<b>V</b>	<b>CONCLUSION .....</b>	<b>165</b>
<b>VI</b>	<b>REFERENCES .....</b>	<b>168</b>
<b>VII</b>	<b>LIST OF PUBLICATIONS .....</b>	<b>188</b>

## SUMMARY

In this study, the process parameters affecting the coating performance of the Precision coater with swirling airflow and the conventional Wurster coater were investigated. The more superior Precision coater was then used to study the conditions favourable for fine particle coating.

Fluid dynamics of the non-swirling airflow in Wurster coating was compared with that of Precision coating under comparable conditions. Mass flow rate measurements indicated that the transport of pellets into the coating zone of the Precision coater was governed largely by suction pressure created by pressure differential across the partition gap. Pellet movement in the Wurster coater depended on a combination of “hydrostatic pressure” of the product in the peripheral staging bed and airflow rate. Mass flow rates in Precision coating were found to increase uniformly with airflow rate and atomizing pressure whereas similar effects were not found with Wurster coating. This shows that mass transport in Precision coating was more responsive to changes in operational variables. Pellets moved through the coating zone in the Precision coater at a faster speed and were set further apart.

Precision-coated pellets had better properties than corresponding Wurster-coated pellets, showing less agglomeration, fewer gross surface defects, more uniform coats, increased flowability, and slower drug release. The surface was well-formed but rougher due to the rapid coat drying with protuberances made by dried spray droplets on the pellet surface. However, the yields were similar for both coating processes, indicating that the rapid drying rate in Precision coating did not contribute significantly to the spray drying effect. A higher degree of agglomeration for Wurster coating was attributed to poorer particle movement conditions and not due to

inadequate drying as the drying efficiencies were found to be similar for both Precision and Wurster coaters. Investigation into particle movement showed higher velocity, better separation and higher trajectories of pellets undergoing Precision coating.

Process parameters for Precision coating, such as airflow rate and partition gap, were studied. It was found that the airflow rate had greater effect on the drying of pellets whereas the partition gap determined the quality of coats formed. Smaller pellets agglomerated primarily from inadequate airflow rate and not due to inadequate particle movement through the partition gap. The agglomeration of larger pellets was less affected by the airflow rate but their movement was restricted by small partition gaps, affecting the deposition of coating material.

With greater understanding of Precision coating, coating of fine particles was carried out by spray coating a commonly used polymeric material, hypromellose onto fine lactose particles. Calcium carbonate nanoparticles were evaluated as an anti-tack agent for fine particle coating because their small sizes made it suitable for being coated onto fine particles and their hydrophobic nature may contribute to the anti-tack property. Calcium carbonate nanoparticles, when used either as a surface-modifying agent or an additive in the film coating material, were found to reduce the agglomeration of lactose particles to varying degrees.

## LIST OF TABLES

Table 1. Examples of different multiple-unit systems.....	5
Table 2. Components of coating formulations. ....	40
Table 3. Conditions used for pellet coating. ....	45
Table 4. Physical properties of base-coated pellets .....	64
Table 5. Process parameters used for the determination of MFR in Wurster and Precision coating.....	67
Table 6. Factorial designs used to study the effects of AF, PG and pellet size.....	70
Table 7. Properties of pellets coated by Wurster and Precision coating. ....	105
Table 8. Surface coverage of lactose with nano-CaCO <sub>3</sub> .....	142

## LIST OF FIGURES

Fig. 1.	Structure of a controlled release-coated particle .....	5
Fig. 2.	Schematic diagram of the air suspension coating process showing the possible products formed under different drying conditions.....	14
Fig. 3.	Schematic diagrams of the coating chamber of (a) bottom-spray, (b) top-spray and (c) tangential-spray air suspension coaters (Arrows show the particle flow paths; Spray nozzles are shaded black).....	16
Fig. 4.	Diagrams of the air distribution plates and associated parts of the (a) Wurster coater and (b) Precision coater, with arrows showing the airflow pattern. ....	21
Fig. 5.	Light microscopy images of uncoated sugar pellets of size 500 to 600 $\mu\text{m}$ .....	39
Fig. 6.	Scanning electron photomicrograph of lactose $\alpha$ -monohydrate particles.....	39
Fig. 7.	Scanning electron photomicrograph of osmium-coated nano- $\text{CaCO}_3$ taken with a scanning electron microscope (SS-550, Shimadzu, Japan).....	39
Fig. 8.	Dimensions of the coating chamber of the (a) Wurster coater and the (b) Precision coater with the associated parts, (i) plenum, (ii) air distribution plate, (iii) partition column, (iv) expansion chamber, (v) retaining filter and (vi) exhaust pipe (not drawn to scale).....	43
Fig. 9.	Schematic diagram of pellet flow in one cycle using the pellet collector in the (a) Wurster coater and (b) Precision coater.....	47
Fig. 10.	Diagram of the MP-1 air handling system showing the locations at which the following process parameters were measured: (a) ambient temperature, (b) ambient humidity, (c) airflow rate, (d) inlet air temperature, (e) product temperature, (f) outlet humidity and (g) outlet temperature. (Arrows show the direction of airflow). ....	50
Fig. 11.	Photographs of the (a) 2 % open area plate, (b) 6 % open area plate, (c) Feidler plate and (d) Tressen mesh of the Wurster coater. ....	65
Fig. 12.	Photograph of the air distribution plate of the Precision coater attached to the swirl accelerator, which is inverted to show the swirl vanes. ....	66



Fig. 13. Photograph of the accelerator inserts of the Precision coater with AI diameters of 20 mm, 24 mm, 30 mm and 40 mm placed in a clockwise manner from top left.....	66
Fig. 14. Influence of PG on MFR in Wurster coating using the Feidler plate (■), 2 % open area plate (▲) and 6 % open area plate (●) at AF(80)AP(1) (represented by dotted lines) and AF(120)AP(3) (represented by solid lines).....	77
Fig. 15. Influence of PG on MFR in Precision coating using AI diameters of 20 mm (■), 24 mm (◆), 30 mm (▲) and 40 mm (●) at AF(80)AP(1) (represented by dotted lines) and AF(120)AP(3) (represented by continuous lines).....	78
Fig. 16. Influence of PG on air velocity in Wurster coating using Feidler plate (■), 2 % open area plate (▲) and 6 % open area plate (●) at AF(80)AP(1) (represented by dotted lines) and AF(120)AP(3) (represented by solid lines).....	80
Fig. 17. Influence of PG on air velocity in Precision coating using AI diameters of 20 mm (■), 24 mm (◆), 30 mm (▲) and 40 mm (●) at AF(80)AP(1) (represented by dotted lines) and AF(120)AP(3) (represented by continuous lines).....	81
Fig. 18. High speed images of pellets moving within the partition column in Wurster coating and Precision coating over an area of 2 cm x 2 cm. (The images were taken at 2770 frames per second) .....	83
Fig. 19. Influence of AI diameter on air velocity in Precision coating at AF(80)AP(1) (represented by dotted line) and AF(120)AP(3) (represented by continuous line). .....	87
Fig. 20. Influence of pellet load on MFR in Wurster coating (■) and Precision coating (□) at AF(80)AP(1) (represented by dotted lines) and AF(120)AP(3) (represented by solid lines). .....	88
Fig. 21. Influence of PG on MFR using pellet load of 700 g (□) and 1000 g (■) in Wurster coating, and 700 g (○) and 1000 g (●) in Precision coating at AF(80)AP(1) (represented by dotted lines) and AF(120)AP(3) (represented by continuous lines). .....	90
Fig. 22. Influence of PG on MFR using pellet size of 500 to 600 μm (□), 710 to 850 μm (■) in Wurster coating and 500 to 600 μm (○) and 710 to 850 μm (●) in Precision coating at AF(80)AP(1) (represented by dotted lines) and AF(120)AP(3) (represented by continuous lines).....	91

Fig. 23. Influence of AF and AP on MFR in (a) Wurster coating and (b) Precision coating.....	94
Fig. 24. Influence of AF and AP on air velocity in (a) Wurster coating and (b) Precision coating.....	95
Fig. 25. Influence of PG on (a) DE, (b) PV, (c) Agg and (d) Yd in Precision coating (clear) and Wurster coating (shaded).....	99
Fig. 26. High speed images of pellet movement in (A) Wurster coating and (B) Precision coating at partition gap of (i) 14 mm, (ii) 18 mm and (iii) 22 mm over an area of 10 mm by 10 mm. (The images were taken at 4000 frames per second).....	101
Fig. 27. Scanning electron photomicrographs of (A) uncoated pellet, (B) base-coated pellet, (C) Wurster-coated pellet at PG of (i) 14 mm, (ii) 18 mm and (iii) 22 mm; and (D) Precision-coated pellet at PG of (i) 14 mm, (ii) 18 mm and (iii) 22 mm. ....	106
Fig. 28. Scanning probe images of the surface of a (a) Wurster-coated pellet and (b) Precision-coated pellet over an area of 25 $\mu\text{m} \times 25 \mu\text{m}$ . ....	107
Fig. 29. Drug release profile of drug-loaded pellets coated by Wurster coating (●) and Precision coating (○). * significant difference in means ( $p < 0.05$ ) .....	110
Fig. 30. Influence of Tp on (a) DE, (b) Agg and (c) Yd in Precision coating.....	112
Fig. 31. Influence of AF on (a) DE, (b) Agg and (c) Yd in Precision coating. ....	114
Fig. 32. Influence of AI diameter on (a) DE, (b) PV, (c) Agg and (d) Yd in Precision coating. ....	116
Fig. 33. Influence of AI diameter on the air velocities at the peripheral (clear) and central (shaded) positions within the partition column in Precision coating. ....	118
Fig. 34. High speed images of pellets moving in Precision coating using accelerator insert (AI) diameters of (a) 20 mm, (b) 24 mm and (c) 30 mm over an area of 10 mm $\times$ 10 mm. (The images were taken at 4000 frames per second).....	120
Fig. 35. Influence of (a) AF and (b) PG on the Agg of Precision-coated pellets. ( $\dagger$ : n = 2) .....	124

Fig. 36. Influence of (a) AF and (b) PG on the Yd of Precision-coated pellets. ( <sup>†</sup> : n = 2).....	125
Fig. 37. Influence of (a) AF and (b) PG on the $\delta E$ of Precision-coated pellets.....	126
Fig. 38. Influence of (a) AF and (b) PG on the RSD of $\delta E$ of Precision-coated pellets.....	127
Fig. 39. Influence of (a) AF and (b) PG on the surface roughness of Precision-coated pellets. ....	128
Fig. 40. Influence of AF on (a) DE, (b) Agg and (c) Yd of Precision-coated pellets of sizes 500 to 600 $\mu\text{m}$ (clear) and 355 to 425 $\mu\text{m}$ (shaded).....	130
Fig. 41. Influence of PG on (a) DE, (b) Agg and (c) Yd of Precision-coated pellets of sizes 500 to 600 $\mu\text{m}$ (clear) and 355 to 425 $\mu\text{m}$ (shaded). ( <sup>†</sup> : n = 2).....	131
Fig. 42. Effect of nano- $\text{CaCO}_3$ concentration on the $D_{10}$ (●), $D_{50}$ (■) and $D_{90}$ (◆) values of HPMC-coated lactose particles. ....	137
Fig. 43. Effect of nano- $\text{CaCO}_3$ concentrations on the span of HPMC-coated lactose particles. ....	138
Fig. 44. Scanning electron photomicrographs of core lactose particles sprayed with (a) water and nano- $\text{CaCO}_3$ suspensions to a nano- $\text{CaCO}_3$ concentration of (b) 0.1 % w/w, (c) 0.2 % w/w, (d) 0.3 % w/w, (e) 0.4 % w/w and (f) 0.5 % w/w. ( $\times 500$ magnification) .....	140
Fig. 45. Scanning electron photomicrographs of core lactose particles sprayed with (a) water and (b) nano- $\text{CaCO}_3$ suspension to a nano- $\text{CaCO}_3$ concentration of 0.5 % w/w. ( $\times 2000$ magnification).....	141
Fig. 46. Effect of nano- $\text{CaCO}_3$ concentrations on the $D_{10}$ (●), $D_{50}$ (■) and $D_{90}$ (◆) values of core lactose particles. ....	143
Fig. 47. Effect of nano- $\text{CaCO}_3$ concentrations on the span of core lactose particles.....	144
Fig. 48. Effect of nano- $\text{CaCO}_3$ concentration on the (a) aspect ratio and (b) sphericity of core lactose particles.....	147
Fig. 49. Effect of nano- $\text{CaCO}_3$ concentration on the (a) Ra and (b) angle of repose of core lactose particles.....	148

Fig. 50. Effect of nano-CaCO <sub>3</sub> concentration on the D <sub>10</sub> (●), D <sub>50</sub> (■) and D <sub>90</sub> (◆) of HPMC-coated lactose particles. ....	150
Fig. 51. Effect of nano-CaCO <sub>3</sub> concentration on the span of HPMC-coated lactose particles. ....	151
Fig. 52. Effect of nano-CaCO <sub>3</sub> concentration on the tack values of neat suspensions (■) and HPMC suspensions (●). ....	152
Fig. 53. Effect of nano-CaCO <sub>3</sub> concentration on the kinematic viscosity, KV, of (a) neat suspensions and (b) HPMC suspensions.....	154
Fig. 54. Effect of nano-CaCO <sub>3</sub> concentration on the surface tension of (a) neat suspensions and (b) HPMC suspensions. ....	157
Fig. 55. FTIR spectra of (a) nano-CaCO <sub>3</sub> , and HPMC films with (b) 0 % w/w (c) 2 % w/w, (d) 4 % w/w (e) 6 % w/w, (f) 8 % w/w and (g) 10 % w/w nano-CaCO <sub>3</sub> .....	159
Fig. 56. Effect of nano-CaCO <sub>3</sub> concentration on the (a) maximum stress and (b) elasticity of the cast HPMC films. ....	161
Fig. 57. Effect of nano-CaCO <sub>3</sub> concentration on the (a) Ra and (b) contact angle of cast films.....	162

## LIST OF SYMBOLS

---

A	Area
AC	Wurster coater (Aerocoater)
AF	Airflow rate (m <sup>3</sup> /h)
Agg	Degree of agglomeration (%)
AI	Accelerator insert
AP	Atomizing pressure (bar)
CM	Chlorpheniramine maleate
CPVC	Critical pigment volume concentration
CSA	Cross-sectional area
D <sub>10</sub> , D <sub>50</sub> and D <sub>90</sub>	Particle diameters at the 10, 50 and 90 percentiles of the cumulative percent undersize plot respectively
DE	Drying efficiency (%)
ΔE	Difference in colour of coated pellets with respect to the initial colour of the pellets
EC	Ethylcellulose
HPMC	Hypromellose
KV	Kinematic viscosity
<i>L, a, b</i>	CIELab units where <i>L</i> indicates lightness and <i>a</i> and <i>b</i> indicate colour directions
M	Pellet load (g)
M <sub>s</sub>	Mass of sample
MFR	Mass flow rate (g/s)
m <sub>g</sub>	Airflow rate (kg/h)
m <sub>l</sub>	Liquid flow rate (kg/h)
Nano-CaCO <sub>3</sub>	Calcium carbonate nanoparticles
N <sub>lactose</sub>	Number of lactose particles

$N_{\text{nano}}$	Number of nano-CaCO <sub>3</sub>
P	Perimeter
PC	Precision coater
PG	Partition gap (mm)
PV	Pellet velocity (m/s)
PVP	Polyvinyl pyrrolidone
r	Radius
$r_l$	Mean radius of lactose particles
$r_n$	Mean radius of nano-CaCO <sub>3</sub>
Ra	Arithmetic mean roughness
RP	Iron oxide red pigment
RSD of $\delta E$	Relative standard deviation of $\delta E$
SA	Surface area
t	Time (s)
TD	True density (g cm <sup>-3</sup> )
Tp	Inlet air temperature (°)
$V_i$	Volume of an individual particle
$V_s$	Volume of sample
$W_A$	Weight of agglomerated pellets (g)
$W_C$	Total weight of coated pellets (g)
$W_T$	Theoretical final weight of coated pellets (g)
$x_i$	Inlet air absolute humidity (kg/kg dry air)
$x_o$	Outlet air absolute humidity (kg/kg dry air)
Yd	Yield (%)

---

**PART I:**

**INTRODUCTION**

## **I INTRODUCTION**

### **A Background**

#### **A.1 Coating of pharmaceutical products**

In the pharmaceutical industry, coating of solid dosage forms is an important process which is used to enhance the properties of the final products (Collett and Moreton, 2001; Hogan, 2001). It is carried out by the application of a thin polymeric film, approximately 25 to 100  $\mu\text{m}$ , onto the surfaces of solid cores. Cores may consist of tablets, pellets, granules, caplets or particles which are loaded or layered with drug (Radebaugh, 1992). Depending on the type of coating material applied, different functions can be achieved (Cole, 1995a; Porter and Bruno, 1990; Horvath and Ormos, 1989). A single layer of coat may serve several functions. Alternatively, several distinct layers of coat made of different materials may be used to impart a combination of properties to the dosage unit (Lehmann, 1994).

The functions of coating are extensive, ranging from basic necessity to aesthetic purposes. Coating can be used to improve the chemical and physical properties of the core. Coats may serve as barriers that protect incompatible or unstable core materials from one another and from environmental elements such as light, oxygen, water and carbon dioxide (Cole, 1995b; Horvath and Ormos, 1989). They may also improve the physical characteristics of core particles by enhancing flow and reducing friability (Cole, 1995b).

One most common use of coating is for enhancing the appearance of the product with colour coating. Such coatings can also facilitate the identification of different dosage strengths and drugs, thereby preventing mistakes in drug administration. By masking unpleasant color, taste or odour and preventing leaching of materials from the cores,



coats can improve patient acceptance of the product (Cole, 1995b; Porter and Bruno, 1990; Horvath and Ormos, 1989).

Controlled or modified-release coating may be used to customize drug release patterns and rates. Sustained drug release can be achieved using coats with rate-controlling properties (Chang and Robinson, 1990). An acid-resistant coat can prevent the release of drugs in the stomach, thus protecting any acid-labile drug from the acidic environment or preventing the drug from damaging the stomach (Huyghebaert *et al.*, 2005). Even more specific targeting of drug release may be achieved using coats that are capable of only dissolving under certain physiological environments (Gupta *et al.*, 2001; Beckert *et al.*, 2003).

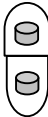

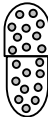
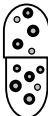
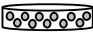
Of utmost importance to the clinical management of diseases is the ability to maintain the drug concentration within the therapeutic window for as long as the treatment is required. Controlling the drug release rate allows drugs to be delivered at a predetermined rate over a fixed time period (Collett and Moreton, 2001). By coating a core with a release rate controlling polymeric film followed by an immediate release drug layer, the composite effects of both an immediate release dose and a sustained release dose can be achieved (Fig. 1). This enables improved treatment of many diseases by preventing system breakthroughs, reducing dosage frequency and improving patient compliance. Moderation of drug release also reduces the incidence and severity of dose-related systemic and local adverse side effects (Collett and Moreton, 2001) such as nausea, vomiting and ulcers from local irritation (Cole, 1995b).

## **A.2 Multiparticulates as coated dosage forms**

Multiparticulates are small discrete particulates that are collated into one dosage entity to form a multiple-unit system (Collett and Moreton, 2001). They are commonly filled into capsule shells and less commonly compressed into tablets (Collett and Moreton, 2001; Tsuchida *et al.*, 2003). Each particulate typically ranges from 0.7 mm to 2 mm in size (Hogan, 2001) and may exist as pellets, granules, sugar seeds (non-pareils), mini-tablets, ion-exchange resin particles, powders and crystals, with drugs being entrapped in or layered around cores (Collett and Moreton, 2001; Hogan, 2001; Porter and Bruno, 1990). The most common shape of multiparticulates is spherical, since a spheroid has minimum surface to volume ratio with a consistent and definable surface for drug release. Thickness of coats on multiparticulates usually ranges from 5 µm to 50 µm, depending on the desired purpose of the coat (Lehmann, 1994). Some examples of multiple-unit systems are described in Table 1.

Coated multiparticulates have several advantages over single-unit systems such as coated tablets or capsules (Bechgaard and Nielsen, 1978). In multiple-unit systems, the total drug dose is divided over many sub-units. Failure of a few units may not be as consequential as failure of a single-unit system. This is apparent in sustained release coated single-unit dosage form, where failure may lead to dose-dumping (Collett and Moreton, 2001). When taken orally, multiparticulates that are released in the stomach are less dependent on gastric emptying and nutritional status than single-unit systems. Their small sizes allow them to pass through the pyloric sphincter easily, reducing intra and inter-subject variations in gastrointestinal transit time (Dechesne and Delattre, 1987; Sugito *et al.*, 1990; Collett and Moreton, 2001) and achieving more consistent drug release profiles (Abrahamsson *et al.*, 1996; Tuleu *et al.*, 1999).

Table 1. Examples of different multiple-unit systems.

Multiple-unit system	Description	Examples
	Capsule filled with minitables	Macrobid <sup>®</sup> , Dilacor <sup>®</sup> XR
	Capsule filled with powder and granules	Cardene <sup>®</sup> SR
	Capsule filled with coated pellets	Inderal <sup>®</sup> LA, Prilosec <sup>®</sup> , Losec <sup>®</sup>
	Capsule filled with pellets with different coat thicknesses	Cardizem <sup>®</sup> CD, Compazine <sup>®</sup> Spansule
	Tablet comprising pellets or micropellets	Toprol <sup>®</sup> XL, Naprelan

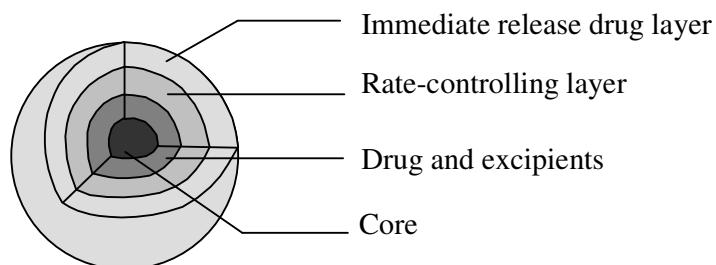


Fig. 1. Structure of a controlled release-coated particle

Their small sizes also enable them to be well-distributed along the gastrointestinal tract, improving absorption and reducing the irritant effect of any irritant drug that single-unit systems may cause to the mucosal lining, especially if lodged for a prolonged period at a particular site (Hogan, 2001).

Smaller multiparticulates can be administered via enteral feeding without having to be crushed, maintaining the functional purpose of the coat. Extremely small multiparticulates consisting of fine particles may be administered by other routes including inhalation (Iida *et al.*, 2005) and epidermal application (Maa *et al.*, 2004). The main pharmaceutical advantage of smaller coated multiparticulates is the ability to be compacted into tablets without having as much damage to the functional coats as compared to larger coated multiparticulates (Ragnarssen *et al.*, 1987; Bodmeier, 1997; Johansson, 1998). The latter have to be filled into capsule shells which is a comparatively less cost effective method than tablet compaction (Alderborn, 2007; Jones, 2007). The animal protein, gelatin, commonly used to make capsule shells, also may incur religious aversion.

Other pharmaceutical advantages of the multi-unit system include easy adjustment of the strength of a dosage unit by changing the number of multiparticulates in the dosage unit; combination of incompatible drugs in a single dosage unit by separating them in different multiparticulates; and combination of multiparticulates with different drug release rates to obtain the desired overall release profile.

### **A.3 Methods of preparing coated multiparticulates**

Various methods are available for the manufacture of coated multiparticulates. The most common method is air suspension coating. Other methods include complex coacervation, interfacial complexation, interfacial polymerization, compression

coating, spray-drying and spray-congealing. These methods can be classified as chemical processes or mechanical processes whereby chemical processes are carried out in liquid media while mechanical processes involve the use of a gas phase at some stage (Thies, 1996).

### **A.3.1 Chemical processes**

The use of chemical processes to coat particulates involves submerging the core particles in a liquid medium. Different types of polymers and chemical reactions can then be used to form coats around the cores.

Coats can be formed by complex coacervation whereby the polymer material is precipitated onto the core surfaces by a change in temperature or by adding a precipitating agent. The coated particles are then collected and dried (Wieland-Berghausen *et al.*, 2002).

Coats can also be formed by interfacial complexation where coating excipients interact with core surfaces to form complexes, leaving a polymeric coat on the surface of the cores (Sriamornsak *et al.*, 1997).

Interfacial polymerization involves the interaction of various monomers at the interface between two immiscible liquid phases to form a polymeric coat on the surface of the cores dispersed in this mixture (Sriamornsak *et al.*, 1997). Nylon microcapsules, polyphthalamide microcapsules, sulfated and carboxylated polyphthalamide microcapsules, polyphenyl ester microcapsules have been produced by this method (Deasy, 1984). However, safety concerns have limited their medical applications. These include toxicity associated with the unreacted monomer and accumulation in the body due to lack of biodegradability. Other disadvantages of this

method are excessive degradation of drugs by reaction with monomers, poor control of drug release due to high permeability and/or fragility of the coat (Deasy, 1984).

### **A.3.2 Mechanical processes**

#### **A.3.2.1 Air suspension coating**

Air suspension or fluid bed coating, is a process in which air is passed through a perforated plate, suspending the substrates to be coated and drying the coats that are sprayed onto the substrates (Jones and Percel, 1994; Deasy, 1984). Air suspension coating is a popular method of coating multiparticulates due to its ability to form high quality, multilayer coatings and its capability of large scale production (Porter and Ghebre-Sellassie, 1994). This method can easily produce multi-layered functional coats by simply changing the type of coating material applied during coating (Jono *et al.*, 2000).

Coating materials used in air suspension coating can be broadly classified as polymer solutions (Lehmann, 1994; Munday and Fassihi, 1989), aqueous polymer dispersions (Ichikawa *et al.*, 2001; Sun *et al.*, 1997; Fukumori, 1994), molten polymers (Barthelemy *et al.*, 1999; Jones and Percel, 1994) and dry powders (Pearnchob and Bodmeier, 2003a, b; Obara *et al.*, 1999). Depending on the material used, the mode of application, mechanism of film formation and characteristics of coat formed would be different.

Polymer solutions are prepared by dissolving the polymer in a suitable solvent. Hot processing air is used to evaporate the solvent, causing the dissolved polymer to increase in concentration and eventually form a dry film over the cores (Hogan, 1995a). The drying capacity of processing air is high. Hence, it may not be necessary to employ high temperatures and the product temperature may be kept below 40 °C by

the cooling effect of the evaporating liquid. This is advantageous for drugs or coating materials which are thermolabile (Jono *et al.*, 2000). Due to the preferential use of water over organic solvents, aqueous solutions of hydrophilic cellulose derivatives such as methylcellulose and hypromellose are commonly used. As the polymers are highly water soluble, films formed are usually fast-dissolving and unsuitable for controlled release applications (Lehmann, 1994).

For aqueous polymer dispersions, hot air is used to dry the applied coating. Discrete polymer particles in the coating dispersion are drawn together, and coalesce to form a continuous film as water evaporates (Hogan, 1995b). The coalescence of polymer particles can be explained by the dry sintering, capillary pressure and wet sintering theories (Fukumori, 1994). Polymer dispersions can be classified as latexes, pseudolatexes and solid dispersions. Latexes such as copoly(methacrylic acid-ethyl acrylate), are prepared by emulsion polymerization. Pseudolatexes such as ethylcellulose, are prepared by emulsification processes while solid dispersions such as hydroxypropyl methylcellulose acetate succinate, are prepared by dispersing the micronized polymeric powder in water. Due to the poor solubility of these polymers in water, their coats commonly have sustained release properties.

Cold air instead of hot air is used in melt coating. Heated molten liquid is atomized and sprayed onto core particles conveyed by the cold air. The molten droplets impinge on the surfaces of cores, covering them with continuous solidified layer coatings. The absence of water in melt coating enables hygroscopic or moisture-sensitive cores to be used. Compared to hot air suspension coating, shorter processing times may be achieved. Coating materials consist of oil based excipients such as hydrogenated vegetable oils and stearic acid with melting points ranging from approximately 50 to

70 °C and waxes such as paraffin or carnauba wax with melting points ranging from approximately 70 to 80 °C. The coats formed may be used for sustained release or taste masking applications (Jones and Percel, 1994).

Powder coating is a relatively less known technique in air suspension coating (Obara *et al.*, 1999). The process involves feeding a powder mixture (e.g. polymer and talc) and spraying liquid components (e.g. plasticizer and binder) concurrently through separate inlets onto a bed of fluidizing substrates. The liquid components enable the powder mixture to adhere to the substrates. Powder-coated particles are subsequently cured to enable complete coalescence of polymer particles for film formation (Pearnchob and Bodmeier, 2003a; Obara *et al.*, 1999). Powder coating has a faster processing time than liquid based coating because only small amounts of water containing plasticizer are used, reducing the drying effort needed (Pearnchob and Bodmeier, 2003a; Obara *et al.*, 1999). However, the coats obtained were found to be more permeable and had many cracks when compared to coatings using conventional organic polymer solutions or aqueous polymer dispersions. Hence, thicker coats were required to produce a similar rate of drug release (Pearnchob and Bodmeier, 2003b).

#### **A.3.2.2 Compression coating**

Compression coating is more suitable for larger multiparticulates, such as minitables. This method requires the use of a tablet press whereby the core is placed on a powder bed of coating material in a die, covered with a top layer of coating powder, then compressed by the punch to form a coated minitab (Shivanand and Sprockel, 1998). This method is not commonly used for coating of multiparticulates because of the high possibility of incomplete or uneven coating when cores are not placed properly (Hogan, 2001).



### **A.3.2.3 Spray drying**

In spray drying, a solution or suspension is sprayed via an atomizing air nozzle placed at the top of a hot chamber. The solvent within the droplets evaporates in the hot environment during the downward fall to form dried particles which are collected at the bottom of the chamber or by a cyclone (Berggren *et al.*, 2004; Wang *et al.*, 2004; Shi and Tan, 2002). Spray drying can be used to produce either microcapsules or microspheres, in which drugs are encapsulated by a polymer layer or dispersed in a polymer matrix respectively. The type of microparticle obtained is dependent on the solubility of drug in the coating solution. Microspheres are produced when the drug is soluble in the coating solution. When the drug is insoluble in the coating solution, microcapsules or microspheres may be produced (Kristmundsdottir *et al.*, 1996). Major disadvantages of using this method to produce microcapsules are the presence of incomplete coats and the low core loading capability of about 20 to 30 % (Thies, 1996).

### **A.3.2.4 Spray congealing**

In spray congealing, molten waxes or fats are sprayed via an atomizing nozzle placed at the top of a cold chamber. The spray may be co-current or counter-current to the cooling air stream. The sprayed droplets solidify during the downward fall to form particles which are collected at the bottom of the chamber (Passerini *et al.*, 2003; Emås and Nyqvist, 2002; Fini *et al.*, 2002; Tobio *et al.*, 2000). Spray congealing is a solvent-free method that can be used to produce microcapsules. High encapsulation efficiency and spherical particles with sustained release properties can be obtained by using the appropriate type and amount of meltable material. Spray congealing may not be suitable for hydrophilic drugs such as verapamil because of poor wetting by the hydrophobic base. This problem may be reduced by using a more hydrophilic wax

such as stearyl alcohol, and/or a surfactant such as soya lecithin (Passerini *et al.*, 2003). As with spray drying, major problems associated with this method are the presence of incomplete coats and the low core loading capability.

## **B Coating of fine particles using air suspension coating**

Coating methods such as complex coacervation, interfacial complexation and interfacial polymerization can be used to coat fine particles. However, these methods are not popular because of their low efficiencies. Spray drying and spray congealing are large scale operations that can be used to coat fine particles but the products formed may not be well-encapsulated. On the other hand, air suspension coating is a feasible alternative to the coating of fine particles due to its capability of large scale production and ability to form multilayer complete coats.

Air suspension coating of particles in millimeter size range is well-established and poses few problems. However, air suspension coating of micron sized particles is challenging. Only few studies have attempted to coat fine particles of micron sizes due to the high tendency of agglomeration, which is detrimental to the quality of the coated products formed (Jono *et al.*, 2000). Fine particles also have higher surface area to volume ratios and require more coating material to achieve similar coat thickness as larger particles of an equivalent volume (Ragnarsson and Johansson, 1988). Coupled with high agglomeration tendency, this makes air suspension coating of fine particles very time consuming. Hence, it is important to understand the causes of agglomeration of particles in air suspension coating in order to overcome it. The aim is to coat each particle discretely and uniformly without causing agglomeration.

Substrate movement, spraying of coating material and evaporation of solvent occur concurrently in air suspension coating. Poor substrate movement commonly occurs

with fine particles due to their inherently poor flow properties and cohesive nature. This results in poor circulation and clumping of substrates, leading to a high tendency for agglomeration. Fine particles are extremely prone to building up of electrostatic charges from the constant movement of particles during fluidization. The electrostatic charges can cause particles to adhere onto the walls of the coating chamber, especially at the partition column where the particle velocities are the highest. This is often referred to as dry quenching. Low spray rates are often employed to reduce agglomeration (Jono *et al.*, 2000). This would result in low humidity in the coating chamber, encouraging the build up of electrostatic charges. Conversely, they can be minimized with the use of wetter coating conditions.

During the wetting process, liquid bridges can form between the particles and agglomeration takes place if the liquid bridges do not break up but solidify, resulting in the permanent fusion of two or more particles (Hemati *et al.*, 2003). The small size of fine particles makes it easy for liquid bridges to form and difficult for them to be broken. In order to prevent agglomeration, the formation of liquid bridges must be minimized or the applied separation forces must be strong enough to break up any liquid bridges that have formed (Fukumori, 1994).

The drying capacity of the air should also be controlled to ensure adequate drying of the wetted particles. Extremely wet condition causes a more serious form of agglomeration which is referred to as wet quenching, whereby the cores are engulfed and fused together by the liquid medium. On the other hand, dry conditions can lead to excess attrition of substrates. Depending on the drying conditions of coating, several products may result (Fig. 2). Hence, the drying condition has to be optimal to prevent undesirable products from forming.

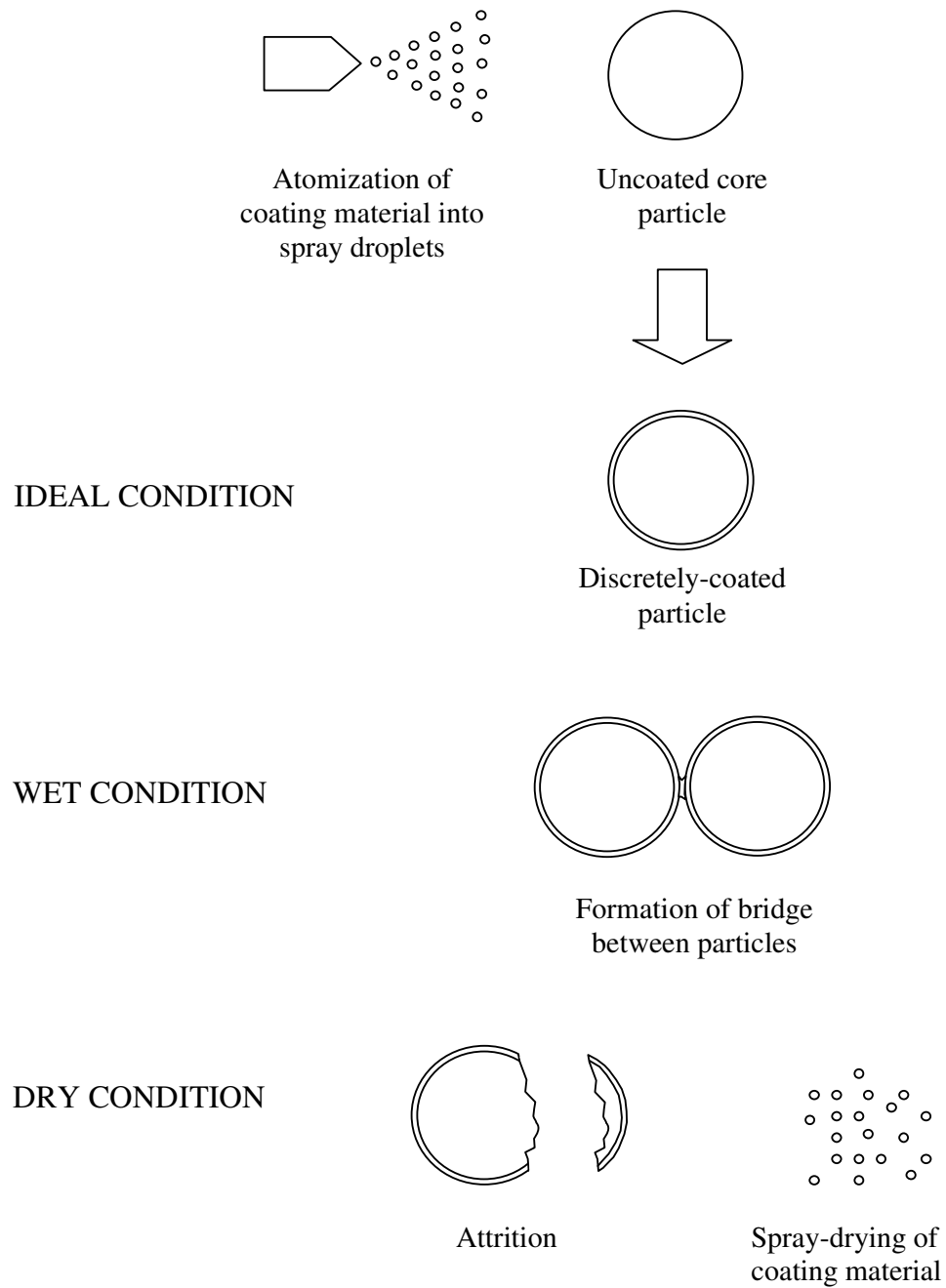


Fig. 2. Schematic diagram of the air suspension coating process showing the possible products formed under different drying conditions.

## **C Factors affecting air suspension coating of multiparticulates**

The factors which may affect air suspension coating of multiparticulates may be broadly classified into four categories: processing equipment, processing conditions, core materials and coating materials. A limited scope of the factors will be discussed in this section. In practice, these factors are dynamic and may interact with one another, making process optimization rather complex. Knowledge of these factors is nevertheless important for air suspension coating because control of these factors ensures consistency of product quality and greater efficiency in coating.

### **C.1 Processing equipment**

The basic components of an air suspension coating system consist of a coating chamber, nozzle(s), pump(s) and filter(s). Constant developments to improve the coating process have led to various equipment setups with different efficiencies and purposes (Bertelsen *et al.*, 1994; Wesdyk *et al.*, 1993; Yang *et al.*, 1992).

#### **C.1.1 Types of air suspension coaters**

Air suspension coaters are generally classified into three types: the bottom-spray, tangential-spray and top-spray coaters (Jones and Percel, 1994), depending on the position of the nozzles (Fig. 3). Among the different forms of air suspension coating, bottom-spray air suspension coating (Fig. 3a) is considered superior for coating fine particles as it enables better flow of particles in the coating zone and imparts high shear forces to the fluidizing particles (Fukumori, 1994). Highly functional multi-layer microcapsules from fine particles as small as 10  $\mu\text{m}$  have been coated by this method (Jono *et al.*, 2000). However, the turbulent air conditions may cause excessive attrition and are not suitable for friable cores.

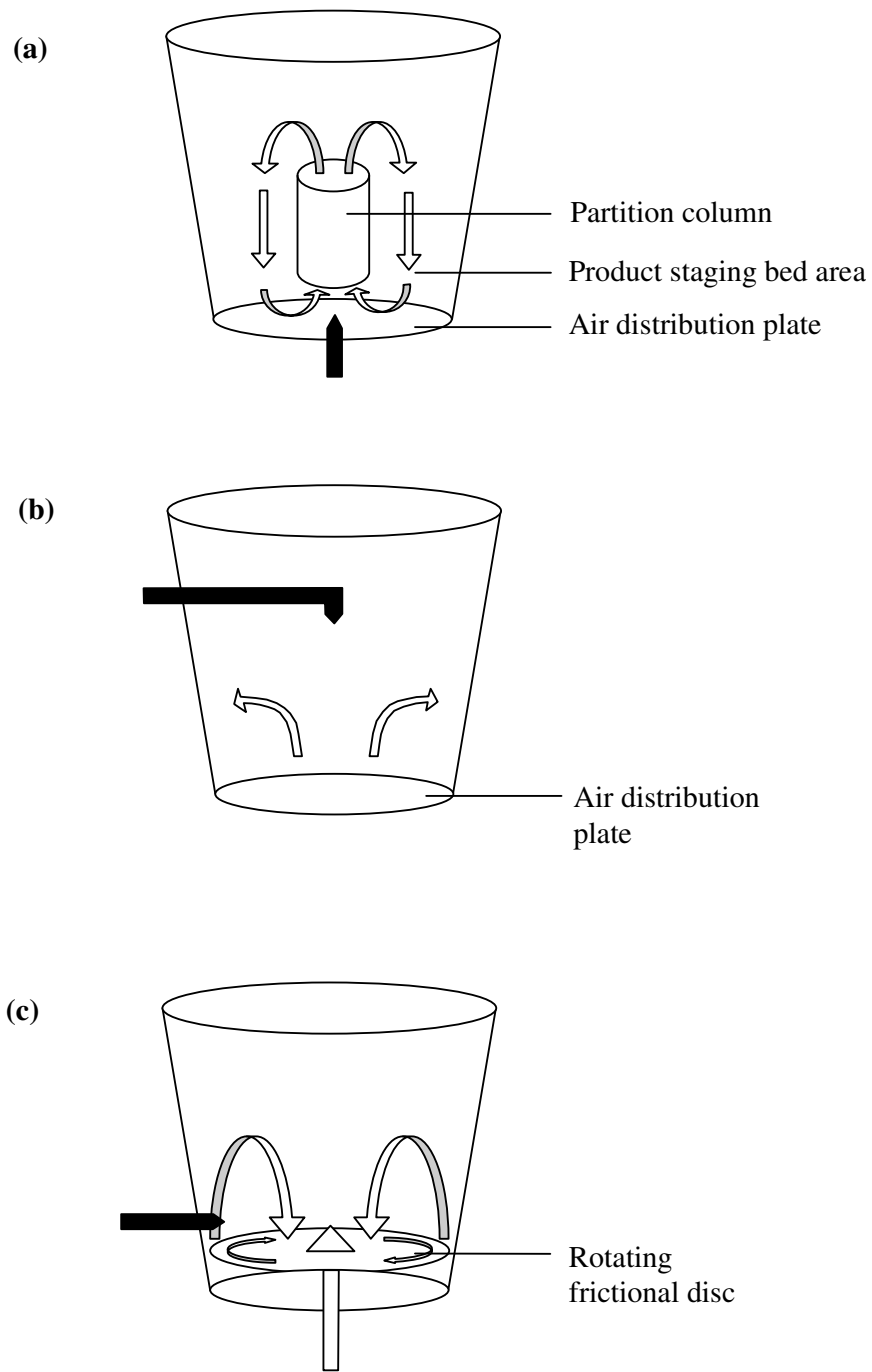


Fig. 3. Schematic diagrams of the coating chamber of (a) bottom-spray, (b) top-spray and (c) tangential-spray air suspension coaters (Arrows show the particle flow paths; Spray nozzles are shaded black).

The bottom-spray air suspension coater (Fig. 3a) uses a hollow partition column, also known as Wurster partition, to restrict the upward movement of the substrates to be coated. The area of air distribution plate directly under the partition column has more perforation than the peripheral region of the air distribution plate, resulting in a comparatively higher central air velocity through the partition column (Porter and Bruno, 1990). This also creates a region of lower pressure which draws the substrates in and lifts particles up through the partition column. As part of the cycle, the substrates from the peripheral product staging bed enter the partition gap into the partition column (horizontal transport zone), move up the partition column (upbed zone), decelerate in the expansion chamber above the partition column (deceleration zone), fall downwards and outwards in an inverted U-shaped trajectory (downbed zone) into the product staging bed area. From the product bed, substrates re-enter the partition column through the partition gap, repeating the fountain-like cyclic flow (Christensen and Bertelson, 1997). Particles receive coating droplets during the passage through the spray zone within the partition column and this cycle is repeated until the desired coating level is achieved.

Top-spray coaters make use of a spray nozzle located at the top of the coating chamber to spray coating material onto the fluidizing substrates in the product bed (Fig. 3b). The particles are supported by a perforated base plate through which fluidizing air is passed through. Due to the longer distance between the spray nozzle and the product bed, top-spray coaters have the highest incidence of coating materials drying before they can impinge on the substrates as compared to the other types of air suspension coaters. The counter current spray droplets against the fluidizing air also tend to promote spray drying. Weak separation forces may result in higher tendency of agglomeration when coating smaller cores.

Tangential-spray coaters make use of a rotating frictional disc to move substrates in a circular manner (Fig. 3c). These coaters have characteristics intermediate between the top-spray and bottom-spray coaters. They can be used to coat particles as small as 200 to 300  $\mu\text{m}$  in diameter as the shear forces applied are intermediate between those of top-spray and bottom-spray coaters. They are also suitable for producing thicker coats and for coating friable cores due to the lower particle trajectories during coating (Fukumori, 1994).

### **C.1.2 Types of bottom-spray air suspension coaters**

The Wurster coater (Wurster, 1953) (Fig. 4a) is the first generation of bottom-spray air suspension coater which has since been extensively used in the pharmaceutical industry for coating of substrates ranging from tablets to powders (Christensen and Bertelson, 1997). It offers excellent heat and mass transfer within the product bed and is able to produce uniform coats (Porter and Bruno, 1990). However, its efficiency for coating powders has been limited due to the propensity of the fine particles to agglomerate during the coating process (Jono *et al.*, 2000). This could be attributed to several weaknesses of the Wurster coating system. As described in section C.1.1, substrates circulate through various regions of the coater in a fountain-like manner. Each region could contribute to agglomeration if process conditions were not optimal.

At the product staging bed, substrates are stored before entering the coating zone. The close contact between substrates may encourage agglomeration if they are insufficiently dried prior to this stage (Christensen and Bertelson, 1997). Substrates then move from the staging bed through the horizontal transport region into the upbed region. If the flow of substrates is not rapid enough at the horizontal transport region, over-wetting may occur and can cause the partition gap to be clogged up with



agglomerated substrates. Moving into the partition column, the tendency of agglomeration becomes very high as this is where substrates are sprayed with coating material. Individual substrates moving up may group up to form clusters whereby close contact will favour agglomeration (Christensen and Bertelson, 1997). It was reported that particles moving up a spouted bed closer to the walls had lower velocities than particles moving in the center, resulting in slower and even downward fall of particles (Bader *et al.*, 1988). This downward fall or recirculation could contribute to poor movement of substrates in the partition column of the Wurster coater. Substrates moving close to the wall may also adhere to the wall if coating material deposited onto the walls do not dry quickly enough.

All these scenarios suggest that the Wurster coater is vulnerable to agglomeration of substrates and unpredictable performance. Therefore, since the invention of the Wurster coater, several modifications have been attempted to improve the coating process in bottom-spray air suspension coaters.

One approach to improve the particle movement within the partition column was to change the design of the partition column. Danelly and Leonard (1978) used a bicylindrical partition column with the Wurster setup instead of the conventional cylindrical partition column as described in Fig. 4a. The bicylindrical partition column, which has a larger circumference at the bottom end and a smaller circumference at the top end, was placed vertically above the air distribution plate. This was used in conjunction with an aerodynamic structure under the air distribution plate which directed all the inlet processing air into the partition column and little air to the product staging bed as substrates were expected to be dried before reaching the product staging bed. The substrates accelerated as they moved up the bicylindrical

partition column due to the narrowing passageway. The improved particle movement up the partition column was found to favour coating. However, due to the large base of the partition column, large amount of energy would be required to produce the airflow to lift the substrates up, especially so for larger substrates. Hence, it would be difficult to scale up such a setup.

The nozzle tip of the conventional Wurster coater is typically placed in the center of the air distribution plate, protruding into the product bed. The gas jet produced by the high pressure atomizing air was reported to cause attrition of substrates by impact collision. To address this problem, slight modifications were made to the conventional Wurster coater to create the Wurster HS. The latter has a spray nozzle placed further from the substrate bed, allowing the atomizing air velocity to decrease prior to contacting the substrate. This reduced the attrition caused by the atomizing air, enabling higher atomizing pressures and higher spray rates to be used (Mehta, 1997).

One of the latest modifications of the conventional Wurster coater is the Precision coater (Walter, 1998), which uses a modified mode of air distribution to improve the Wurster coating process (Fig. 4b). It has a swirl accelerator under the air distribution plate which swirls and accelerates the processing air to impart spin and high velocity to the substrates as they transit through the partition column (Mehta, 1997). Based on a similar concept employed by Danelly and Leonard (1978), a bicylindrical insert, with narrower opening at the top, is placed in the central part of the air distribution plate to accelerate the inlet air. This insert is referred to as the accelerator insert.

Like the Wurster HS, the nozzle tip of the Precision coater is positioned just below the upper surface of the accelerator insert, whereby it does not come into contact with the substrates being coated. This would reduce the attrition caused by the atomizing air.

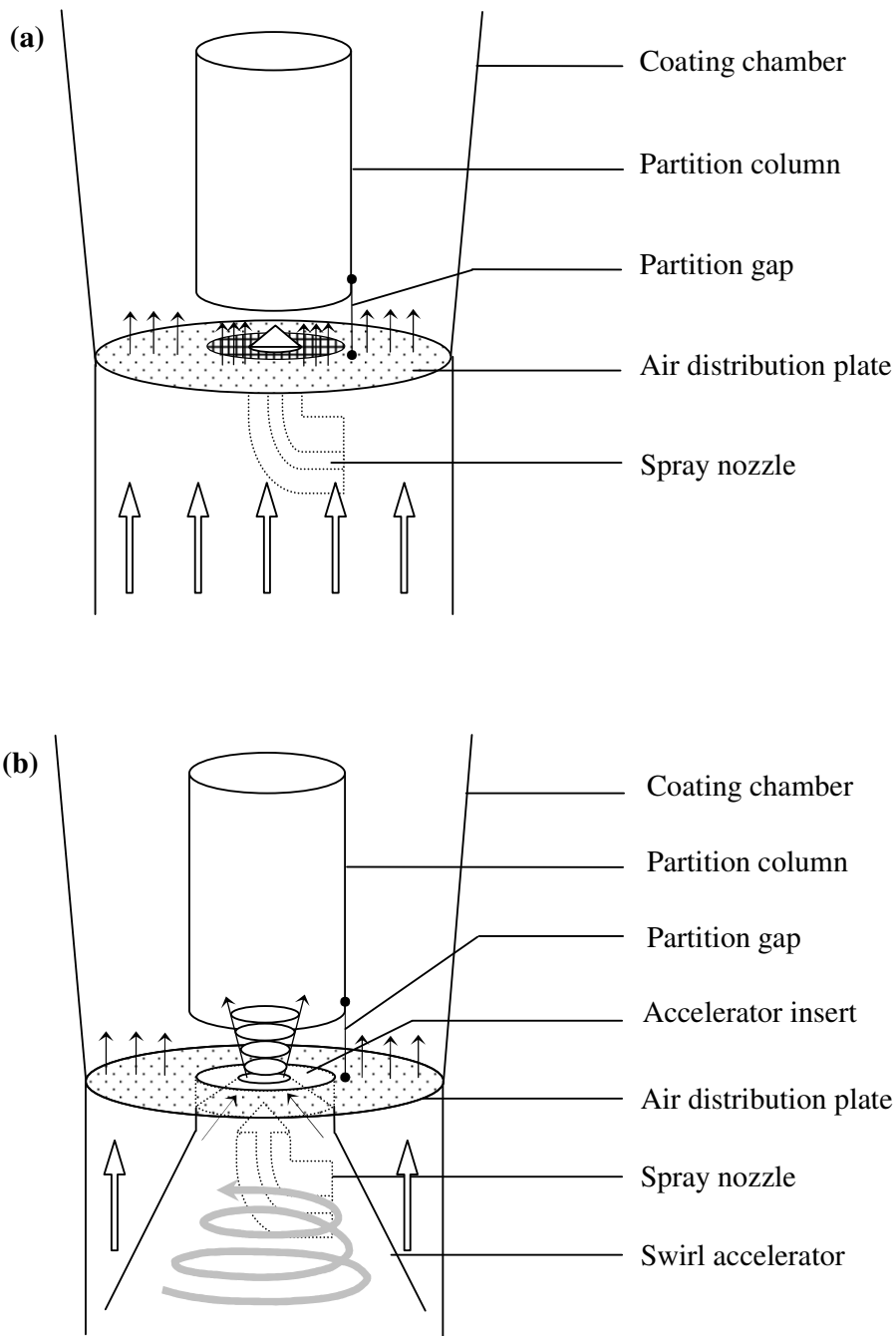


Fig. 4. Diagrams of the air distribution plates and associated parts of the (a) Wurster coater and (b) Precision coater, with arrows showing the airflow pattern.

A number of studies had reported that swirling airflow was able to improve heat transfer rates (Ozbey and Soylemez, 2005; Kevat *et al.*, 2005; Yilmaz *et al.*, 2003; Yilmaz *et al.*, 1999; Algifri *et al.*, 1988) and mixing of components (Ozbey and Soylemez, 2005) as compared to non-swirling airflow. This was attributed to the longer flow paths of swirling airflow which increased the energy dissipated by friction and caused angular acceleration to the flow (Yilmaz *et al.*, 2003), in addition to the increased pressure drop near the central rotation axis of swirling airflow which increased the velocity of flow (Yilmaz *et al.*, 1999; Shtern *et al.*, 1998). The degree of swirl is dependent on the amount of tangential motion corresponding to the amount of axial motion (Ozbey and Soylemez, 2005). The centre of a swirling air has also lower pressure, hence improved coating droplet spreading can be expected. These effects would be beneficial in bottom-spray coating for the spreading of deposited coating droplets and drying of the coatings, possibly increasing the coating efficiency and improving coat quality attributes.

## **C.2 Processing conditions**

### **C.2.1 Temperature**

The inlet drying air is usually heated before passing into the coating chamber to enhance the evaporation of coating material sprayed onto the cores. Control of the air temperature is important as it affects the quality of coats formed. Generally, excessively dry environment leads to spray drying effect and attrition while over-wetting causes agglomeration (Maronga and Wnukowski, 1998). The optimal temperature allows the evaporation of solvent to take place at a rate that is sufficiently slow for adequate spreading of spray droplets and coalescence of polymer particles, and fast enough to avoid agglomeration and drug migration into the liquid layer (Yang and Ghebre-Sellassie, 1990).

When the temperature of the air is too high, sprayed droplets dry quickly and do not coalesce when impinged on the core particles. This forms discontinuous coats which are rough and porous and will not impart the desired controlled release properties of a functional coat (Fukumori, 1994). The high temperatures may also cause spray drying of atomized droplets before they reach the cores, resulting in loss of coating material and thinner coats. Spray dried coating materials may also be embedded in the film coats, disrupting the continuity (Oliveira *et al.*, 1997; Ronsse *et al.*, 2007).

On the other hand, when the temperature is too low, a longer time is required for coat drying and this allows soluble drug to migrate from the cores into the moistened coat layer. The dissolved drug reduces the surface tension of the liquid layer, lowering the capillary forces required for deformation and coalescence of spray droplets. Drug embedded in the resultant coat may dissolve on contact with dissolution media, resulting in a porous and more permeable coat. If the temperature is lower than the minimum film formation temperature, coalescing would not occur, resulting in discontinuous porous films (Oliveira *et al.*, 1997).

### **C.2.2 Humidity**

In addition to the temperature, humidity of the inlet drying air also affects the drying of coated particles. The relationship between temperature and relative humidity or moisture content of air at different atmospheric pressures may be derived from psychrometric charts (Shallcross, 1997). The evaporation of solvent from sprayed droplets depends on the vapour pressure difference between the wet particle surface and the surrounding air. Inlet air with lower humidity has a low vapour pressure and will enhance the evaporation of the solvent in the sprayed droplets.

### **C.2.3 Conveying airflow rate**

Conveying airflow or fluidizing airflow is responsible for the circulation and drying of substrates during coating. Insufficient airflow may not provide sufficient drying air to circulate the substrates and remove the moisture from the deposited sprayed droplets during coating and consequently result in a high degree of agglomeration. However, excessively high airflow rates can increase attritive conditions causing erosion of friable cores or stress cracks in coats and may also augment the spray drying effect. For functional coats, this can result in loss of the desired release properties (Cole, 1995b). The suitable airflow rate is unique for each coating equipment and also depends on product characteristics such as particle density, size, and shape (Christensen and Bertelsen, 1997).

### **C.2.4 Atomizing air pressure**

Pneumatic nozzles are commonly used for spraying of coating materials in air suspension processes. These nozzles make use of air pressure to shear the coating materials into atomized droplets. Higher atomizing air pressures result in smaller spray droplets (Wan *et al.*, 1995) and are required to prevent agglomeration, especially when coating smaller substrates (Hemati *et al.*, 2003). When the atomizing pressure is too high, the spray droplets can be propelled away too quickly and this does not promote droplet-core contact. High atomizing air pressure also increases the attrition of cores and can produce more fines. On the other hand, low atomizing pressure causes the formation of coarse spray droplets, which dry slowly and encourage the formation of liquid bridges between the cores, leading to increased agglomeration of the substrates being coated (Heng *et al.*, 1999).

### **C.2.5 Spray rate**

High spray rates increase the propensity for agglomeration and result in formation of less uniform coats, while low spray rates increase the coat uniformity (Singh *et al.*, 1996). Low spray rates also enable smaller spray droplets to be formed which would reduce agglomeration, especially when coating smaller substrates (Jones and Percel, 1994). However, if the spray rate is too low, fast drying of the droplets could prevent coalescence of polymer particles, resulting in poorly formed coats (Heng *et al.*, 1999).

### **C.2.6 Partition gap**

A partition column is present for bottom-spray air suspension coaters. The partition gap may be defined as the vertical distance between the bottom of the partition column and the surface of the air distribution plate (Fig. 4). Appropriate adjustment of the partition gap ensures proper substrate circulation through the spray zone and up the partition column (Christensen and Bertelsen, 1997). It was recognized as an important factor in determining the success of coating small substrates (Deasy, 1984) and was found to affect the drug release profile of coated pellets (Porter and Ghebre-Sellassie, 1994). This was attributed to its influence on the flow of pellets into the partition column and the exposure of pellets to the coating droplets in the spray zone (Fitzpatrick *et al.*, 2003; Shelukar *et al.*, 2000). If the partition gap is too large, there may be insufficient pressure differential to draw particles in and up the partition column. The resultant slow and sluggish flow of particles through the partition column would increase agglomeration (Deasy, 1984). However, when the partition gap is too small, restriction to the passage of particles into the partition column may cause a loss of spray material due to the scarcity of particles passing through the spray zone.

### **C.3 Characteristics of core materials**

#### **C.3.1 Size**

Smaller cores have higher surface area to volume ratios and require more coating material to achieve similar coat thickness as larger cores of an equivalent total volume (Ragnarsson and Johansson, 1988). Smaller cores fluidize higher and suspend longer in the expansion zone, thus reducing the cycling rate. They are also accelerated faster in the partition column resulting in a shorter time spent in the spray zone (Wesdyk *et al.*, 1993). This may result in loss of coating material to the surrounding wall and thinner coats to be formed as compared to larger particulates coated under similar conditions. This phenomenon was found to vary with different air suspension coating equipment used (Wesdyk *et al.*, 1993; Husson *et al.*, 1991).

#### **C.3.2 Shape**

Spherical particles have the lowest surface area to volume ratio compared to particles of other shapes. They do not have any large protuberances and hence, will be equally exposed to the coating spray over time to enable the formation of a uniform coat. On the other hand, needle-like cores are less evenly coated as the surfaces are unequally exposed to the coating spray. They tend to be friable and produce fines that may be embedded in the coat during the coating process. On dissolution, embedded fines produce pores for drugs to leach out from the coat and allow easy drug passage and faster drug release (Chopra *et al.*, 2002). Spherical particles have the best flow properties compared to particles of other shapes. Thus, spherical cores facilitate easy movement during coating and help to minimize the likelihood of agglomeration.



### **C.3.3 Surface roughness**

Cores with rough surfaces tend to develop more uneven coats than smooth cores of equivalent size (Johansson and Alderborn, 1996). Uneven raised ridges receive thinner coats, which possess lower mechanical strength. Thus, the films at these sites show a greater tendency to stretch or break arising from internal stress during drying. The rougher surfaces also contribute to friction resulting in sluggish flow of particles during coating. This could lead to poor fluidization and erratic particle movement through the spray zone leading to a higher opportunity for agglomeration.

### **C.3.4 Porosity**

Porosity of cores can affect the film formation process when aqueous polymeric dispersions are used for coating. Pores may retain liquid by capillary forces and slow down the evaporation of solvent during the coating process. This hinders the coalescence of polymer particles, resulting in a more porous coat with a faster drug release profile (Tunon *et al.*, 2003). Highly porous cores may also encourage infiltration of coating material into the cores during coating, forming uneven coats and causing core constituents to be dissolved into the coat.

### **C.3.5 Properties of drug**

The concentration of drug within cores can influence the quality of coats formed (Ouriemchi *et al.*, 1994; Wan and Lai, 1991). A high concentration of drug on the surface of the core also increases interaction between drug and polymer coat, which may result in poor film adhesion. It can also cause migration of drug into the coat layer and disrupt the continuity of the applied coat.

Leaching of drug into the coat during coating can change the surface characteristics of the coat, such as surface roughness or hydrophobicity, and bring about difficulties in spreading of coating material over the surface. As a consequence, liquid bridges between cores can be formed more easily, increasing the agglomeration tendency. Some drugs may react with coating dispersions by salt formation, complexation, ester hydrolysis, ring opening or cyclization. The reaction can alter coat properties especially if reaction products are poorly soluble or large in size (Sadeghi *et al.*, 2003).

### **C.3.6 Properties of excipient**

Excipients with low aqueous-solubility can affect the quality of coats formed. The low miscibility with water prevents proper film formation, resulting in coats with poor integrity. This causes poor film adhesion to the cores which may hasten the disintegration of the coats during further processing or drug administration (Sousa *et al.*, 2002).

Different excipients used in the formation of cores result in cores with differences in sphericity, hardness and density. Excipients with better spheronizing abilities produce cores which are more spherical, regular in size, harder and denser. It was reported that microcrystalline cellulose had better spheronizing ability than other fillers such as maize starch, calcium hydrogen phosphate dehydrate, glucose and lactose (Eerikainen and Lindqvist, 1991). This resulted in cores that were more suitable for coating as they had better flow properties and showed lower incidences of attrition.

## **C.4 Components of coating formulation**

### **C.4.1 Solvent**

Volatile organic solvents were widely used for coating in the past. However, since the 1970s, the use of organic solvents for coating formulations had gradually lost popularity and was replaced by water due to toxicity and safety concerns (Cole, 1995b; Hogan, 1995b). The use of water as the liquid media for coating applications has led to various problems and challenges. Water has a higher heat of capacity than volatile organic solvents and requires longer drying times or higher drying temperatures. This may be detrimental to heat and moisture sensitive drugs (Thoma and Bechtold, 1999; Faroongsarng and Peck, 1991 and 1992). Aqueous coating preparations also require a higher amount of coating material than organic preparations to achieve the same sustained drug release profile. This is because of the higher tendency of forming porous coats from aqueous coating preparations (Thoma and Bechtold, 1999).

### **C.4.2 Polymer**

There are many types of polymers that can be used for air suspension coating. They may be classified according to their origin as being natural, semi-synthetic or synthetic. Natural polymers include zein (O'Donnell *et al.*, 1997), alginate (Abletshauser *et al.*, 1993), chitosan (Kim *et al.*, 2003), pectin (Pillay and Fassihi, 1999), shellac (Chang *et al.*, 1990) and rosin (Fulzele *et al.*, 2002). Semi-synthetic polymers include ethylcellulose (Shi and Tan, 2002; Porter, 1989), cellulose acetate (Shivanand and Sprockel, 1998) and hypromellose (Wan and Lai, 1991). Synthetic polymers include methacrylic acid copolymers (Musko *et al.*, 2001; Savage and Rhodes, 1995; Husson *et al.*, 1991). Natural polymers and their derivatives are commonly used due to their low toxicity. Synthetic polymers may contain residual

monomers, plasticizers, softeners and fillers and needed to be carefully evaluated for their potential toxicity (Leszek, 1987). The most commonly used coating polymers for the coating of sustained release multiparticulates are ethylcellulose, methacrylic acid copolymers and cellulose acetate (Savage and Rhodes, 1995).

The solid content, type and molecular weight of polymers used would influence the viscosity of the coating preparation. Viscous coating preparations have poorer flow properties and higher tendency of nozzle clogs (Mazzone *et al.*, 1987). They spread less readily on the cores, increasing agglomeration tendency (Heng *et al.*, 1996) and hinder coalescence of polymer particles on the substrate.

Different grades of the polymer used can also affect the quality of coats formed. Low molecular weight grades of ethylcellulose formed films with cracks and flaws, while high molecular weight grades were able to produce good quality controlled drug release films (Rowe, 1986). It was subsequently found that as the molecular weight of a polymer increased, the mechanical strength also increased until the critical molecular weight beyond which the mechanical properties did not improve further (Rowe, 1997).

#### **C.4.3 Plasticizers**

Plasticizers increase film elongation, decrease elastic modulus and tensile strength of the film by lowering glass transition temperature. They can be added to polymers to form softer and more pliable polymer coats (Hogan, 1995b). Suitability of a plasticizer depends on its ability to interact with the polymer chains (Gutierrez-Rocca and McGinity, 1994). Plasticizers can be classified as polyols (e.g. glycerol, propylene glycol, polyethylene glycol), organic esters (e.g. phthalate esters, dibutyl sebacate, citrate esters, triacetin) or oils/glycerides (e.g. castor oil, acetylated

monoglycerides, fractionated coconut oil). Recently, n-alkenyl succinic anhydrides were found to be effective plasticizers for ethylcellulose coats (Tarvainen *et al.*, 2003).

Plasticizers reduce the incidence of flaws and cracks in coats especially with cores that swell on contact with water (Sun *et al.*, 1997). Lack of plasticizer or loss of plasticizer from the polymer coat through evaporation (permanence), migration to the cores or migration into packaging materials caused the coats to become brittle and form cracks (Hogan, 1995b).

#### **C.4.4 Colorants**

Colorants are compounds which add colour to the product. They are usually used for decorative purposes or as indicators of coating uniformity (Heng *et al.*, 1999, Chan *et al.*, 2001). Some pigments may have anti-tack properties and may be added to the coating formulation to reduce agglomeration of core particles during coating (Chopra and Tawashi, 1985). Water-soluble colorants are known as dyes and water-insoluble colorants, pigments. Pigments are considered to be superior to dyes because they are chemically more stable and have higher opacity which enhances protection against light.

The type of colorant used may affect the stability of the coating formulation. An example is the aluminium lake which was found to be incompatible with both ionic and non-ionic polymeric dispersions. Non-ionic polymeric dispersion changes the surface charge of the aluminium lakes causing them to aggregate. With ionic polymeric dispersions, aluminium lakes release electrolytes due to the incompatible pH, causing aggregation of the polymers (Nyamweya *et al.*, 2001).

The concentration of the pigment used may also affect the characteristics of the coat formed. At concentrations below the critical pigment volume concentration, the permeability of the coat to water and air was not affected (Hogan, 1995b). However, when concentration of pigments went beyond the critical pigment volume concentration, marked changes in mechanical property, appearance and permeability of the coats were found (Gibson *et al.*, 1988).

#### **C.4.5 Anti-tack agents**

Insoluble additives, soluble salts, plasticizers and film formers can act as anti-tack agents. They are commonly added to the coating formulation to reduce agglomeration of substrates undergoing coating.

Insoluble additives such as talc, kaolin, calcium carbonate, magnesium stearate, glyceryl monostearate and silicon dioxide have been widely used as anti-tack agents (Felton and McGinity, 2002; Wesseling *et al.*, 1999; Lehmann, 1997; Wan and Lai, 1993; Ghebre-Sellassie *et al.*, 1986, 1987). However, they had been found to cause detrimental effects to the coating formulation and coat properties, depending on their properties and interaction with other film coat constituents. They may cause flocculation and precipitation of polymer, increase viscosity of the coating formulation (Nagai *et al.*, 1997; Aulton *et al.*, 1997) and affect coat properties such as mechanical strength, appearance, moisture permeability and drug release (Wan and Lai, 1993; Okhamafe and York, 1984a, b).

The effects of insoluble film coat additives were reportedly dependant on their particle size, morphology, surface area and density (Felton and McGinity, 2002). Generally, the smaller the insoluble additive, the more effective and less detrimental it will be. For fine particle coating, smaller insoluble additives would be favoured over

larger ones. Smaller insoluble additives, if well-dispersed, will have a lower tendency to clog the spray nozzle especially when smaller sized nozzle tips are used for the coating onto fine cores.

Sodium chloride and sodium citrate are soluble salts that have anti-tack properties. They reduce the viscosity of the coating formulation by salting out the polymer. Less viscous coating preparations would spread better over the surfaces of substrates, enhancing the drying of coats, thereby preventing agglomeration of pellets during coating. These salts also can increase drug release from the coated particulates as they dissolve and form pores in the coat when exposed to aqueous media, (Yuasa *et al.*, 1997; Nakano and Yuasa, 2001).

Plasticizers such as polyethylene glycol, triacetin, triethyl citrate and film formers such as vinylpyrrolidone/vinyl acetate copolymers and polyvinyl pyrrolidone have been investigated as anti-tack agents (Heng *et al.*, 1996). Polyvinyl pyrrolidone was found to be superior to polyethylene glycol as an anti-tack agent under similar conditions due to its higher viscosity lowering effect (Wong *et al.*, 2002).

Besides being used as additives, anti-tack agents may be used as physical barriers to prevent sticking of underlying coats. Polyethylene glycol, when applied as an overcoat, was found to prevent sticking or agglomeration of Eudragit-coated particulates during storage (Ghebre-Sellassie *et al.*, 1987).

**PART II:**

**HYPOTHESES AND OBJECTIVES**



## II HYPOTHESES AND OBJECTIVES

Pharmaceutical coating has come a long way from tablet to pellet coating. Advancing further is the coating of even smaller particles such as powders, which allows for new applications in drug administration and delivery. Currently, there is a lack of knowledge in the field of pharmaceutical technology to enable efficient and feasible coating of fine particles. Hence, this project was targeted at establishing the science of coating with a view to advance the development of fine particle coating.

The Wurster coater, a bottom spray air suspension coater, is one of the most common coaters employed in the pharmaceutical industry for the coating of pellets. While Wurster coating is well-established, it has many weaknesses which limit the size of particles that it can efficiently handle to about 500  $\mu\text{m}$  in diameter. The newer Precision coater utilizes swirling airflow to improve the coating process. It was hypothesized that the coating performance of the Precision coater was superior to that of the Wurster coater. Fluid dynamics and thermodynamics in Wurster and Precision coating would be compared to elucidate the differences in the transport of particles and drying conditions. Differences in their coated products would also be assessed.

Proper selection of process conditions is important in the coating of small particles. The drying condition in the coater is important during coating, as excessively dry environment would lead to spray-drying effect and attrition while over-wetting causes agglomeration. It was hypothesized that an optimal drying efficiency would be necessary for desirable product characteristics. Hence, the temperature and airflow rate, which could affect the overall drying efficiency of the coater, would be studied to determine the relationship between drying efficiency and product characteristics. It was also hypothesized that optimal particle movement was important in enhancing

coating. Accelerator insert diameter, airflow rate and partition gap are the major process parameters that could affect the particle movement in Precision coating, hence their influence on the quality of coated products and their suitability for coating smaller particulates would be investigated.

By understanding the conditions favourable for coating smaller particulates, formulation factors affecting fine particle coating could then be studied with minimal influences from the equipment setup and process conditions.

Core particles with different properties may affect the degree of agglomeration during coating. Calcium carbonate nanoparticles (nano-CaCO<sub>3</sub>) are potentially useful for modifying the surfaces of core particles due to their small sizes and hydrophobic nature. It was hypothesized that nano-CaCO<sub>3</sub>, when coated onto lactose particles, would modify their characteristics and influence the subsequent film coating. Hence, the effect of nano-CaCO<sub>3</sub> on the properties of the core lactose particles and their impact on subsequent coating with hypromellose would be investigated.

Insoluble excipients, including CaCO<sub>3</sub>, have been shown to be effective anti-tack additives in coating formulations. However, the effects of nanoparticulate additives on coating were not well-established. It was hypothesized that nano-CaCO<sub>3</sub> was an effective anti-tack agent for hypromellose in the coating of fine particles. Hence, the effectiveness of nano-CaCO<sub>3</sub> in reducing agglomeration of core lactose particles during coating would be evaluated. The effects of nano-CaCO<sub>3</sub> on the properties of the coating formulations and cast films would be studied to elucidate the mechanism of anti-tack action.

**PART III:**

**EXPERIMENTAL**

### **III EXPERIMENTAL**

#### **A Materials**

##### **A.1 Core particles**

###### **A.1.1 Sugar pellets**

For the study of fluid dynamics without coating, sugar pellets of size fractions 500 to 600  $\mu\text{m}$  and 710 to 850  $\mu\text{m}$  (Non-pareil seeds, JRS Pharma LP, USA) were used. For coating studies, sugar pellets of size fractions 355 to 425  $\mu\text{m}$  and 500 to 600  $\mu\text{m}$  (Fig. 5) from a different source (Nu-pareils, Hanns G. Werner GmbH + Co., Germany) were used as substrates for coating as the pellets were visibly less friable and considered more suitable for evaluation of coat properties.

###### **A.1.2 Lactose particles**

Lactose  $\alpha$ -monohydrate particles (80M lactose, Meggle, Germany) were used as cores for fine particle coating (Fig. 6). The lactose was fractionated by sieving with 125  $\mu\text{m}$  and 250  $\mu\text{m}$  aperture size sieves to produce a narrower size fraction prior to coating. The fractionated lactose particles had a median size of  $166 \pm 1.8 \mu\text{m}$ , a span of  $1.04 \pm 0.03$  and true density of  $1.53 \pm 0.001 \text{ g cm}^{-3}$ .

##### **A.2 Coating materials**

Components used for the coating formulations are listed in Table 2. The concentrations of components used for each coating formulation were varied according to the intended purpose of the coat. As such, the formulae are specified in the respective sections. Deionised water was used as the vehicle for all the coating media.

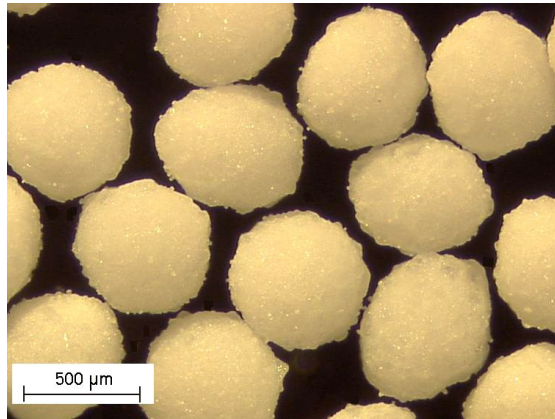


Fig. 5. Light microscopy images of uncoated sugar pellets of size 500 to 600 μm.

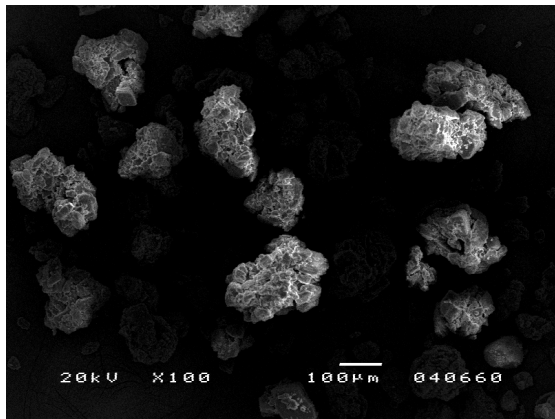


Fig. 6. Scanning electron photomicrograph of lactose α-monohydrate particles.

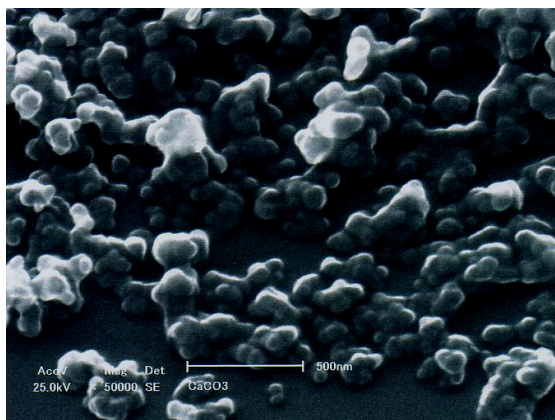


Fig. 7. Scanning electron photomicrograph of osmium-coated nano-CaCO<sub>3</sub> taken with a scanning electron microscope (SS-550, Shimadzu, Japan).

Table 2. Components of coating formulations.

<b>Component</b>	<b>Function</b>	<b>Source</b>
Hypromellose (HPMC) <sup>†</sup>	Film former	Methocel E3 Premium LV EP, DOW Chemical, US
Polyvinyl pyrrolidone (PVP)	Co-film former	Plasdone C-15, ISP Technologies, USA
Iron oxide red pigment (RP)	Colorant	Sicopharm Red 30, BASF Corporation, Germany
Chlorpheniramine maleate (CM)	Drug	Chlorpheniramine maleate BP, Merck, USA
Ethylcellulose (EC) coating dispersion	Sustained release coat	Surelease, Colorcon, USA
Calcium carbonate nanoparticles (nano-CaCO <sub>3</sub> ) <sup>*</sup>	Anti-tack agent	CC-1, Nanomaterials Technology, Singapore

<sup>†</sup> HPMC had a apparent viscosity of 3 cP and molecular weight of about 20 kDa (Keary, 2001).

<sup>\*</sup> Nano-CaCO<sub>3</sub> had a mean diameter of  $99.4 \pm 22.8$  nm as determined from measuring the diameter of 50 particles randomly picked out from Fig. 7. It had a true density of  $2.66 \pm 0.003$  g cm<sup>-3</sup>.

## **B Method**

### **B.1 Coating**

#### **B.1.1 Preparation of coating materials**

Hypromellose solutions were prepared using a magnetic stirrer to disperse the HPMC powder in a beaker of hot water at 80 °C for 5 min, followed by adding ice cold water to the dispersion. The amount of hot and cold water used was each approximately 40 % of the total amount of the coating material to be prepared. The mixture was stirred for 10 min and allowed to hydrate overnight in the refrigerator at about 5 °C. The next day, PVP, RP, CM and nano-CaCO<sub>3</sub> were added to the HPMC solution and additional water was added to make up to volume. Preparations with RP were homogenized for 5 minutes prior to coating. EC coating material was prepared according to the manufacturer's instruction by diluting the Surelease from 25 % w/w solids to 15 % w/w solids with water prior to use.

Nano-CaCO<sub>3</sub> was supplied as a paste of nano-CaCO<sub>3</sub> in water. Immediately before every use, the percentage solids in the paste was determined using a moisture balance (EB 330 MOC, Shimadzu, Japan) which gave the weight of solids left after evaporation to dryness. To prepare the coating formulations, water was added to an accurately weighed amount of paste to give a 10 % w/w suspension. The paste was dispersed in water by first stirring with a glass rod and then by agitation in an ultrasonic bath for 10 min. The appropriate weight of this concentrated suspension was added to HPMC solution or water to prepare nano-CaCO<sub>3</sub> HPMC suspensions or neat nano-CaCO<sub>3</sub> suspensions respectively.

### **B.1.2 Equipment for coating**

Precision coating was carried out using the Precision coater (PC: Precision coater, GEA Aeromatic-Fielder, UK) and Wurster coating was carried out using the Wurster coater (AC: Aerocoater, GEA Aeromatic-Fielder, UK) (Fig. 8). The coaters were fitted using the same air handling system (MP-1 Multi-processor, GEA Aeromatic-Fielder, UK), partition column and conical acrylic coating chamber. Each coater was equipped with a two-fluid spray nozzle which had similar nozzle tip diameter (1 mm), air cap opening diameter (2.5 mm) and nozzle tip protrusion (1 mm from the flushed position).

### **B.1.3 Standard procedure for coating**

The coating system was pre-heated at an inlet air temperature ( $T_p$ ) of 70 °C and airflow rate (AF) of 80 m<sup>3</sup>/h for 30 min prior to coating. At the start of each run, substrates were loaded into the coating chamber and fluidized at a low airflow rate of 20 m<sup>3</sup>/h and inlet air temperature of the respective run until a product temperature of 45 °C was reached. The appropriate AF and atomizing pressure (AP) were then activated and the coating material was fed to the spray nozzle using a peristaltic pump (504U, Watson-Marlow, UK).

Throughout the run, the beaker of coating material was agitated using a magnetic stirrer (SP46920, Barnstead/Thermolyne, USA), while the weight of the coating material sprayed was monitored using a weighing balance (Libror EB3200H, Shimadzu, Japan). At least 2 coating runs were done for each condition.

Coated products were dried in the oven at 60 °C (with the exception of ethylcellulose-coated pellets at 35 °C) for 12 h. After being cooled to room temperature, products were stored in sealed plastic bags and used for further tests.



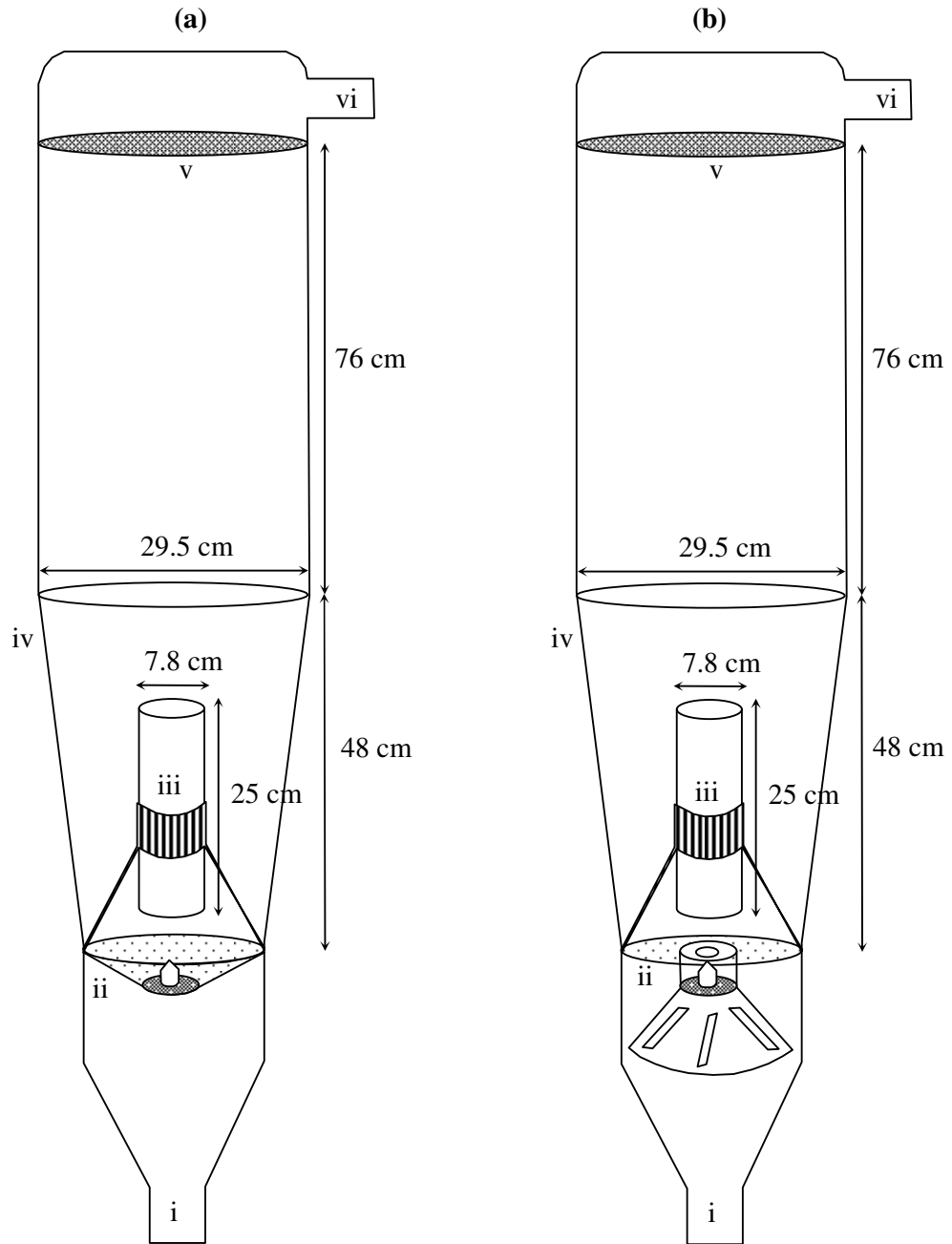


Fig. 8. Dimensions of the coating chamber of the (a) Wurster coater and the (b) Precision coater with the associated parts, (i) plenum, (ii) air distribution plate, (iii) partition column, (iv) expansion chamber, (v) retaining filter and (vi) exhaust pipe (not drawn to scale).

#### **B.1.4 Conditions used for pellet coating**

Conditions used for pellet coating are described in Table 3. Pellets were base-coated before being used in all the studies. This was done to reduce the friability of the pellets and to prevent infiltration of coating materials into the core.

Conditions for agglomerative coating were chosen to deliberately encourage agglomeration. As partition gap (PG) may affect the outcome of coating, agglomerative coating was carried out over a range of partition gaps in both coaters.

Colour coating was carried out at a lower spray rate than agglomerative coating to avoid agglomeration. Approximately 2 g of colour-coated pellets were sampled at 0.4, 0.8, 1.2, 1.6 and 2.0 % w/w coating levels. The weight of pellets sampled was considered negligible as the pellet load of 1000 g was relatively much larger.

Pellets used for ethylcellulose coating were first base-coated with a highly water-soluble drug (chlorpheniramine maleate) which was used as an indicator to evaluate the sustained release properties of the ethylcellulose coats produced by both coaters. A low coating level of 2 % w/w ethylcellulose was used to form thin coats which would allow better differentiation of coat quality.

### **B.2 Evaluation of process characteristics**

#### **B.2.1 Determination of mass flow rate**

Several methods have been used to quantify and describe the fluid dynamics of particles in air suspension processes, including positron emission particle tracking (Fitzpatrick *et al.*, 2003; Stein *et al.*, 2000; Parker *et al.*, 1997), radioactive particle tracing (Cassanello *et al.*, 1999), magnetic particle tracing (Shelukar *et al.*, 2000; Xu and Turton, 1997) and optical fiber probe techniques (Jose *et al.*, 1998).

Table 3. Conditions used for pellet coating.

Process parameters	Coating Method				
	Base coating	Agglomerative coating	Colour coating	Base coating with drug	Ethylcellulose coating
Coater	AC	AC and PC	AC and PC	PC	AC and PC
Coating formula*	HPMC 5% PVP 1%	HPMC 5% PVP 1%	HPMC 5% PVP 1% RP 0.67%	HPMC 5% PVP 1% CM 2%	EC 15%
Load (kg)	3	1	1	3	1
AF (m <sup>3</sup> /h)	100	80	80	100	100
AP (bar)	2	1.5	1.5	2	2
Tp (°C)	70	70	70	70	65
PG (mm)	18	14, 18, 22	18	18	18
Spray rate (g/min)	14	14	10	14	14
Coating level (% w/w) <sup>†</sup>	2	6	2	8	2

\* The amount of constituent used is expressed as a percentage of the total weight of coating material prepared.

<sup>†</sup> Coating level was defined as the theoretical increase in dry weight of samples after coating as a percentage of the initial weight of the samples before coating.

Due to high cost and technological complexity of the reported methods, a simpler yet effective method was devised by using a pellet collection system to determine the pellet mass flow rate (MFR) in order to describe the fluid dynamics of particles in air suspension coaters.

There were certain limitations associated with this method, mainly being a subjective assessment of the end-point and the use of non-steady state measurements. However, errors associated with these limitations were minimized as all the experiments were carried out systematically using the same air handling system, and upon start of equipment, it was quick to reach steady state conditions, within a few seconds. Overall, this improvised method was potentially useful for the characterization of particle fluid dynamics in the coaters.

The pellets were placed in the coating chamber and leveled using a spatula. The pellet collector consisted of fine netting (mesh size of 180  $\mu\text{m}$ ) held by a metal frame and was fitted above the pellet bed between the partition column and internal wall of the chamber (Fig. 9a(i) and 9b(i)). During each run, the airflow and atomizing air were activated simultaneously, transporting the pellets from the product bed to the pellet collector. The pellet collector served to collect the pellets, preventing further cycling of the pellets (Fig. 9a(ii) and 9b(ii)). The time (t) taken for a certain pellet load (M) to flow into the pellet collector was used to calculate the mass flow rate (MFR):

$$\text{MFR} = \frac{M}{t} \qquad \text{Equation 1}$$

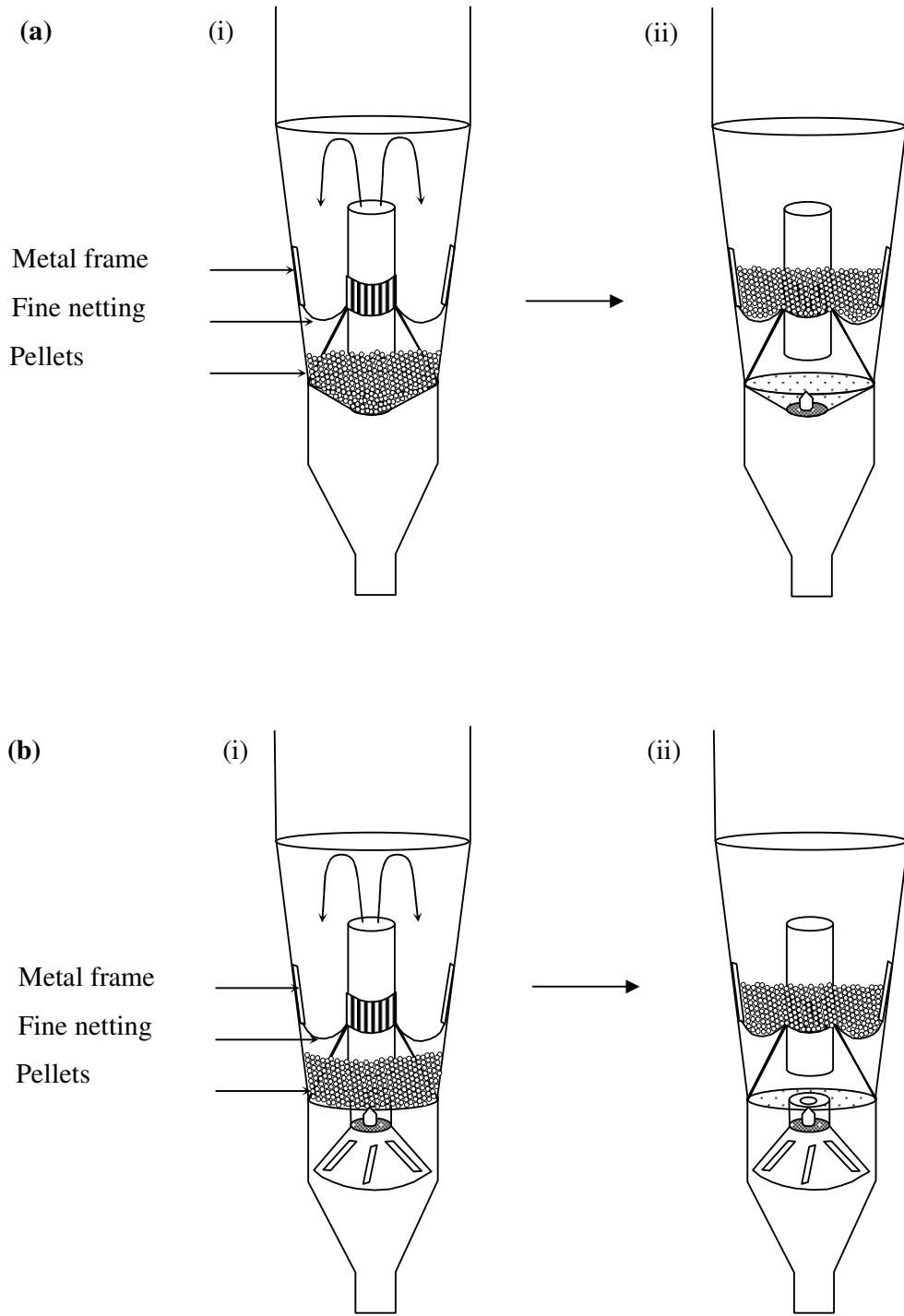


Fig. 9. Schematic diagram of pellet flow in one cycle using the pellet collector in the (a) Wurster coater and (b) Precision coater.

### **B.2.2 Determination of pellet velocity**

The partition column is the region where pellets are coated as they move through the spray zone. Images of pellets moving within the partition column were captured by a high speed camera (Motionpro HS-4, Redlake, USA). This was carried out by using transparent acrylic partition column and coating chamber, which enabled photography from outside of the coater. In order to obtain sharp images, the acrylic partition column was cleaned before each run and images were captured without spraying the coating material to avoid blurring of the images from material deposition on the partition column. Pellet velocities (PV) were determined by tracking the speeds of 30 randomly chosen pellets using slow speed playback video mode. Most of the pellets were observed to be moving up the partition column, while few were falling downwards. Only pellets that were moving upwards were tracked.

### **B.2.3 Determination of air velocity**

Air velocities within the partition column in Precision coating were measured using a digital micromanometer (8705 DP-CALC, TSI, US). The L-shaped probe was inserted into the coating chamber through an opening whereby a rubber stopper held the probe in place and sealed the opening. The probe was placed with the tip positioned vertically in the direction of airflow with the tip positioned in the center of the partition column or at the periphery of the partition column (30 mm from the center point).

The reading on the digital display was reset to zero before the initiation of each run. After starting each run, the conditions were allowed to stabilize at for at least 1 min before taking the air velocity reading. Three readings were obtained for each condition and the values averaged.

#### **B.2.4 Determination of process conditions**

During pellet coating, process conditions including inlet air relative humidity, inlet air temperature, outlet air temperature and outlet air relative humidity were continuously recorded. The positions whereby the process parameters were measured are shown in Figure 10.

The relative humidity was measured using humidity transmitter (I-1000, Rotronic Instruments, UK) and temperature was measured using dry bulb temperature element (PT-100, Testtemp, UK). Measurements were taken every 10 s with a data acquisition system (Orchestrator Ver. 2.5.0.0., Measuresoft Development, Ireland) linked to the MP-1. Baseline inlet and outlet conditions were monitored before the start of coating. Inlet ambient air was maintained at about 50 % RH and 25 °C.

#### **B.2.5 Determination of drying efficiency**

The drying efficiency (DE) was defined as the ability of the incoming air to remove the moisture introduced into the system. A DE of 100 % would indicate that the outlet air carried all the moisture from the inlet air as well as from the liquid spray material. Hence, DE may be calculated from the following equation,

$$DE(\%) = \frac{m_g X_o}{m_g X_i + m_l} \times 100 \quad \text{Equation 2}$$

where  $m_g$  is the airflow rate (kg/h),  $m_l$  is the liquid flow rate (kg/h),  $X_i$  is the inlet air absolute humidity (kg/kg dry air) and  $X_o$  is the outlet air absolute humidity (kg/kg dry air). The process conditions used for analysis were taken from 20 min to 60 min after the start of the run, whereby the conditions had stabilized. The absolute humidity was determined from the psychrometric chart of water-air system at 1 atmospheric pressure using dry bulb temperature and relative humidity (Shallcross, 1997).

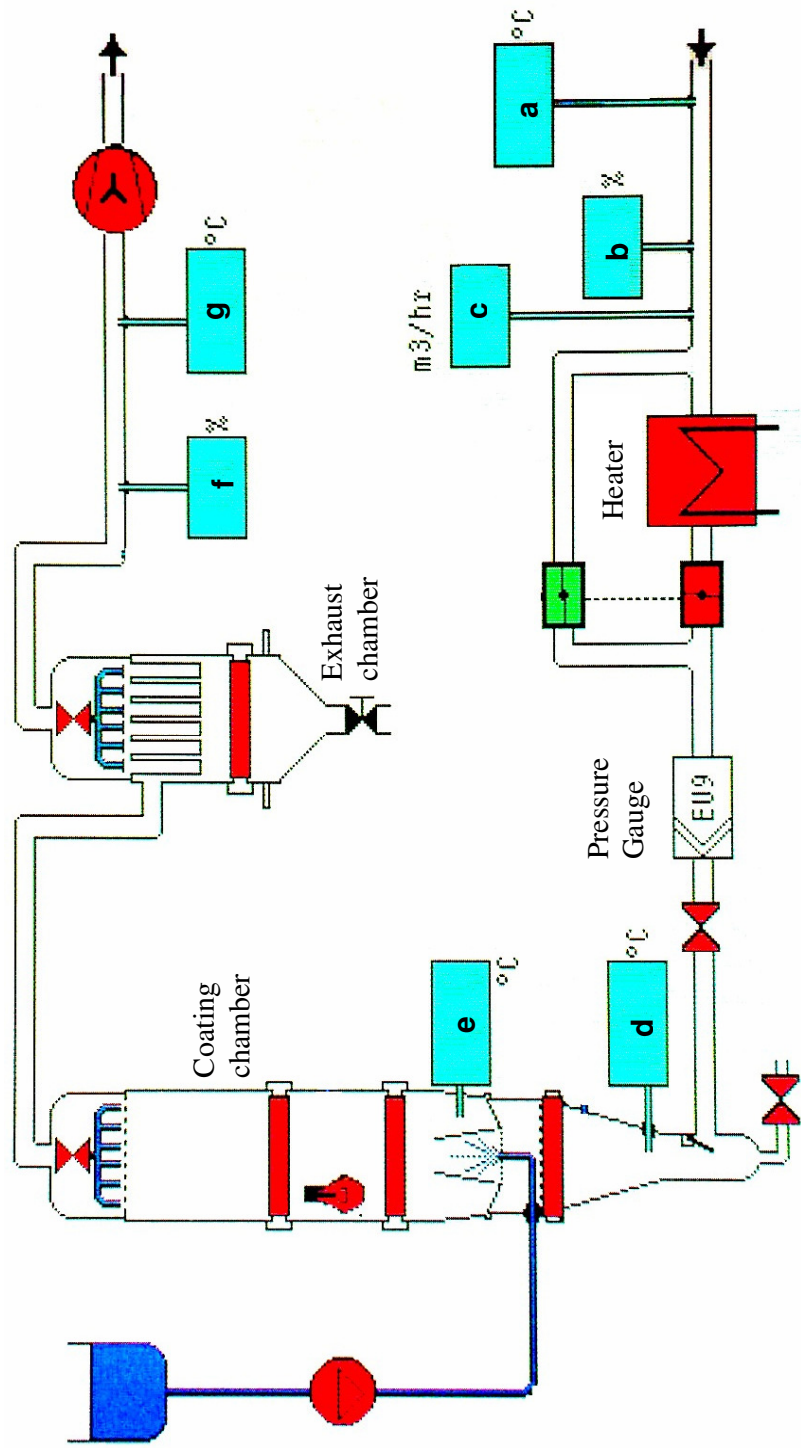


Fig. 10. Diagram of the MP-1 air handling system showing the locations at which the following process parameters were measured: (a) ambient temperature, (b) ambient humidity, (c) airflow rate, (d) inlet air temperature, (e) product temperature, (f) outlet humidity and (g) outlet temperature. (Arrows show the direction of airflow).



### **B.3 Evaluation of product characteristics**

#### **B.3.1 Characterization of pellets**

##### **B.3.1.1 Determination of flow properties**

Angle of repose, angle of fall and angle of difference of the coated pellets were determined using a powder tester (PT-N, Hosokawa, Japan). Only unagglomerated pellets were used for this test. Pellets were fed through a funnel onto a fixed circular base, forming a cone. The cone was caused to collapse by dropping a weight off a fixed distance three times. An angle pointer was used to determine the angles of inclination of the initial cone (angle of repose) and collapsed cone (angle of fall). The angle of difference was derived from the difference between the angle of inclination of the initial cone and collapsed cone. Five replicated measurements were obtained for each sample and results averaged.

##### **B.3.1.2 Determination of pellet shape**

Images of 30 randomly chosen pellets of each size fraction were obtained using a stereomicroscope (SZH, Olympus, Japan) linked to an image analysis program (Microimage, Olympus, Japan). Sphericity was determined from the area (A) and perimeter (P) of the images using Equation 3,

$$\text{Sphericity} = \frac{4\pi A}{P^2} \quad \text{Equation 3}$$

Sphericity values range from 0 to 1, whereby perfectly spherical pellets have a sphericity value of 1 and shapes that deviate from that of a sphere have lower sphericity values.

### **B.3.1.3 Determination of degree of agglomeration**

After coating, the pellets were weighed and passed through sieves of aperture sizes 355 and 500  $\mu\text{m}$  for the pellets of size fraction 355 to 425  $\mu\text{m}$ , and 500 and 710  $\mu\text{m}$  for pellets of size fraction 500 to 600  $\mu\text{m}$ . Agglomerated pellets were retained by the larger aperture size sieve, while fines passed through the smaller aperture size sieve. Fines were removed from the products after coating. The remaining pellets were weighed to determine the total weight of coated pellets ( $W_C$ ). The degree of agglomeration (Agg) was the percent by weight of agglomerated pellets ( $W_A$ ) to  $W_C$ :

$$\text{Agg}(\%) = \frac{W_A}{W_C} \times 100 \quad \text{Equation 4}$$

### **B.3.1.4 Determination of yield**

The yield (Yd) was the final weight of coated pellets ( $W_C$ ) as a percentage of the theoretical final weight ( $W_T$ ). The theoretical final weight of the pellets was the sum of the weight of pellet load and the solid content of the coating material applied.

$$\text{Yd}(\%) = \frac{W_C}{W_T} \times 100 \quad \text{Equation 5}$$

### **B.3.1.5 Determination of surface roughness and morphology**

Pellet surface roughness was determined using a scanning probe microscope (SPM-9500J, Shimadzu, Japan). The SPM uses a cantilever with a sharp tip (probe) at its end to scan the sample surface. When the probe is brought into proximity of the sample surface, forces between the tip and the sample lead to a deflection of the cantilever. The deflection is measured using a laser spot reflected from the top of the cantilever into an array of photodiodes and a 3D image is generated.

The pellets were mounted onto a double-side adhesive tape on the sample holder. The probe was scanned over an area of  $25\ \mu\text{m} \times 25\ \mu\text{m}$  on the apex of each pellet using the dynamic mode at a scan rate of 1 Hz. The degree of surface roughness was expressed by the arithmetic mean roughness (Ra) where a higher value indicates greater surface roughness. Eight unagglomerated pellets were randomly selected from each batch and analyzed. No sample pretreatment was required.

#### **B.3.1.6 Determination of surface morphology**

Unagglomerated pellets were mounted on an aluminium stud using carbon paint. Samples were pretreated by gold sputtering (JFC-1100, Jeol, Japan) prior to examination under a scanning electron microscope (JSM-5200, Jeol, Japan).

#### **B.3.1.7 Determination of colour and colour uniformity**

For colour-coated pellets, the tristimulus colorimeter (Chroma Meter CR-241, Minolta, Japan) was used to determine the colour over a 0.3 mm diameter circular spot on the apex of each pellet. The light source, standard illuminant D65, consisted of average daylight including ultraviolet wavelength region. Colour measurements were taken in *Lab* colour space, also referred to as CIELab units, which was defined by CIE (Commission internationale de l'éclairage) in 1976 and described by Chan *et al.* (2001). *L* indicates lightness and *a* and *b* indicate colour directions, where *+a* is the red direction, *-a* is the green direction, *+b* is the yellow direction and *-b* is the blue direction.

Colour measurements were made for 30 randomly chosen pellets for each batch. The colour difference ( $\delta E$ ) of each spot with respect to the initial colour of the pellets before colour coating was defined by Equation 6,

$$\delta E = \sqrt{(L_c - L_w)^2 + (a_c - a_w)^2 + (b_c - b_w)^2} \quad \text{Equation 6}$$

where the subscript “c” refers to the coloured sample and “w” refers to the white base-coated pellets. The colour variation between pellets was indicated by the relative standard deviation of  $\delta E$  (RSD of  $\delta E$ ), in which the higher the value, the greater the colour variation.  $\delta E$  of the coloured pellets produced from each coating condition was represented by the summation of mean  $\delta E$  for 0.4, 0.8, 1.2, 1.6 and 2 % w/w coating levels. RSD of  $\delta E$  of the same pellets were determined for each coating level and averaged to give the average RSD of  $\delta E$  for each coating condition (Heng *et al.*, 1999).

#### **B.3.1.8 Determination of drug release profile**

Drug release profiles of pellets coated with drug (CM) and EC coats were obtained using the USP paddle method. A dissolution tester (72-RL, Hanson Research, USA) with dissolution vessels containing 900 ml of deaerated distilled water maintained at  $37 \pm 1$  °C and stirred with a paddle at 100 rpm was used.

Pellets of about 5 g containing approximately 100 mg of drug were accurately weighed and used for each dissolution run. At preselected intervals, 4 ml samples were collected using an automated sampler (Dissoette 27-6A, Hanson Research, USA). Liquid removed by sampling was not replaced and this loss in volume of the dissolution medium was taken into consideration during calculation. The amount of drug was determined spectrophotometrically at 262 nm with reference to the Beer’s plot of the standard drug solutions. Triplicates were carried out for each batch of coated pellets.

## **B.3.2 Characterization of lactose particles**

### **B.3.2.1 Determination of particle size**

Size of lactose particles was determined using the dry powder module of a laser diffraction particle size analyzer (LS230, Beckman Coulter, US). Three measurements were made for each lactose batch and the values averaged. Particle size distribution was described by the  $D_{10}$ ,  $D_{50}$  and  $D_{90}$ , which were the size of the particles at the 10, 50 and 90 percentiles of the cumulative percent undersize plot respectively. The size distribution of the particles, span, was calculated using the following equation:

$$\text{Span} = \frac{D_{90} - D_{10}}{D_{50}} \quad \text{Equation 7}$$

### **B.3.2.2 Determination of true density**

The true density of lactose was obtained using a helium pycnometer (Pentapycnometer, Quantachrome, USA) according to the USP method. Lactose was oven dried at 80 °C for 2 hr and cooled in a desiccator prior to testing. The true density (TD) was derived by dividing the mass of lactose used with the true volume of the lactose as determined by the helium pycnometer. Three measurements were obtained for each sample and the values averaged to give the TD.

### **B.3.2.3 Determination of flow property**

Angle of repose of lactose was determined using a powder tester (PT-N, Hosokawa, Japan). The sample was fed through a funnel onto a fixed circular base to form a powder cone. The angle of repose was determined by an angle pointer positioned parallel to the inclined cone surface. For each sample, five replicated measurements were carried out using fresh cones and the angle of repose determined by the mean of the five readings obtained.

#### **B.3.2.4 Determination of particle shape**

Images of particles were obtained with a stereomicroscope (SZH, Olympus, Japan) and processed using an image analysis program (Microimage, Olympus, Japan). Particles were scattered over a slide and imaged. Only single unagglomerated particles were analyzed for sphericity and aspect ratio. Sphericity of particles was determined from the area (A) and perimeter (P) of the images obtained according to Equation 3. Aspect ratio was the ratio of major axis and the minor axis of the ellipse equivalent to the object. The values were obtained from 50 randomly selected particles.

#### **B.3.2.5 Determination of surface roughness**

Due to the small sizes of lactose particles, it was technically difficult to position the cantilever probe of the SPM onto their surfaces. Hence, the surface roughness of lactose particles was obtained using an optical profiling system (NT1100, Wyko, USA). The optical profiler splits a beam of light into two and directs it onto the sample surface. The light is reflected back to create an interference pattern, which is used to derive the image of the sample.

Particles were scattered over a slide and imaged using a 20 x objective with a 2 x filter, under VSI mode. Curvature/tilt and low pass filter were used as post-processing steps. For each particle, surface roughness measurement of a 50  $\mu\text{m}$  by 50  $\mu\text{m}$  spot was obtained. The averaged arithmetic mean height (Ra) obtained for each respective spot was used as the parameter for quantifying surface roughness. Sample pretreatment was not required. Ten particles were analyzed for each batch and the mean Ra obtained.

### **B.3.2.6 Determination of surface morphology**

Lactose particles were mounted on an aluminium stud using double-sided adhesive tape made of carbon. Samples were pretreated by gold sputtering (JFC-1100, Jeol, Japan) prior to examination under a scanning electron microscope (JSM-5200, Jeol, Japan).

### **B.3.2.7 Determination of surface coverage of lactose with nano-CaCO<sub>3</sub>**

Mathematical calculations could estimate the degree of coverage of the surfaces of the lactose particles by nano-CaCO<sub>3</sub> for different concentrations of nano-CaCO<sub>3</sub>. The calculations were based on the assumption that the surface area (SA) of a lactose particle would be approximately equal to the cross-sectional area (CSA) of all the nano-CaCO<sub>3</sub> that would form a single saturated layer around the lactose particle. To simplify the calculations, lactose particles and nano-CaCO<sub>3</sub> were approximated to be spherical in shape.

The surface area of a lactose particle could be determined from the general equation

for the SA of a sphere, 
$$SA = 4\pi r_1^2 \quad \text{Equation 8}$$

where  $r_1$  refers to the mean radius of lactose.

The CSA of nano-CaCO<sub>3</sub> may be determined from the following equation:

$$CSA = \pi r_n^2 \quad \text{Equation 9}$$

where  $r_n$  refers to the mean radius of nano-CaCO<sub>3</sub>.

From equation 8 and 9, the number of nano-CaCO<sub>3</sub> required for 100 % coverage of a

lactose particle is estimated to be  $\frac{SA}{CSA}$ .

Hence, the percentage coverage of the lactose with nano-CaCO<sub>3</sub> (% coverage) may be determined from the number of lactose particles (N<sub>lactose</sub>) and nano-CaCO<sub>3</sub> (N<sub>nano</sub>) present in the sample according to Equation 10.

$$\% \text{ coverage} = \frac{N_{\text{nano}}}{N_{\text{lactose}} \times \frac{SA}{CSA}} \times 100 \quad \text{Equation 10}$$

The percentage coverage would be greater than 100 % when the number of nano-CaCO<sub>3</sub> present exceeded that required to form a single saturated layer around the lactose particle.

The number of particles present in a specific mass of sample is the volume of the sample divided by that of an individual particle. The volume (V<sub>s</sub>) of a specific mass of sample (M<sub>s</sub>) may be calculated using its true density (TD) according to Equation 11.

$$V_s = \frac{M_s}{TD} \quad \text{Equation 11}$$

The volume (V<sub>i</sub>) of an individual particle may be calculated using Equation 12.

$$V_i = \frac{4}{3} \Pi r^3 \quad \text{Equation 12}$$

where r refers to either r<sub>l</sub> or r<sub>n</sub> for lactose particle or CaCO<sub>3</sub> nanoparticle respectively.

From Equations 11 and 12, the number of particles present in the sample is estimated

to be  $\frac{V_s}{V_i}$ .

### **B.3.3 Characterization of coating formulations**

#### **B.3.3.1 Determination of tackiness**

Tackiness of the coating material was measured using a tensile tester (E-Z Test, Shimadzu, Japan) according to the technique developed by Wan and Lai (1992). The tensile tester was fitted with a cylindrical-shaped acrylic plastic test probe with a



diameter of 4 cm and a water-jacketed base plate of 8 cm in diameter. Fresh samples were prepared immediately before measurement. 2 ml of sample was spread evenly over the base plate and the probe lowered until it laid flat on the base plate. After 10 s, the load exerted by the probe was reset to zero after which the probe was raised at a speed of 5 mm min<sup>-1</sup>. Tackiness was indicated by the tack value determined from the maximum pull force per unit area required to separate the probe from the base plate containing the coating material. A higher tack value signified greater tackiness of the coating material. The temperature of the base plate was kept at 25 °C during measurement by using a water jacket. For each coating material, tack measurement was repeated 10 times with new samples and the mean used as the tack value.

#### **B.3.3.2 Determination of viscosity**

Kinematic viscosity (KV) of the coating material was measured using a rotational viscometer with the concentric cylindrical setup (ThermoHaake RheoStress 1, HAAKE Instruments, Germany). Fresh samples were prepared immediately before measurement. During measurement, the temperature of the sample was maintained at 25 °C by a thermocontroller water jacket (ThermoHaake Circulator DC30, HAAKE Instruments, Germany) and the shear rate was increased from 50 rad s<sup>-1</sup> to 400 rad s<sup>-1</sup>. For each coating material, 3 viscosity measurements were carried out using fresh samples each time. Kinematic viscosities at the shear rate of 250 rad s<sup>-1</sup> were obtained and averaged to give the kinematic viscosity value.

#### **B.3.3.3 Determination of surface tension**

Surface tension of the coating material was measured using a torsion balance with a platinum ring (Model OS, White Electrical Instrument, UK). Fresh samples were prepared and equilibrated to room temperature of 25 °C immediately before

measurement. The platinum ring was lowered until it made contact with the surface of the coating material and raised slowly until it detached from the surface. The surface tension was determined at the point of detachment. Triplicates were carried out for each sample and the averaged result used as the mean surface tension of the sample.

#### **B.3.4 Characterization of cast films**

5 ml of coating material was placed in a Petri dish with a diameter of  $9.5 \pm 0.2$  cm. The filled Petri dish was placed on a leveled surface in an oven and dried for 24 h at 40 °C. The dried films were carefully peeled and kept in a desiccator for at least 1 week before analysis. Thickness of the cast films was measured using a digital micrometer (Mitutoyo, Tokyo, Japan). Only samples within the thickness of 40  $\mu\text{m}$  to 60  $\mu\text{m}$  were used for further analysis.

##### **B.3.4.1 Determination of FTIR spectra**

The films were cut with a sharp pen knife to form fine pieces which were easily incorporated with potassium bromide. FTIR spectra were obtained (IRPrestige-21, Shimadzu, Japan) with 200 mg potassium bromide disks containing 1 % w/w of film samples over the wavenumber of 4000 to 400  $\text{cm}^{-1}$ . Each spectrum was obtained from the average of 400 scans at a resolution of 2  $\text{cm}^{-1}$ . Three spectra were obtained for each type of cast film. One representative spectrum was used for qualitative analysis.

##### **B.3.4.2 Determination of mechanical properties**

The mechanical properties of cast film were determined using a tensile tester with a 100 N load cell (E-Z Test, Shimadzu, Japan). The films were cut into strips measuring 7 cm in length and 1 cm in width. Each strip was clamped on both ends leaving 5 cm of the film being exposed. The force detected by the load cell was reset to zero before

the top clamp was raised. Using a crosshead speed of  $10 \text{ mm min}^{-1}$ , the film was stretched vertically until it gave a clean break. The maximum stress and elasticity were obtained from the force curve using the software program. For each formulation, results for 10 film strips were obtained and averaged.

#### **B.3.4.3 Determination of surface roughness**

Surface roughness of cast films was obtained using an optical profiling system (NT1100, Veeco Instruments, USA) with 20 x objective and 2 x magnification under VSI mode. Only the top-side of the film that had not been in contact with the Petri dish during cast film formation was used for surface roughness measurements. The surface roughness of each spot,  $10 \mu\text{m}$  by  $10 \mu\text{m}$  in size, was obtained after post-processing by plane fit and low pass filter. 60 spots were analyzed for each type of film. The arithmetic mean height ( $R_a$ ) was used to evaluate surface roughness, whereby a higher value signified a rougher surface. The mean  $R_a$  of the 60 spots were used to represent the surface roughness of the film.

#### **B.3.4.4 Determination of wettability**

The ability of water to spread on the cast films was determined by the sessile drop method using the FTÅ contact angle analyzer (FTÅ200, First ten Ångstroms, USA). A strip of film was adhered onto a flat surface using double sided tape. Approximately  $8 \mu\text{l}$  of water of Milli-Q quality was dispensed by a syringe pump through a 27 gauge flat-tip needle onto the surface of the cast film. The contact angle at the three-phase contact point of the sessile drop was determined by axisymmetric drop shape analysis using the software of the contact angle analyzer. A smaller contact angle indicates better wettability of the film. The mean value of 10 contact angles was reported for each film sample.

## **B.4 Experimental designs used**

### **B.4.1 Comparison of bottom-spray air suspension coaters on pellet coating**

#### **B.4.1.1 Study of the fluid dynamics in Wurster and Precision coaters**

The fluid dynamics in both coaters were compared under standardized conditions. Pellet mass flow rate, pellet velocity, air velocity and high speed images of pellets moving up the partition column were used to describe the fluid dynamics. The experiments were conducted over a range of parameters in a controlled environment of approximately 25 °C and 50 % RH. In order to avoid the confounding factors such as changes in flow properties and weight of pellets, all experiments were conducted without liquid spray. The pellets were base-coated according to the conditions specified in Table 3 to reduce their friability.

The physical properties of the base-coated pellets are presented in Table 4. Two size fractions of pellets, 500 to 600 µm and 710 to 850 µm, were used. The smaller pellets (500 to 600 µm) had significantly poorer flow and packing properties than the larger pellets (710 to 850 µm) ( $p < 0.05$ ) albeit both had good flow properties and similar sphericities.

For the Wurster coater, three different air distribution plates were studied. These included the 2 % open area plate (Fig. 11a), 6 % open area plate (Fig. 11b) and Feidler plate (Fig. 11c). The open area was defined as the total area of perforations of the air distribution plate. The perforations, which were circular holes of 3 mm in diameter, were distributed evenly over the plates. These were used in conjunction with a Tressen mesh (Fig. 11d) to prevent the product from falling through the holes. The Feidler plate had an open area of 2 % which was made up of holes that were smaller than those of the open area plates. The holes were tapered such that the

diameter on the air-side was 1.6 mm and product-side was 0.71 mm. All three air distribution plates were funnel-shaped with similar inclination of 20 °.

For the Precision coater, the standard air distribution plate consisting of a horizontal perforated plate attached to the swirl accelerator was used (Fig. 12). The plate had a graduated open area from 2.0 % on the outside to 1.5, 1.0, 0.5 and 0 % towards the middle. The holes were tapered with a diameter of 0.8 to 1.0 mm on the airside and 0.7 mm on the product side. The accelerator insert (AI), a detachable solid cylinder with an opening in the middle, made up the central part of the air distribution plate. The diameter of the openings (AI diameter) were 20, 24, 30 and 40 mm (Fig. 13).

The ranges of parameters studied are listed in Table 5. In all the tests, MFR were determined at low and high airflow rates (AF) and atomizing pressures (AP). For ease of reference, the processing conditions are denoted as AF( $x$ )AP( $y$ ) where  $x$  represents the airflow rate (m<sup>3</sup>/h) and  $y$  represents the atomizing pressure (bar). Low airflow conditions are defined as AF(80)AP(1) and high airflow conditions as AF(120)AP(3).

Unless specified otherwise, the following conditions were employed: size of pellets in the range of 710 to 850 µm, pellet load of 700 g, Wurster coater fitted with the Feidler plate and partition gap of 18 mm, and Precision coater fitted with AI diameter of 24 mm and partition gap of 10 mm. All runs were carried out in triplicates.

Table 4. Physical properties of base-coated pellets

<b>Parameters</b>	<b>Size of pellets (<math>\mu\text{m}</math>)</b>	
	<b>500 to 600</b>	<b>710 to 850</b>
Angle of repose ( $^{\circ}$ ) *	$31.4 \pm 0.3$	$30.1 \pm 0.5$
Angle of fall ( $^{\circ}$ ) *	$23.6 \pm 1.3$	$21.1 \pm 0.8$
Angle of difference ( $^{\circ}$ ) *	$7.8 \pm 1.6$	$9.0 \pm 0.9$
Sphericity	$0.89 \pm 0.01$	$0.89 \pm 0.01$

\* 2 sample t-test shows significant difference in means ( $p < 0.05$ )



(a)



(b)



(c)



(d)

Fig.11. Photographs of the (a) 2 % open area plate, (b) 6 % open area plate, (c) Feidler plate and (d) Tressen mesh of the Wurster coater.



Fig. 12. Photograph of the air distribution plate of the Precision coater attached to the swirl accelerator, which is inverted to show the swirl vanes.

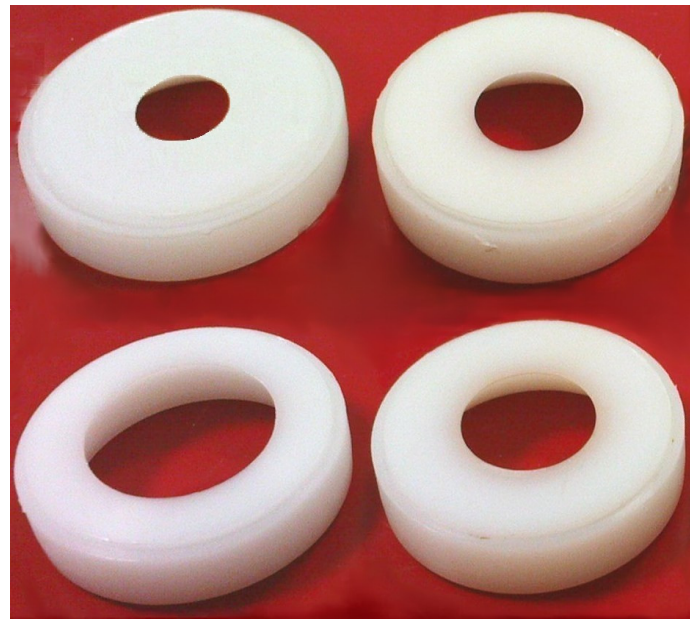


Fig. 13. Photograph of the accelerator inserts of the Precision coater with AI diameters of 20 mm, 24 mm, 30 mm and 40 mm placed in a clockwise manner from top left.



Table 5. Process parameters used for the determination of MFR in Wurster and Precision coating.

<b>Process parameter</b>	<b>Setting</b>
PG (mm)	4 to 22
AI diameter used in Precision coating (mm)	20, 24, 30, 40
Type of air distribution plate used in Wurster coating	Feidler plate (2%) Open area plate (2 %, 6 %)
AF (m <sup>3</sup> /h)	80, 90, 100, 110, 120
AP (bar)	1, 1.5, 2, 2.5, 3
Pellet size (µm)	500 to 600, 710 to 850
Pellet load (g)	500, 700, 850, 1000

#### **B.4.1.2 Study of drying efficiency and pellet movement in Wurster and Precision coaters**

Base-coated pellets of size fraction 500 to 600  $\mu\text{m}$  were used. Pellets were coated by Wurster and Precision coaters using agglomerative coating conditions (Table 3). As the PG may affect the outcome of coating, the experiment was carried out over a range of PGs (14, 18 and 22 mm) in both coaters. Three coating runs were carried out for each coating condition, unless otherwise specified. The drying efficiency, pellet velocity, degree of agglomeration and yield were determined.

#### **B.4.1.3 Study of the coated products of Wurster and Precision coaters**

Pellets of size fraction 500 to 600  $\mu\text{m}$  were used in this study. Pellets were base-coated prior to agglomerative coating, colour coating and ethylcellulose coating using both coaters (Table 3). Three coating runs were carried out for each coating condition, unless otherwise specified. Coated pellets were analyzed for degree of agglomeration, yield, flow property, surface roughness, surface morphology, colour, colour uniformity and drug release rate.

### **B.4.2 Influence of processing conditions for Precision coating**

#### **B.4.2.1 Effects of inlet air temperature and airflow rate on pellet coating**

Base-coated pellets of size fraction 500 to 600  $\mu\text{m}$  were used. Pellets were coated by Precision coating using agglomerative coating conditions at a partition gap of 18 mm (Table 3). Coating conditions studied included  $T_p$  of 60, 65, 70, 75 and 80  $^{\circ}\text{C}$  and AF of 60, 70, 80, 90 and 100  $\text{m}^3/\text{h}$ . When AF was studied,  $T_p$  of 70  $^{\circ}\text{C}$  was used. When  $T_p$  was studied, AF of 80  $\text{m}^3/\text{h}$  was used. Three coating runs were carried out for each coating condition, unless otherwise specified. Drying efficiency, degree of agglomeration and yield were determined.

#### **B.4.2.2 Effects of accelerator insert diameter on pellet coating**

Base-coated pellets of size fraction 500 to 600  $\mu\text{m}$  were used. Pellets were coated by Precision coating using agglomerative coating conditions at a partition gap of 18 mm (Table 3). The AI diameters studied were 20, 24 and 30 mm. Three coating runs were carried out for each coating condition, unless otherwise specified. Drying efficiency, degree of agglomeration, yield, pellet velocity and air velocity were determined.

#### **B.4.2.3 Effects of airflow rate and partition gap on the coated pellets**

Base-coated pellets of size fraction 500 to 600  $\mu\text{m}$  were used. Pellets were coated by Precision coating using agglomerative coating and colour coating conditions (Table 3). The coating methods were carried out at AF of 60, 70, 80, 90 and 100  $\text{m}^3/\text{h}$  and PGs of 6, 10, 14, 18 and 22 mm. When AF was studied, PG of 18 mm was used. When PG was studied, AF of 80  $\text{m}^3/\text{h}$  was used. Three coating runs were carried out for each coating condition, unless otherwise specified. Coated pellets were analyzed for degree of agglomeration, yield, colour, colour uniformity and surface roughness.

#### **B.4.2.4 Effects of airflow rate, partition gap and pellet size on pellet coating**

Base-coated pellets of size fraction 500 to 600  $\mu\text{m}$  and 355 to 425  $\mu\text{m}$  were used. Pellets were coated by Precision coating using agglomerative coating conditions (Table 3). Two  $2^2$  factorial designs were used to study the effects of pellet size and AF and the effects of pellet size and PG (Table 6). Three coating runs were carried out for each coating condition, unless otherwise specified. The drying efficiency, degree of agglomeration and yield were determined.

Table 6. Factorial designs used to study the effects of AF, PG and pellet size.

<b>Factorial design 1</b>		<b>Factorial design 2</b>	
<b>Pellet size (<math>\mu\text{m}</math>)</b>	<b>AF (<math>\text{m}^3/\text{h}</math>)</b>	<b>Pellet size (<math>\mu\text{m}</math>)</b>	<b>PG (mm)</b>
355 to 425	60	355 to 425	6
355 to 425	80	355 to 425	18
500 to 600	60	500 to 600	6
500 to 600	80	500 to 600	18

### **B.4.3 Influence of calcium carbonate nanoparticles as a surface modifying agent on Precision coating of lactose particles**

For each batch, 600 g of lactose particles were coated by Precision coating. Surface modification was carried out by coating the lactose particles with nano-CaCO<sub>3</sub> neat suspensions. The neat suspensions consisted of 30 g of water with different amounts of nano-CaCO<sub>3</sub>. Immediately after surface modification, 300 g of 10 % w/w HPMC solution was sprayed. After coating, particles were oven-dried at 60 °C for 12 h before being used for further testing. The amount of nano-CaCO<sub>3</sub> used was expressed as a percentage of the amount of lactose used and ranged from 0 to 0.5 % w/w. Coating was carried out in triplicates.

Airflow rate of 20 m<sup>3</sup>/h, T<sub>p</sub> of 70 °C, AI diameter of 24 mm, PG of 10 mm, spray rate of 4 g/min and AP of 2 bars were employed for the surface modification of lactose. The condition for surface modification was selected to minimize agglomeration of lactose particles by using a high AP and low spray rate.

Similar condition, except a higher spray rate of 10 g/min, was used for the HPMC coating. The higher spray rate, together with the viscous 10 % w/w HPMC solution, was deliberately used to induce agglomeration of the lactose particles. This would enable differences in Agg to be magnified and detected more easily.

To obtain surface modified lactose particles for analysis, lactose particles were coated with neat nano-CaCO<sub>3</sub>, omitting the HPMC coating. After coating, particles were oven-dried at 60 °C for 12 h before being used for further testing. Coating was carried out in triplicates. Properties of surface modified lactose particles determined were particle size, span, aspect ratio, sphericity, flowability, surface roughness and surface morphology. HPMC-coated lactose particles were analyzed for particle size and span.

#### **B.4.4 Influence of calcium carbonate nanoparticles as an anti-tack additive on Precision coating of lactose particles**

For each batch, 600 g of lactose particles were coated by Precision coating. Different amounts of nano-CaCO<sub>3</sub> were incorporated into 300 g of 10 % w/w HPMC coating solution and sprayed onto the lactose particles. After coating, particles were oven-dried at 60 °C for 12 h before being used for further testing. Coating was carried out in triplicates. The amount of nano-CaCO<sub>3</sub> used was expressed as a percentage of the HPMC and ranged from 0 to 10 % w/w. The condition used was AF of 20 m<sup>3</sup>/h, Tp of 70 °C, AI diameter of 24 mm, PG of 10 mm, spray rate of 10 g/min and AP of 2 bars. This condition was chosen to induce agglomeration of the lactose particles. This would enable differences in Agg to be magnified and detected more easily.

Coated particles were analyzed for size and span. Coating formulations were analyzed for tackiness, kinematic viscosity and surface tension. Cast films were analyzed for chemical interaction, surface roughness, mechanical properties and wettability.

#### **B.5 Statistical analysis**

Independent-sample t test was used to compare 2 sample sets for equality. One-way ANOVA was used to compare more than 2 sample sets with Tukey's test as the post-hoc analysis. Sample means were significantly different if  $p < 0.05$ . Minitab Release 14 statistical software was used for all the tests.

**PART IV:**

**RESULTS AND DISCUSSION**

## **IV RESULTS AND DISCUSSION**

### **A Study of conditions suitable for coating**

In order to study the coating of fine particles effectively, it was first necessary to understand the processing equipment and conditions that could affect the coating process. Unsuitable equipment setup or process conditions could lead to an unstable process which in turn result in unpredictable performance. This would make the products of fine particle coating highly variable. Hence, the coating equipment and process conditions were first studied to better understand the conditions favourable for coating fine particles. In this series of experiments, pellets were used instead of fine lactose particles as the characteristics of coated pellets could be more thoroughly assessed than those of coated fine particles.

#### **A.1 Comparison of bottom-spray air suspension coaters on pellet coating**

The traditional Wurster coater reportedly encountered many difficulties in the coating of small particulates due to weaknesses in particle transport. Hence, there was a great need for a superior coater in order to process smaller particulates more efficiently. The Precision coater, with its swirling airflow, was identified to be a solution to the problems faced with the use of the Wurster coater. To test the hypothesis that the coating performance of the Precision coater was superior to that of the Wurster coater, a comparative evaluation of both coaters was carried out. Process characteristics as well as product characteristics were compared under standardized conditions.



### **A.1.1 Study of the fluid dynamics in Wurster and Precision coaters**

The primary aim of the following set of studies was to investigate the influence of the different airflow patterns of the Wurster and Precision coaters on the fluid dynamics and the possible effects on the coated products. Fluid dynamics was found to be important in controlling product quality and productivity in bottom-spray air suspension coaters (Sudsakorn and Turton, 2000; Shelukar *et al.*, 2000). A good knowledge of the mechanisms affecting the transport of particles will enable the possible impacts on performance of coating in these processes to be assessed. Pellet mass flow rate, pellet velocity, air velocity and high speed images of pellets were used to study the fluid dynamics in Wurster and Precision coating.

The influences of coater configuration (partition gap, air distribution plates, accelerator inserts) and operating conditions (pellet load, pellet size, airflow rate, atomizing air) on the fluid dynamics of Wurster and Precision coating were evaluated.

#### **A.1.1.1 Influence of partition gap in Wurster and Precision coating**

The partition gap (PG) was defined as the vertical distance between the bottom of the partition column and the surface of the air distribution plate (Fig. 4). It was recognized as an important factor in determining the success of coating of small particles using the Wurster coater (Deasy, 1984) and was found to affect the drug release profile of coated pellets (Porter and Ghebre-Sellassie, 1994). This was attributed to its influence on the flow of pellets into the partition column and the exposure of pellets to the coating droplets in the spray zone (Fitzpatrick *et al.*, 2003; Shelukar *et al.*, 2000).

For both Wurster and Precision coaters, the MFR increased, reached a peak, and decreased with increasing PG (Fig. 14 and 15). The PG was like a doorway for the pellets. When the PG was too small, it restricted the passage of pellets, resulting in the low MFR. As the PG increased, the MFR increased because the passage of pellets was facilitated by the larger gap. However, the pressure differential across the PG also decreased. As such, the MFR reached a peak at an optimal PG, whereby the PG was small enough for the generation of sufficient pressure differential but large enough to facilitate flow of pellets through. When the PG was increased further, the decrease in pressure differential caused the MFR to decrease. Pellets failed to move up the partition column when the PG was too large.

The variation in MFR in Precision coating was significantly greater than that in Wurster coating when the PG was varied (Fig. 14 and 15). Therefore, adjustment of PG would likely affect Precision coating more than Wurster coating. As PG would affect the pressure differential across the PG, its greater influence on MFR in Precision coating indicates that the transport of pellets in Precision coating was more dependent on the pressure differential across the PG than in Wurster coating. On the other hand, pellet flow in Wurster coating was more affected by the inlet air blowing the pellets up the partition column.

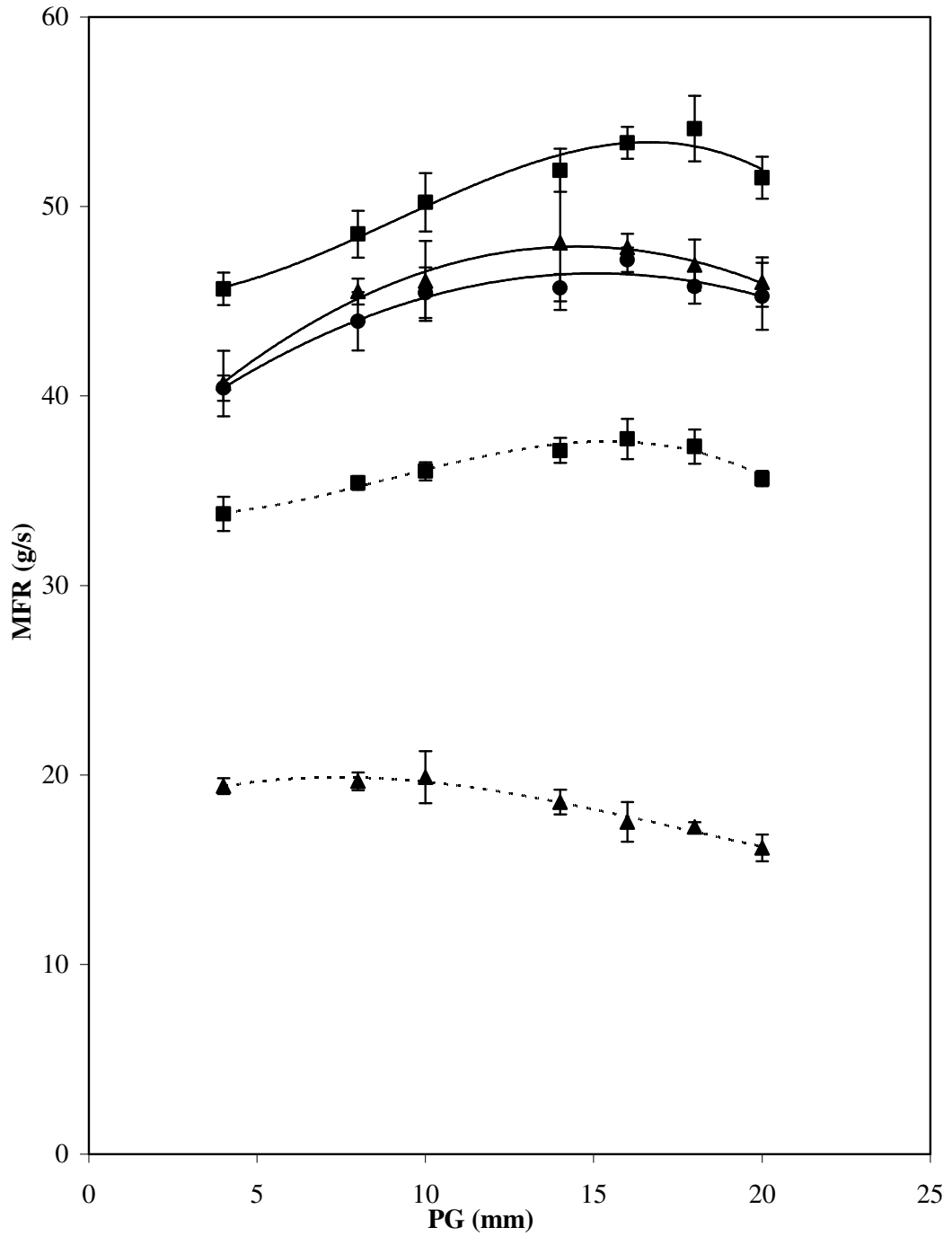


Fig. 14. Influence of PG on MFR in Wurster coating using the Feidler plate (■), 2 % open area plate (▲) and 6 % open area plate (●) at AF(80)AP(1) (represented by dotted lines) and AF(120)AP(3) (represented by solid lines).

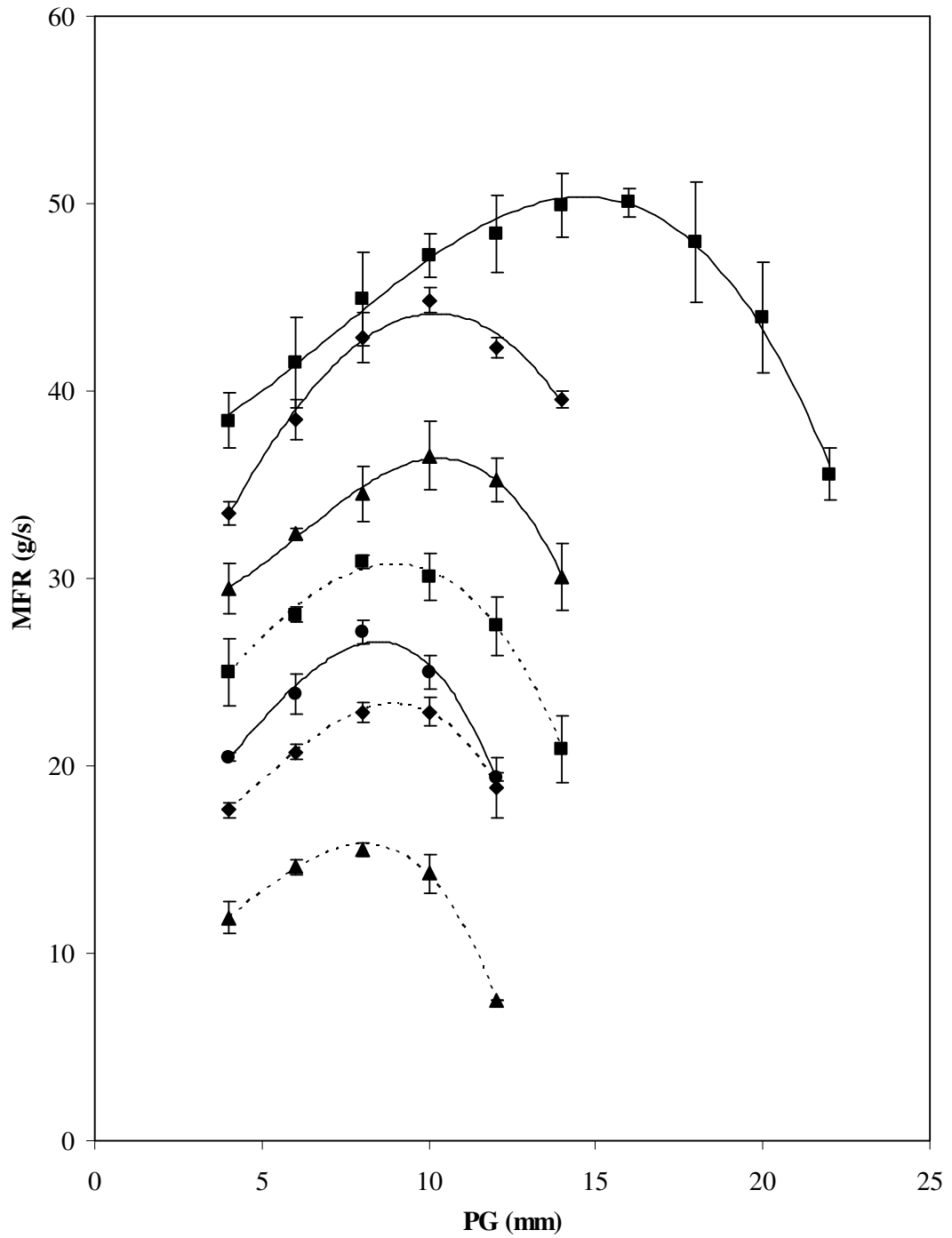


Fig. 15. Influence of PG on MFR in Precision coating using AI diameters of 20 mm (■), 24 mm (◆), 30 mm (▲) and 40 mm (●) at AF(80)AP(1) (represented by dotted lines) and AF(120)AP(3) (represented by continuous lines).

The reason for the difference in dependence of MFR on the pressure differential could be explained by the air velocities within the partition columns of Wurster and Precision coaters. In the Wurster coater, the air velocity within the partition column shows an increasing trend with increase in PG for all the air distribution plates used (Fig. 16). This could be due to the contribution of airflow from the peripheral air distribution plate into the partition column. In the Precision coater, air velocity remained similar and even decreased with the AI diameter of 20 mm when the PG was increased (Fig. 17). The increase in air velocity in the Wurster coater compensated for the decrease in pressure differential when PG was increased and this aided in the transport of pellets up the partition column, accounting for the smaller drop in MFR with the increase in PG. In the Precision coater, the air velocity within the partition column remained relatively stable with changes in PG, hence the MFR was more adversely affected by the decreased pressure differential when the PG was increased.

Pellet velocity determined from high speed photography was higher for Precision coating ( $5.3 \pm 1.1$  m/s) than for Wurster coating ( $1.5 \pm 0.2$  m/s) while the MFR in Precision coating was significantly lower than that in Wurster coating under both low and high airflow conditions (Fig. 14 and 15). This shows that MFR values did not represent mean pellet velocities but rather, the number of pellets moving up the partition column within a fixed time interval. Pellet flow through the partition column in Precision coating was scarcer than in Wurster coating. This was observed visually and also in the images obtained by high speed photography (Fig. 18).

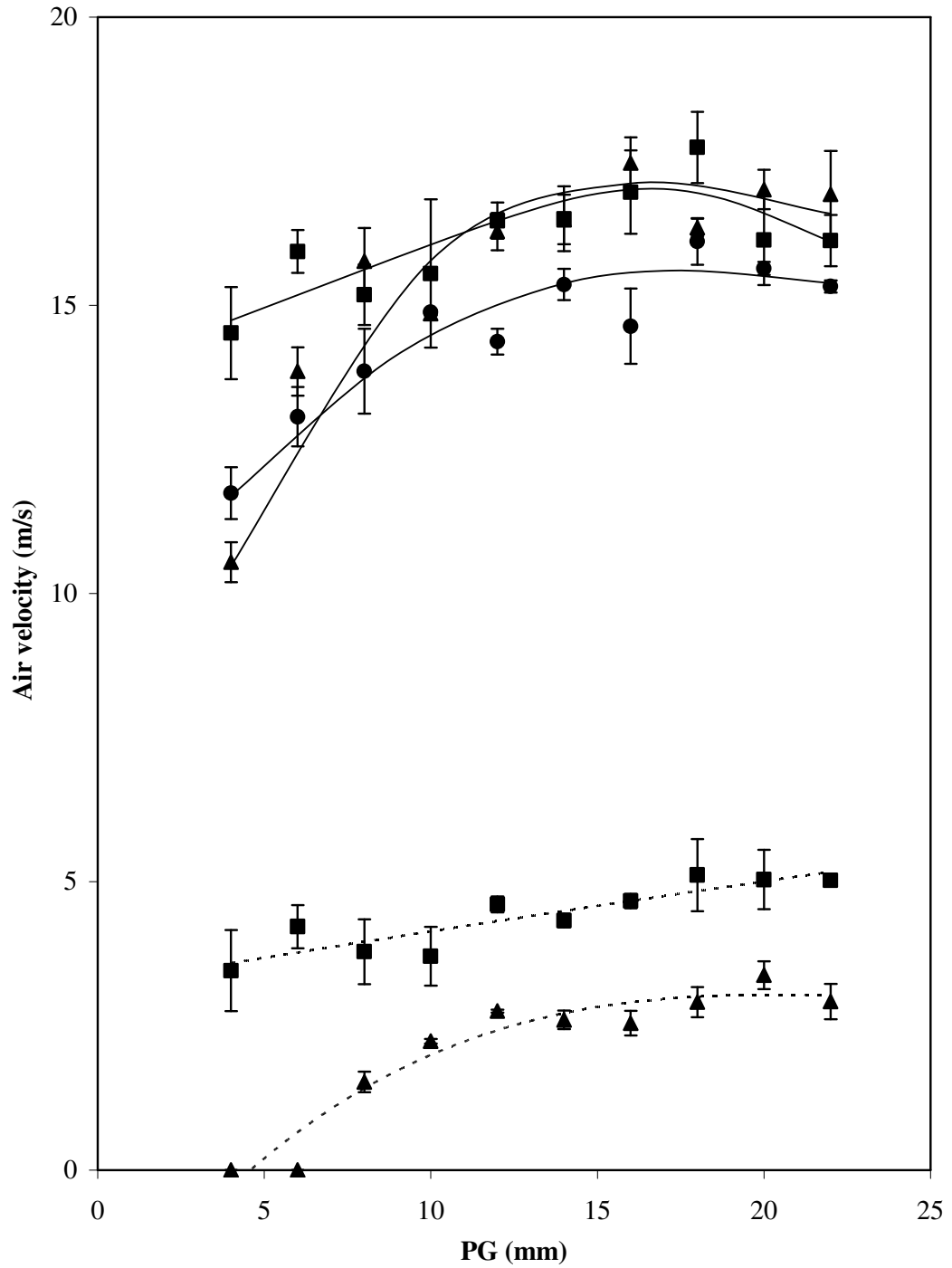


Fig. 16. Influence of PG on air velocity in Wurster coating using Feidler plate (■), 2 % open area plate (▲) and 6 % open area plate (●) at AF(80)AP(1) (represented by dotted lines) and AF(120)AP(3) (represented by solid lines).

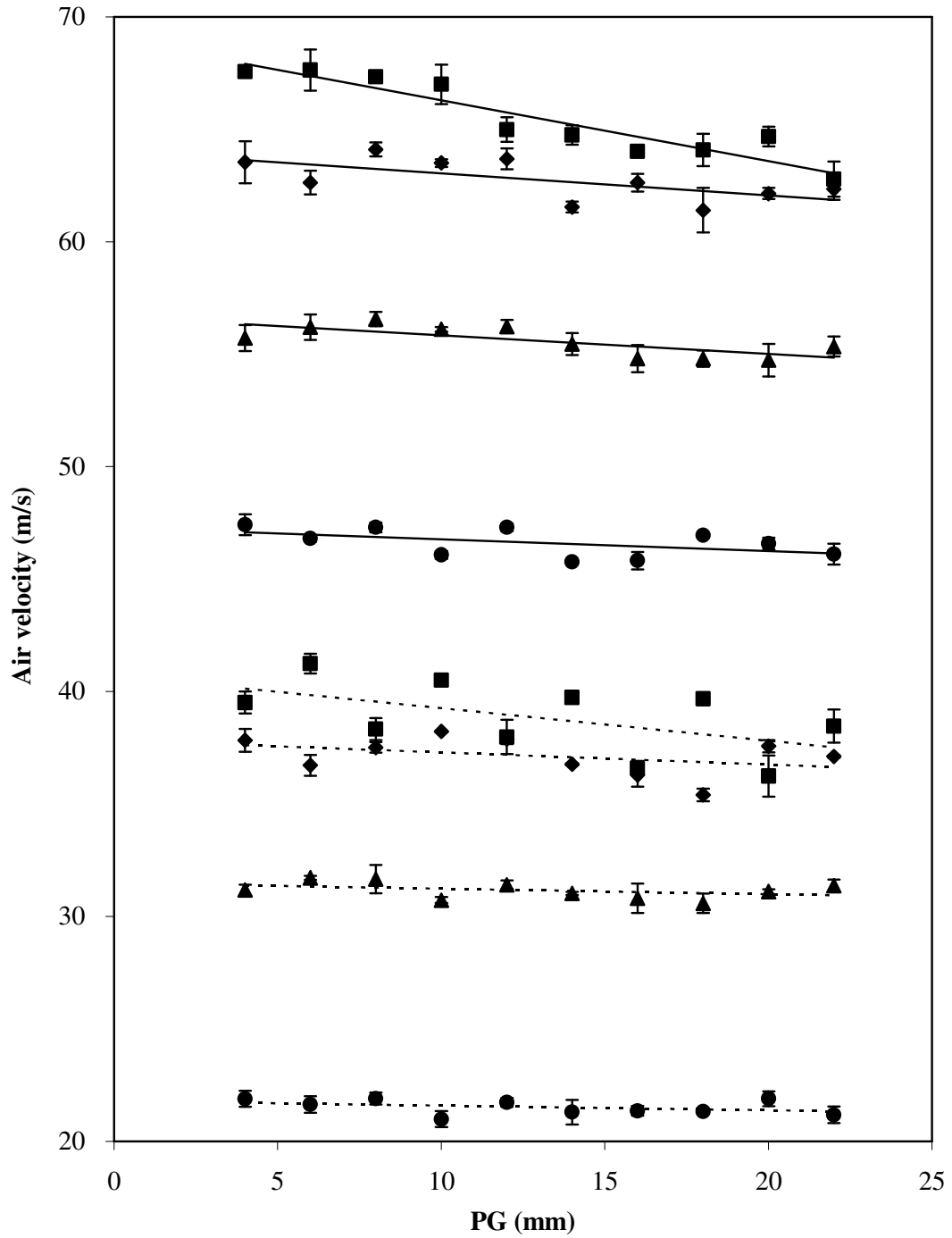


Fig. 17. Influence of PG on air velocity in Precision coating using AI diameters of 20 mm (■), 24 mm (◆), 30 mm (▲) and 40 mm (●) at AF(80)AP(1) (represented by dotted lines) and AF(120)AP(3) (represented by continuous lines).

The scarcer flow in Precision coating indicates that there was better particle separation which could lead to reduced agglomeration, but it might cause coating material to be lost to the surrounding partition column wall or spray-dried and not deposited onto the particle surfaces. This loss of spray material could however be compensated by the high air velocities. The air velocities ranged from 0 to 18 m/s in Wurster coating (Fig. 16) and 21 to 68 m/s in Precision coating (Fig. 17) for both set of airflow conditions. The higher air velocities in Precision coating would have brought about the higher pellet velocities which would compensate for the loss of spray material by increasing the passage of pellets through the spray zone.

The higher MFR in Wurster coating might be beneficial in increasing the exposure of pellets to the spray zone. On the other hand, it could increase the propensity to agglomerate during coating if the pellets were too close to one another in the partition column. Coupled with lower air velocities, the partition column would be congested with slower moving pellets, and would further increase the propensity for pellet agglomeration during coating.



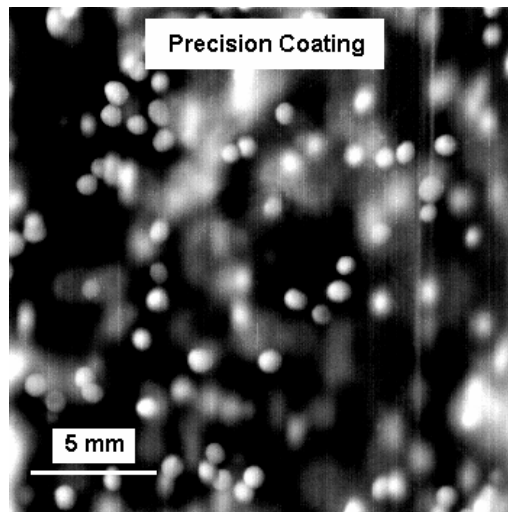
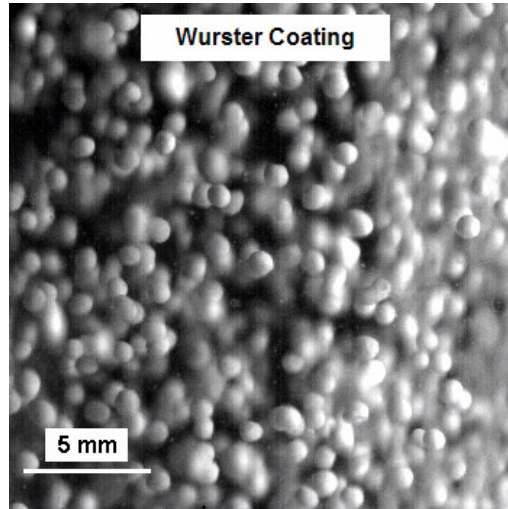


Fig. 18. High speed images of pellets moving within the partition column in Wurster coating and Precision coating over an area of 2 cm x 2 cm. (The images were taken at 2770 frames per second)

Moving from low to high airflow conditions, MFR increased in both coating processes but the aforementioned trends were still observed (Fig. 14 and 15). This shows that increasing airflow conditions increased the rate at which pellets transited through the PG without affecting the mechanisms of pellet flow. There was an increase in the optimal PG in Precision coating when the processing conditions were higher (Fig. 15), whereas there was no significant change in optimal PG in Wurster coating (Fig. 14). At AF(80)AP(1), optimal PG in Precision coating fitted with the 20 mm accelerator insert was 8 mm and increased to 16 mm at AF(120)AP(3) (Fig. 15). From the previous discussion, it could be seen that pressure differential had a greater influence in Precision coating than Wurster coating for the transport of pellets into the coating zone. Hence, it may be inferred that the optimal PG was dependent on the strength of pressure differential across the PG.

When the PG was further increased beyond the optimal point, a maximum gap was reached. Beyond this PG, the pellets failed to pass into the pellet collector. This was attributed to the lower pressure differentials generated at larger PGs. The maximum PG was generally higher in Wurster coating than in Precision coating (Fig. 14 and 15). This shows that the decrease in pressure differential had less influence on pellet transport in Wurster coating than in Precision coating. The sloping funnel-shaped air distribution plate in Wurster coating facilitated pellet flow towards the partition column and the center of the air distribution plate was perforated allowing air to push the pellets up the partition column, making transport of pellets less reliant on pressure differential. In Precision coating, the air distribution plate was horizontal and the accelerator insert was non-perforated, except for the central opening, making transport of pellets dependent on the pressure differential across the PG to draw pellets inwards and up the partition column.

#### **A.1.1.2 Influence of air distribution plates in Wurster coating**

Under high airflow conditions, the MFR obtained with the Feidler plate was significantly higher than those obtained with the 2 % and 6 % open area plates, but the latter two MFR values were not significantly different (Fig. 14). Under low airflow conditions, the Feidler and 2 % open area plates resulted in clearly different MFR. The MFR for 6 % open area plate could not be determined because of very poor pellet flow conditions. The air velocity in the partition column of the 6 % open area plate was so low that it could not be measured (Fig. 16). This indicates that the 6 % open area plate was directing too much air to the peripheral product staging bed and not adequately directing air through the partition column to create effective transport of pellets up the partition column.

There were only slight differences in the MFR obtained using 2 % and 6 % open area plates at high airflow conditions (Fig. 14) indicating that the percent open area in the periphery of the air distribution plate had little influence on the transport of pellets up the partition column. The 2% open area plate and the Fiedler plate had similar open areas but the MFR obtained with the Fiedler plate was significantly higher. The main difference between the latter 2 plates was the material used for the central part of the air distribution plate which was more perforated than the periphery of the air distribution plate. The central part of the Feidler plate consisted of a simple mesh with pore size of ~200  $\mu\text{m}$  and ~36 % perforation, whereas the central area in the open area plates consisted of an interlocking Tressen mesh, which probably imparted greater resistance to airflow and hence a lower MFR. The same Tressen mesh was used with both open area plates, thus explaining their similarities in MFR.

#### **A.1.1.3 Influence of accelerator inserts in Precision coating**

Mass flow rate obtained with the 20 mm accelerator insert was the highest, followed by the 24, 30 and 40 mm accelerator inserts (Fig. 15). MFR using the 40 mm accelerator insert could not be determined at AF(80)AP(1) because of the poor flow. This effect was also seen in a study using optical probe technique in a conical spouted bed, where the solid cycle rate and solid cross flow into the spout decreased with an increase in air inlet diameter (Jose *et al.*, 1998).

Accelerator inserts with smaller diameters for inlet air generated higher air velocities (Fig. 19). This would increase the pressure differential across the PG and impart greater acceleration to particles passing through the spray zone. However, high air velocities may cause particles to hit onto the top of the chamber causing attrition.

#### **A.1.1.4 Influence of pellet load in Wurster and Precision coating**

Linear relationships ( $R^2 > 0.99$ ) exist between MFR and pellet load in Wurster coating and Precision coating (Fig. 20). This behavior was also seen in a conical spouted bed whereby the solid flow rate increased with increasing stagnant bed height (Jose *et al.*, 1998). This was probably due to the increased pressure of the increased load in the peripheral staging bed, which pushed the pellets through the PG. This pressure is analogous to “hydrostatic pressure”. The MFR increased to a significantly greater extent in Wurster coating than in Precision coating, showing a greater influence of “hydrostatic pressure” on the transport of pellets. This indicates that Wurster coating was more dependent on the feeding of pellets to the PG for transport, a contributory factor being the sloping air distribution plate.

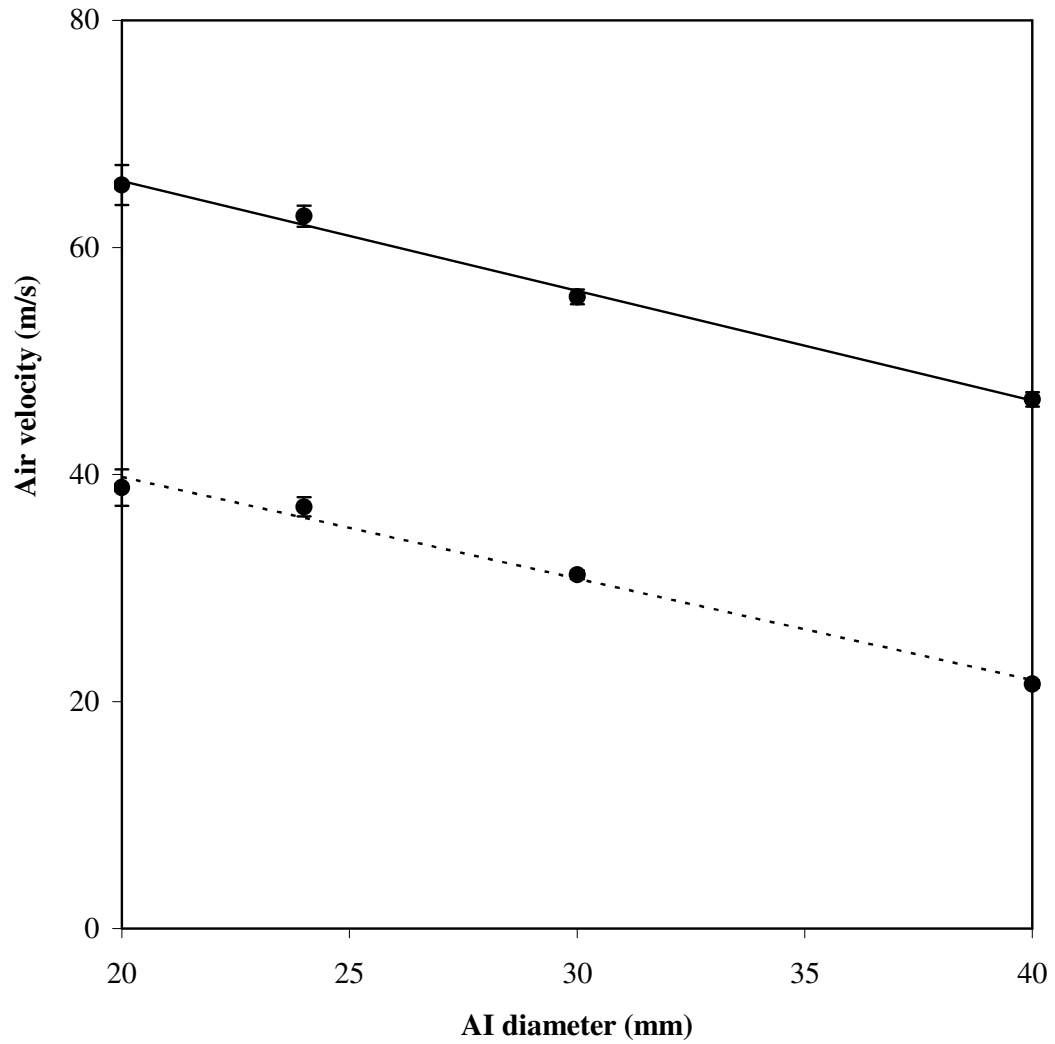


Fig. 19. Influence of AI diameter on air velocity in Precision coating at AF(80)AP(1) (represented by dotted line) and AF(120)AP(3) (represented by continuous line).

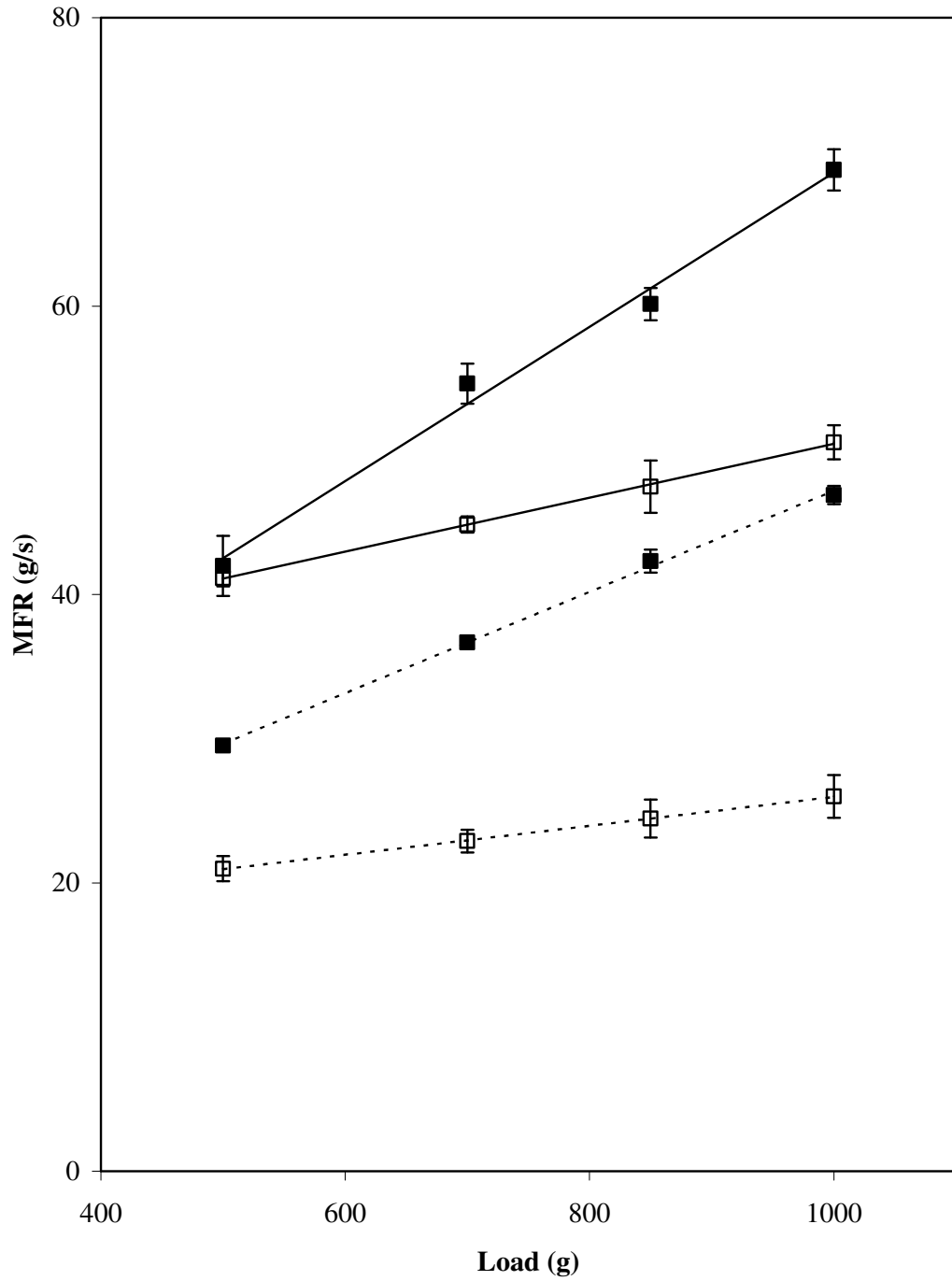


Fig. 20. Influence of pellet load on MFR in Wurster coating (■) and Precision coating (□) at AF(80)AP(1) (represented by dotted lines) and AF(120)AP(3) (represented by solid lines).

This shows that flow properties of the substrate played an important role in particle transport in Wurster coating. The minimal effect of “hydrostatic pressure” on MFR in Precision coating further substantiated its dependence on pressure differential for transportation whereby transport would be limited by pressure differential. Suction by differential pressure may offer more controlled particle movement, however, there may be greater difficulties when processing larger particles.

The effect of “hydrostatic pressure” was also seen in Fig. 21, where the effect of PG on MFR was studied using 700 and 1000 g of pellets in both coaters. Optimal PGs were similar between the corresponding loads in both coaters, suggesting that they were not affected by change in load.

#### **A.1.1.5 Influence of pellet size in Wurster and Precision coating**

In Wurster coating, larger pellets (710 to 850  $\mu\text{m}$ ) had slightly lower MFR than smaller pellets (500 to 600  $\mu\text{m}$ ) at low airflow conditions (Fig. 22). This was in agreement with the findings of Fitzpatrick *et al.* (2003), which show that larger tablets had longer cycle times than smaller tablets at the same conditions in a tabletop Wurster coater. This was also observed in a conical spouted bed using glass spheres of different sizes (Jose *et al.*, 1998). This behavior can be explained by Newton’s Second Law of Motion whereby acceleration is proportional to the force exerted and inversely proportional to the mass of the object. When higher airflow conditions were used, contrasting results were observed (Fig. 22).

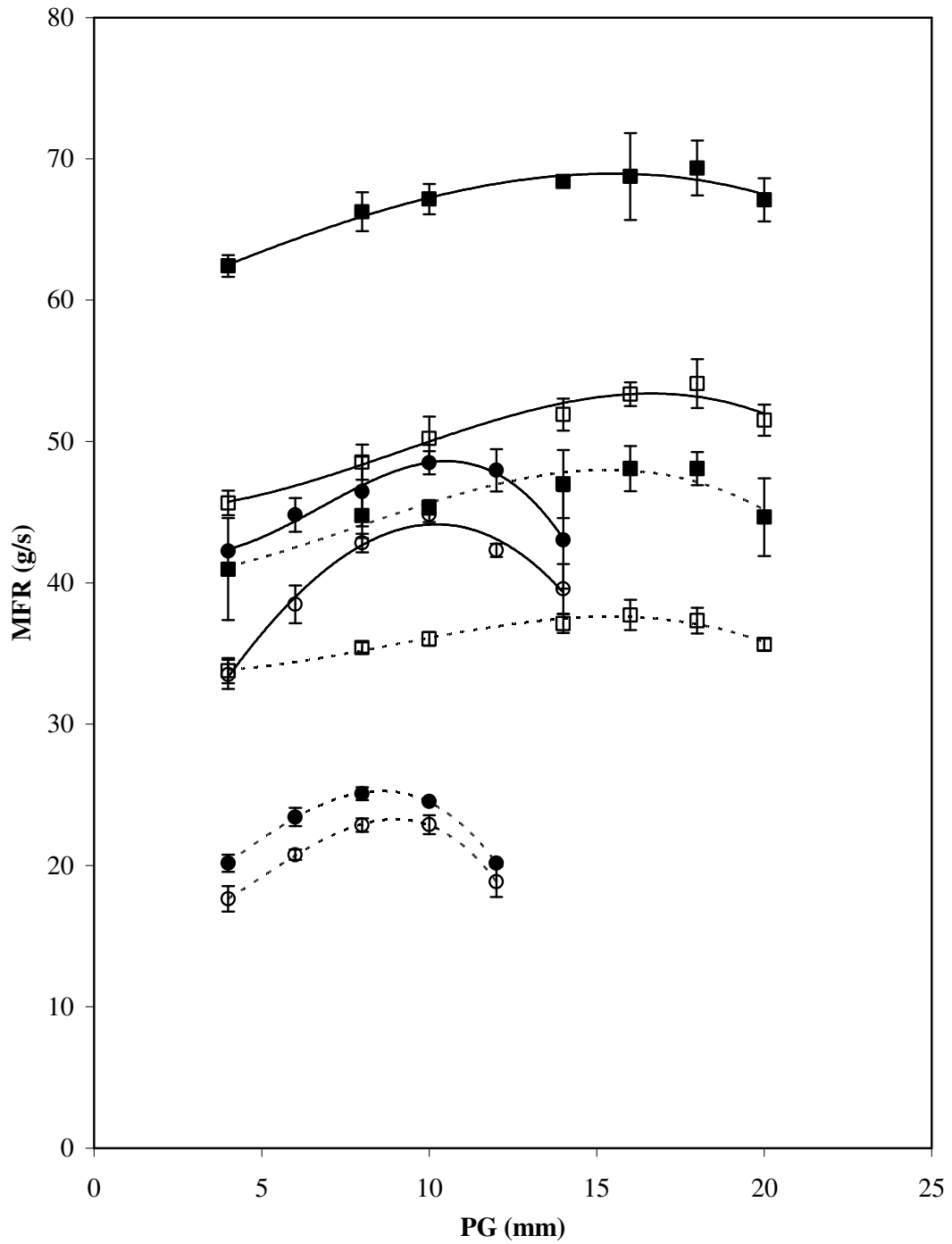


Fig. 21. Influence of PG on MFR using pellet load of 700 g (□) and 1000 g (■) in Wurster coating, and 700 g (○) and 1000 g (●) in Precision coating at AF(80)AP(1) (represented by dotted lines) and AF(120)AP(3) (represented by continuous lines).



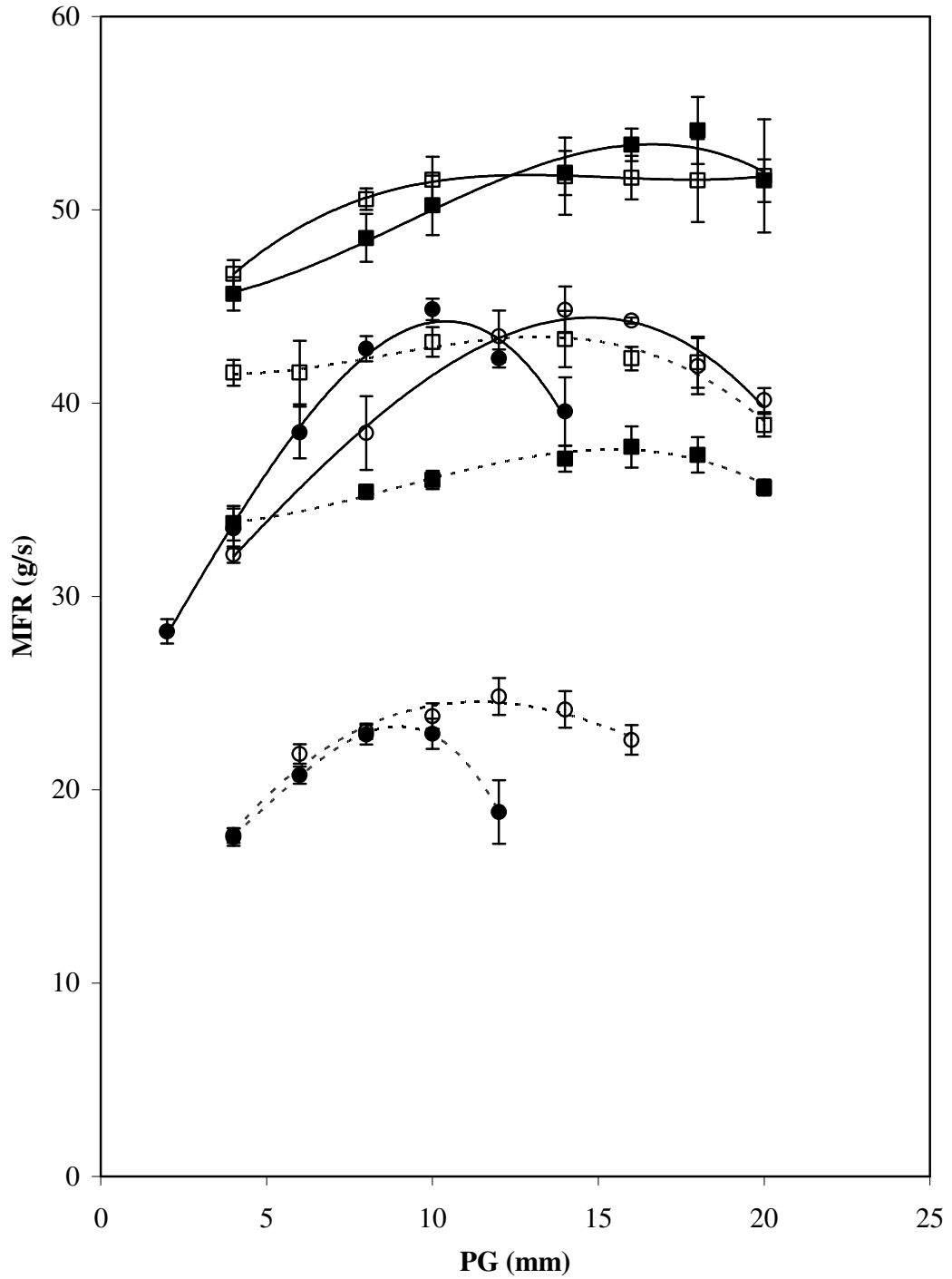


Fig. 22. Influence of PG on MFR using pellet size of 500 to 600 μm (□), 710 to 850 μm (■) in Wurster coating and 500 to 600 μm (○) and 710 to 850 μm (●) in Precision coating at AF(80)AP(1) (represented by dotted lines) and AF(120)AP(3) (represented by continuous lines).

Smaller pellets had similar MFR as bigger pellets despite the higher central acceleration as explained above. This may be due to the higher trajectories of smaller pellets at high airflow conditions, causing them to be suspended in air for a longer time before finishing a cycle. Although this may aid in drying of the particles, it may also cause the substrate bed height to decrease excessively, resulting in scarce pellet flow through the partition column and over-wetting.

Of greater significance was the “air curtain” effect created in the Wurster coater. As the increased airflow rate effected mainly airflow peripheral to the spray nozzle, there was the development of an effective air curtain effect at the peripheral region of the spray zone as the airflow rate was increased. This prevented the pellets from moving through the PG. Smaller pellets tended to be more affected by this air curtain effect and faced greater difficulties traversing from the peripheral staging area into the spray zone and partition column.

In Precision coating, MFR of both sizes of pellets were similar at both airflow conditions. Conditions governing material mass flow in Precision coating were less affected by small differences of individual particle characteristics and more dominated by mass conveyance effects contributed by the increased airflow rate. However, the optimal PG obtained with the different sizes were different (Fig. 22). The higher optimal PG of smaller pellets were probably due to the poorer flow which caused greater resistance while passing through the PG as compared to the larger pellets. In addition, the lower mass of smaller pellets would enable transport of pellets through the partition column at lower pressure differentials, hence resulting in larger optimal PG.

#### **A.1.1.6 Influence of airflow rate and atomizing pressure in Wurster and Precision coating**

Airflow rate (AF) and AP are the main forces resulting in the pneumatic transport and drying of coated particles in bottom-spray coaters. Excessively high AF and AP may result in attrition and increase spray drying effect. Therefore, AF and AP have to be appropriately adjusted to suit the particles to be coated. In this study, it was assumed that the AP in both coaters were comparable as the dimensions of the nozzle and the source of compressed air were similar.

For Wurster coating, the increases in MFR reached maxima, then leveled off at high AP of 2.0, 2.5 and 3.0 bars and could not be further increased by increasing AF beyond 100 m<sup>3</sup>/h (Fig. 23a). In the latter situation, manipulation of AF and AP would not be useful for adjusting flow of pellets during coating. For Precision coating, the MFR increased linearly with increasing AF and AP (Fig. 23b).

The trend observed with an increase in AF in Wurster coating was also observed in other studies (Fitzpatrick *et al.*, 2003; Shelukar *et al.*, 2000). Fitzpatrick *et al.* (2003) determined the cycle time of tablets in a tabletop Wurster coater using positron emission particle tracking. The results show that the mean cycle time decreased at a decreasing rate with an increase in AF. The same trend was observed by Shelukar *et al.*, 2000 using magnetic tracing technique, where the tablet cycle time was obtained during actual coating runs in a Wurster coater.

Increase in AF caused the MFR in the Wurster coater to level off notably at high AP from 2 bars onwards (Fig. 23a). This trend could be due to the effect of the funnel-shaped air distribution plate on the flow of the pellets (Fig. 8b) which was also seen in the findings of Shelukar *et al.*, 2000.

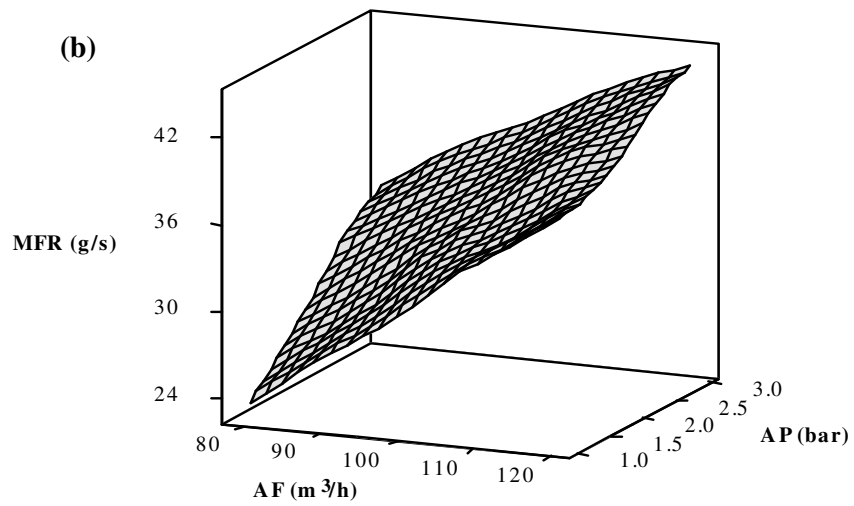
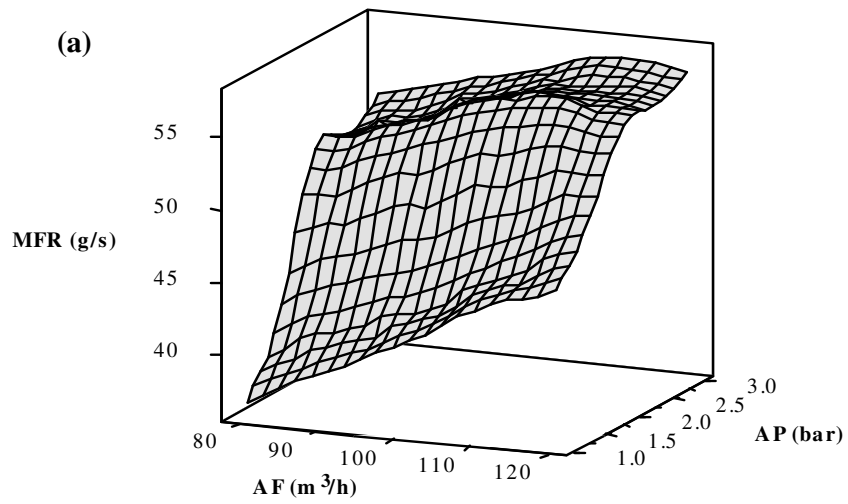


Fig. 23. Influence of AF and AP on MFR in (a) Wurster coating and (b) Precision coating.

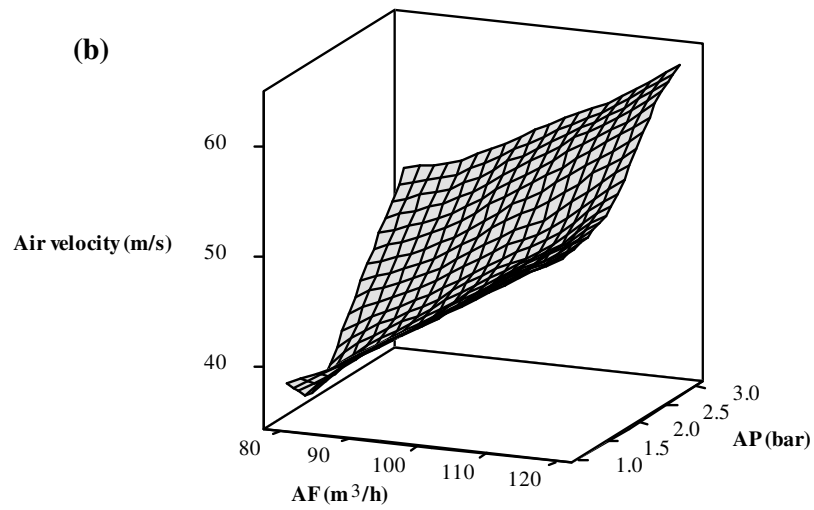
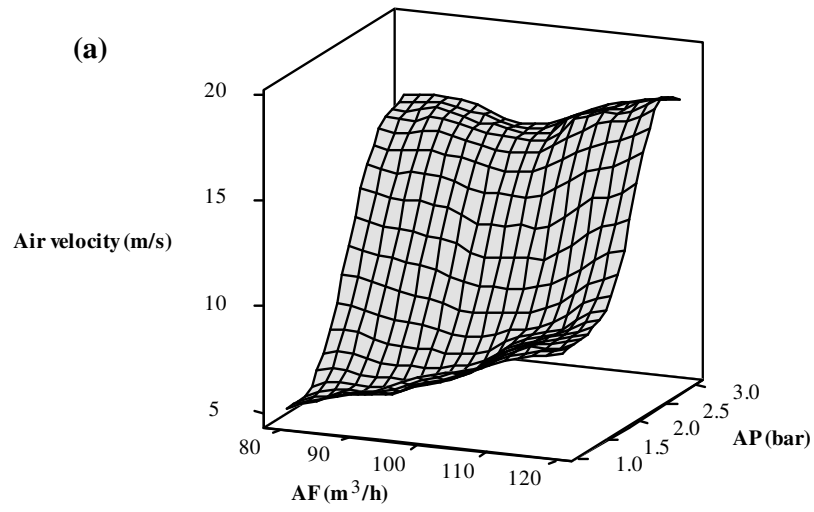


Fig. 24. Influence of AF and AP on air velocity in (a) Wurster coating and (b) Precision coating.

At low airflow conditions, the slope of the funnel-shaped air distribution plate greatly enhanced the movement of the pellets, contributing to the geometric increase in MFR. When high airflow conditions were used, although the air velocities in the partition column were found to increase (Fig. 24a), pellet flow through the PG was probably limited by the resistance of pellet flow by the counteracting “air curtain” effect.

In Precision coating, MFR was proportional to the AF and AP (Fig. 23b) and closely correlated with the air velocities obtained at the same settings (Fig. 24b). Increasing AF and AP would have caused a proportional increase in pressure differential across the partition column, and hence particle trajectories would be increased. MFR could therefore be adjusted by varying AF and AP according to the needs of a particular run. This further substantiates that pellets were drawn into the partition column primarily by pressure differential generated across the partition column.

In Wurster coating, increase in AP up to 2 bar caused the MFR to increase considerably, followed by leveling off in MFR (Fig. 23a). This leveling off was only observed in Wurster coating and not in Precision coating (Fig. 23b). The spray nozzle in Wurster coating was set higher relative to the product bed than in Precision coating. When higher AP was used, the air pressure could be so strong that it created an outward pressure to the entry of product into the partition column, limiting the flow of pellets from the product bed into the partition column. Air velocity also shows similar tapering beyond the AP of 2.5 bar, indicating that some air was directed out through the PG and not up the partition column (Fig. 24a).

From the study of fluid dynamics in Wurster and Precision coating, the pellet collector system was shown to be useful in the study of pellet movement in the two bottom-spray air suspension processes. The findings indicate that the particle

transport in Wurster coating was largely governed by the “hydrostatic pressure” of the product in the peripheral staging bed and airflow rate. In Precision coating, it was governed largely by suction pressure created by pressure differential across the PG. Pellets moving through the spray zone in Wurster coating was found to be closer and slower than those of Precision coating, suggesting that the extent of agglomeration would be much greater in Wurster coating. Thus, knowledge of fluid dynamics in both coaters enables better understanding of their possible impacts on coating.

#### **A.1.2 Study of drying efficiency and pellet movement in Wurster and Precision coaters**

From the previous study, it was strongly indicated that fluid dynamics in both Wurster and Precision coaters were different. In this section, the drying efficiency and pellet movement in both coaters were compared.

The thermodynamics describe the heat and mass balances in the coater which are important for the optimal deposition and drying of coating material sprayed onto the core particles. Hence, the thermodynamic conditions in the two processes were studied to determine the influence of drying conditions on the coated pellets. The thermodynamics of air suspension coating processes have been studied using temperature measurements (Jiménez *et al.*, 2006), moisture determination (Alden *et al.*, 1988), humidity measurements (Maronga and Wnukowski, 1997 and 1998) and enthalpies of actual and adiabatic air (Larsen *et al.*, 2003).

In this study, a new method utilizing “Equation 2” was used to determine the drying efficiency (DE) of the coating processes. This equation determined the absolute moisture content of the outlet air as a percentage of the absolute moisture fed into the coater during coating. DE was used as the parameter to determine the ability of the

coater to handle moisture fed into the system. A DE of 100 % was the maximal obtainable and indicates that all the moisture fed into the system was removed in the outlet air. Absolute moisture content was used as it represented the actual amount of moisture present in the air irrespective of the temperature. It is a better descriptor of the drying condition of the air as compared to relative humidity, which may fluctuate with the temperature. The moisture content of the inlet air included the moisture from the ambient air in addition to the moisture present in the coating formulations.

The DE and particle movement in swirling airflow of Precision coating were compared with those in non-swirling airflow of Wurster coating. While comparing both airflow patterns, the impact of the PG was also studied as it was found to influence the fluid dynamics of particles moving up the partition column in the coater. Increasing PG can result in more particles moving in from the peripheral product staging bed into the partition column but the pressure differential may be lowered, resulting in sluggish pellet movement into and up the partition column. This was observed in the earlier study of the effects of PG on MFR.

#### **A.1.2.1 Drying efficiency in Wurster and Precision coaters**

Differences of airflow pattern in the Wurster and Precision coaters affected the DE to different extents (Fig. 25a). DE in Precision coating remained high (95 % to 98 %) over the PGs studied, showing that almost all the moisture introduced into the system was removed by the drying air. This led to the low Agg of pellets obtained (Fig. 25c). However, the DE in Wurster coating decreased from 98 % to 92 % and the Agg of pellets increased with increasing PGs (Fig. 25c).



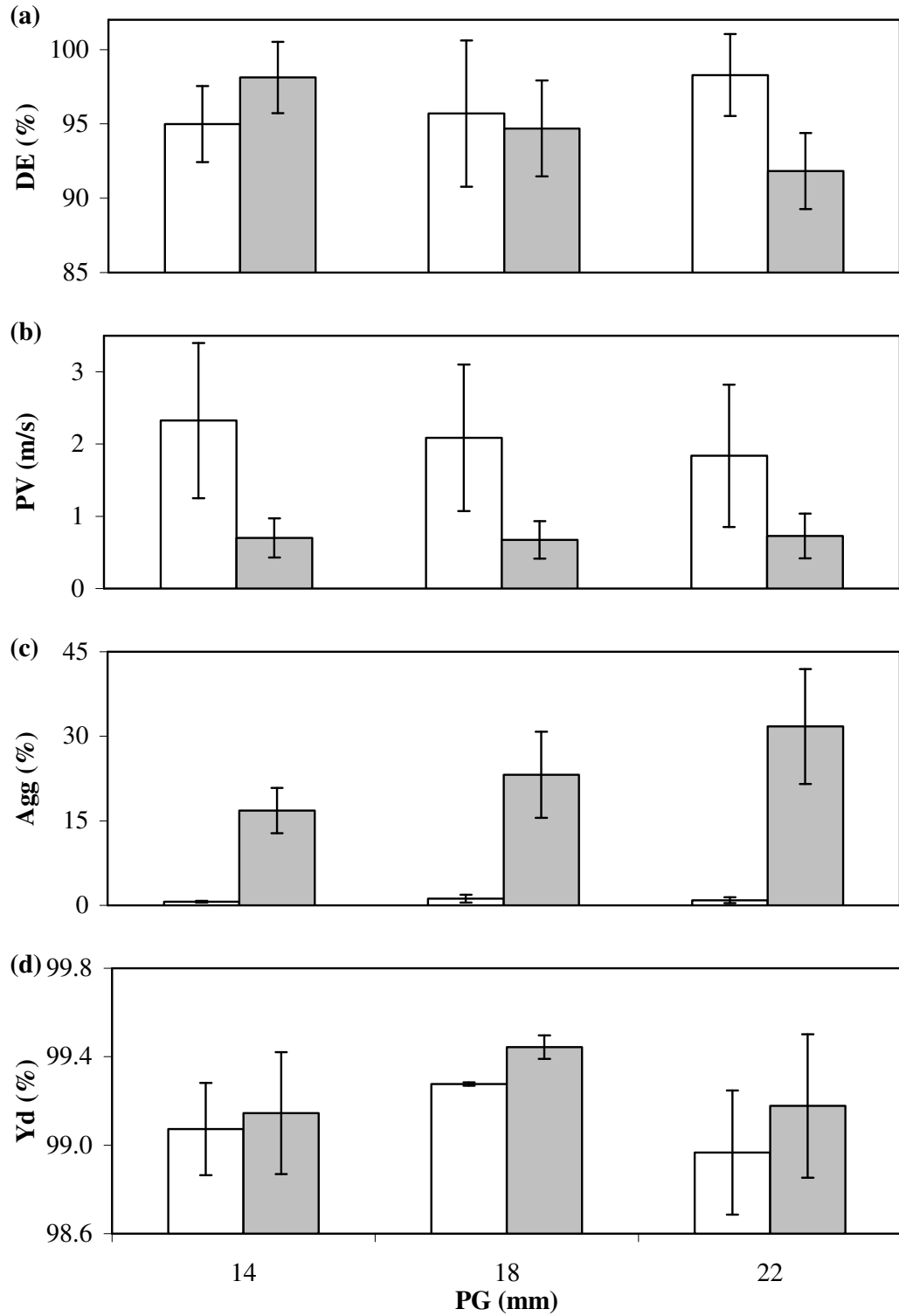


Fig. 25. Influence of PG on (a) DE, (b) PV, (c) Agg and (d) Yd in Precision coating (clear) and Wurster coating (shaded).

Despite the similar DE values ( $p < 0.05$ ) in both airflow patterns at PG 18 mm, the Agg values of pellets were much lower in Precision coating than in Wurster coating (Fig. 25c). This indicates that it was not just insufficient drying condition that had contributed to Agg, but rather, other factors relating to pellet movement in Wurster coating had also contributed to the development of agglomerates.

#### **A.1.2.2 Pellet movement in Wurster and Precision coaters**

High speed photography, at 4000 frames per second, showed that the pellets moving within the partition column in Precision coating were less packed and moved at a more disorderly fashion than in Wurster coating across for all the PG studied (Fig. 26). This indicates that there was better pellet separation in the spray zone in Precision coating, decreasing the tendency for collisions and formation of liquid bridges between pellets undergoing coating. This could be attributed to the accelerator insert used in Precision coating which was not perforated but had a central opening (Fig. 13). This design caused a high velocity airflow in the centre, which sucked in pellets and sent them strongly up the partition column, rather than being dependent on “hydrostatic pressure” aided by the fluidizing peripheral air and blown up the partition column as in Wurster coating. The latter resulted in denser pellet distribution in the coating zone which encouraged agglomeration.

As the PG was increased, the amount of pellets moving into the partition column in Wurster coating increased whereas the quantity of pellets entering the partition column in Precision coating would correspond to the suction pressure exerted by the inlet air (Fig. 26).

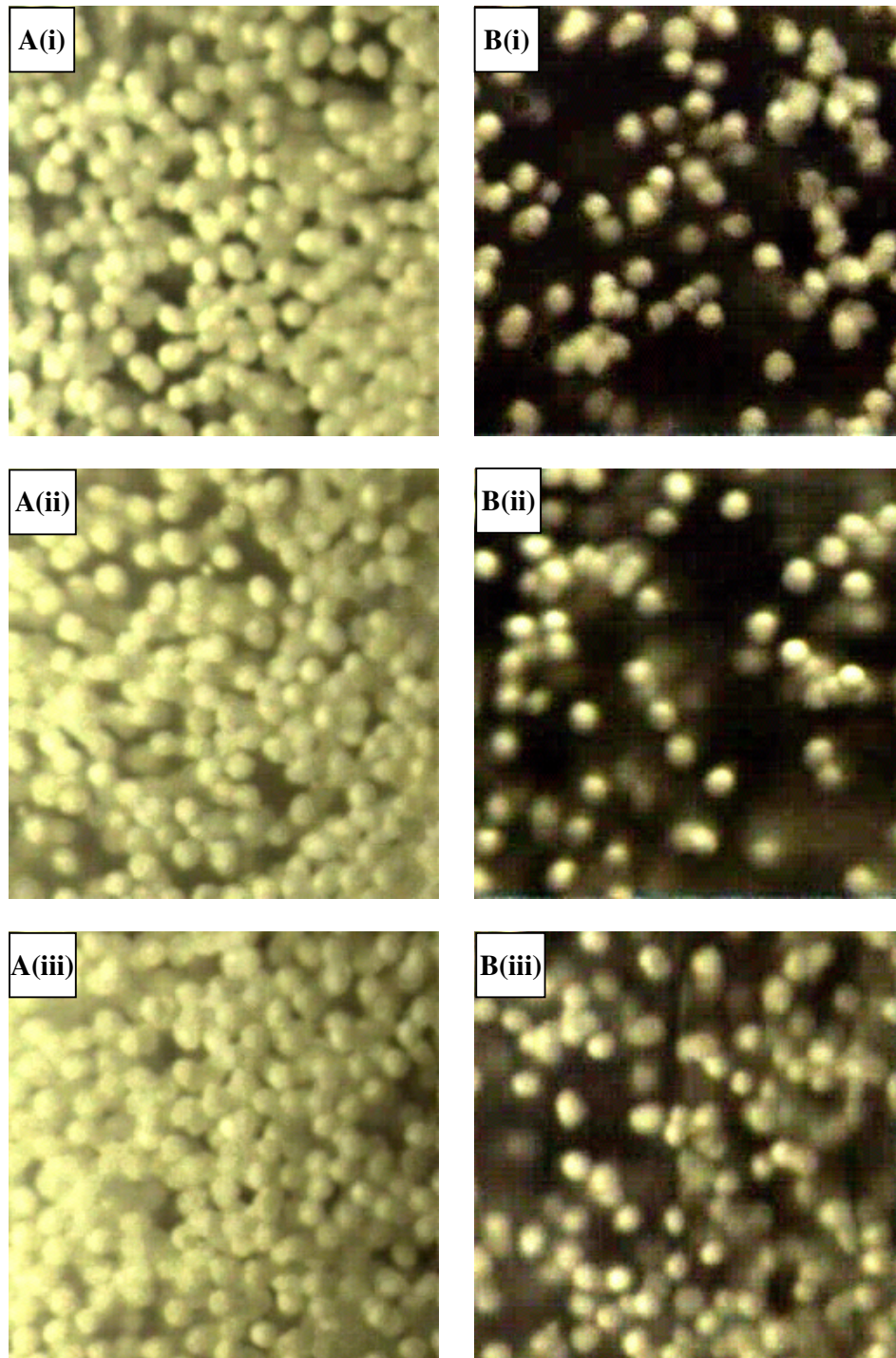


Fig. 26. High speed images of pellet movement in (A) Wurster coating and (B) Precision coating at partition gap of (i) 14 mm, (ii) 18 mm and (iii) 22 mm over an area of 10 mm by 10 mm. (The images were taken at 4000 frames per second)

In addition, the PV in Precision coating was about 3 times higher than that of Wurster coating (Fig. 25b). The faster pellet movement through the spray zone in the partition column would result in less coating material deposited per pellet with each passage through the coating zone and faster drying of the pellets during each coating cycle, thus reducing the Agg. It also enabled the pellets to reach a greater height in the coating chamber, increasing their exposure to the drying air in the chamber. From high speed video playback, pellets were observed to be moving up the partition column in a more disorderly fashion than in Wurster coating. This would have encouraged the breaking of any conjoined pellets with interconnecting bridges, which were earlier formed when the pellets collided and coalesced.

The Yd values were similar for Precision coating with PG of 14 mm and 22 mm, showing that the amounts of spray drying effect and attrition were similar (Fig. 25d). However, there was a marked increase in Yd at PG of 18 mm. The same trend was observed for Wurster coating. This suggests that there was an optimal PG for pellet flow into the partition column.

A very narrow PG would restrict pellet flow into the partition column, leading to scarcity of pellets in the spray zone and loss of spray material to the inner wall of the partition column. On the other hand, a very wide PG would allow a heavy pellet load to enter the partition column, resulting in sluggish and crowded material flow and longer transit time through the spray zone. In the latter situation, the longer transit time caused more coating material to be deposited onto the pellets during each passage through the spray zone. As such, pellet coats took a longer time to dry and the coated pellets could have adhered onto the walls of the partition column, causing a drop in the Yd.

The higher Agg in Wurster coating was not due to inadequate drying conditions as the drying efficiency was found to be similar in both precision and Wurster coating. Poor particle movement in Wurster coating as compared to Precision coating was observed by high speed photography showing that higher pellet velocity, better pellet separation and higher trajectories in Precision coating prevented the agglomeration of particles during coating.

### **A.1.3 Study of the coated products of Wurster and Precision coaters**

With better understanding of the coating process in the Wurster and Precision coaters, the next step was to determine their impacts on product characteristics.

As discussed in section A.1.2, a large difference in Agg was observed between Precision coating and Wurster coating (Fig. 25c). The lower Agg in Precision coating indicates that there was better pellet drying and separation during the coating process. This could be attributed to the swirling airflow which swirled and accelerated the pellets during their passage through the spray zone, providing shear force to break any liquid bridges that may be present between adhering pellets, thus preventing agglomeration from occurring. The swirling airflow increased the speed at which pellets passed through the spray zone, preventing excessive wetting.

From the scanning electron photomicrographs of pellets (Fig. 27), it could be observed that the pellets were coated differently. The coats obtained using Wurster coating (Fig. 27C(i-iii)) show many gross defects as highlighted in the photomicrographs, whereas Precision coating gave relatively good coats with much less observable gross defects (Fig. 27D(i-iii)). These gross defects were probably picking of the coats which occurred due to transient coalescence or sticking by liquid bridges between pellets that later broke off. This was a sign of over-wetting in

Wurster coating which was not observed in Precision coating despite the use of identical coating conditions.

Not considering the defects in the Wurster-coated pellets, uncoated pellets were observed to be the roughest, followed by pellets coated by Precision coating and lastly, pellets coated by Wurster coating. This was substantiated by surface roughness values obtained by scanning probe microscopy, which show that uncoated pellets had the highest mean surface roughness value of 540 nm, and that the surfaces of coats obtained by Precision coating were significantly rougher than those by Wurster coating (Table 7).

The rougher surface in Precision coating was probably due to the better contoured ellipsoidal footprints of the spray droplets which appeared as clearly demarcated and overlapping mosaic-like leaves (Fig. 28b). In contrast, the footprints of droplets formed by Wurster coating appeared to have merged together and beaten-down, creating a smoother surface (Fig. 28a). The conditions of slower drying and more frequent collisions had contributed to less rough films. The observation in Precision coating was probably indicative that the spray droplets dried more rapidly after they were deposited. The appearance of dried deposited spray droplets as clear well-demarcated footprints also provided evidence that the pellets were well-separated from each other as they passed through the spray zone and transited from the partition column. Collisions amongst the pellets would flatten the droplets' footprints as they dried.

Table 7. Properties of pellets coated by Wurster and Precision coating.

<b>Parameter</b>	<b>Wurster coating</b>	<b>Precision coating</b>
Angle of repose (°) *	34.3 ± 0.6	33.7 ± 0.5
Surface roughness, Ra (nm) *	221.2 ± 73.3	304.9 ± 90.1
Colour, $\delta E$	155.9 ± 5.2	157 ± 1.6
RSD of $\delta E$ (%)*	24.9 ± 1.33	14.2 ± 0.45

\* 2 sample t-test shows significant difference in means ( $p < 0.05$ )

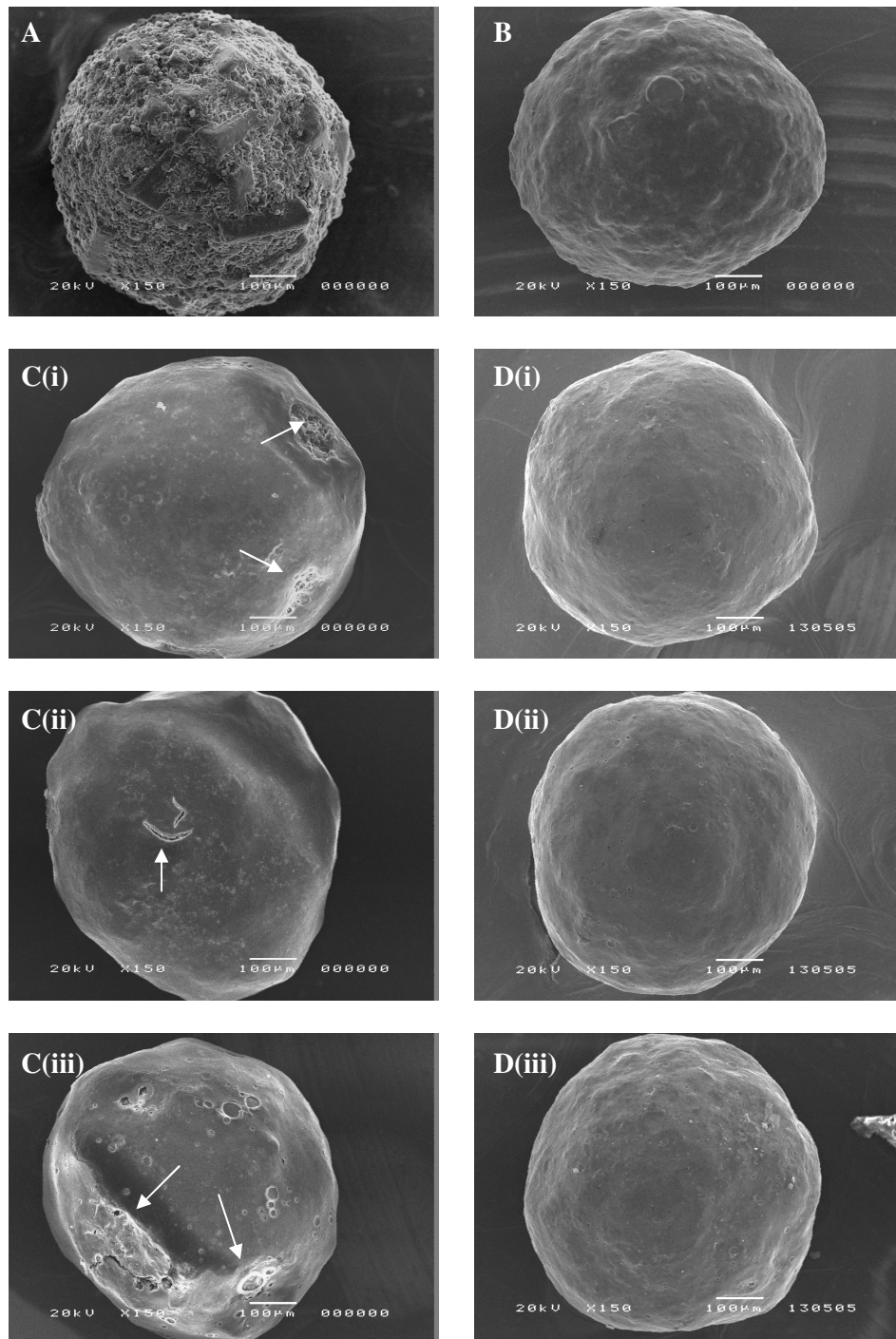


Fig. 27. Scanning electron photomicrographs of (A) uncoated pellet, (B) base-coated pellet, (C) Wurster-coated pellet at PG of (i) 14 mm, (ii) 18 mm and (iii) 22 mm; and (D) Precision-coated pellet at PG of (i) 14 mm, (ii) 18 mm and (iii) 22 mm.



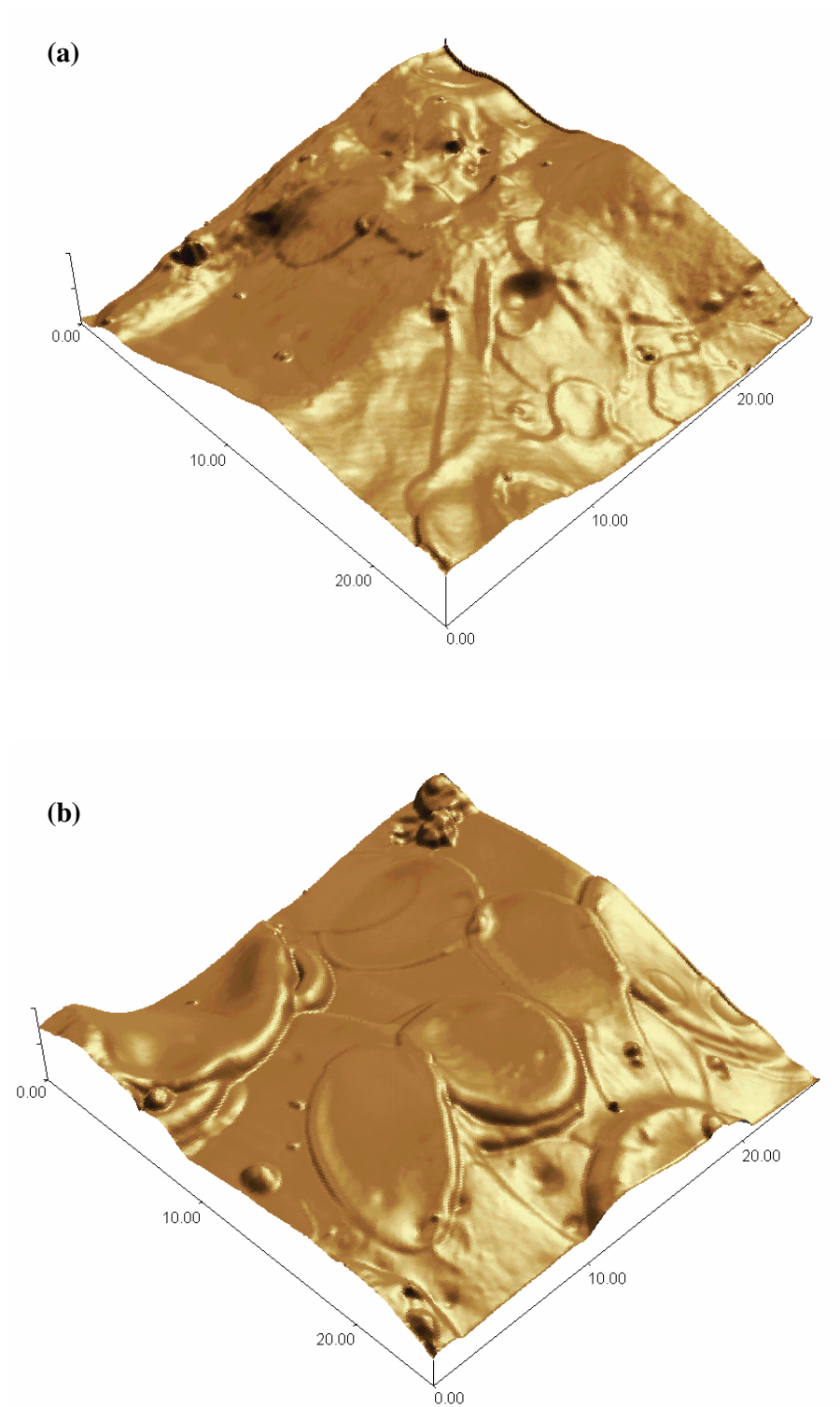


Fig. 28. Scanning probe images of the surface of a (a) Wurster-coated pellet and (b) Precision-coated pellet over an area of  $25\ \mu\text{m} \times 25\ \mu\text{m}$ .

The surface roughness of pellets contributed by gross defects was not reflected in the determined Ra value as the very rough pitted areas of the coated pellets were deliberately avoided during roughness measurements. Nevertheless, the overall pellet surface roughness was evident in the flow and packing studies. Angle of repose shows that coated pellets obtained by Precision coating flowed better and had better packing properties than those obtained by Wurster coating (Table 7). Gross defects observed in Fig. 27C(i-iii) were the most likely explanation for this observation as they caused higher friction between the pellets during flow and packing.

Despite the more disorderly and higher pellet velocities in Precision coating as discussed earlier in section A.1.2.2, there were little differences observed between the Yd obtained in both coating processes (Fig. 25d). The Yd was a measure of the amount of coating material deposited onto the pellets. This indicates that loss of coating material by spray-drying effect or attrition was comparable in both coating processes, showing that the increased particle movement was not detrimental to the pellets being coated.

The colour differences,  $\delta E$ , were also similar (Table 7), substantiating the above results that the amount of coating material deposited were comparable. However, the RSD of  $\delta E$ , which described the coating uniformity, was found to be significantly lower in Precision coating (Table 7).

The more uniform coating observed in Precision coating shows that there was enhanced pellet movement. This could again be attributed to the higher turbulence generated by the swirl accelerated airflow. The swirling action increased the flow path of pellets and the exposure of their surfaces to the spray material. In addition, it

would likely cause circumferential rotation of the pellets as they flow through the coating zone, resulting in a more uniform coat. However, in the non-swirling airflow of Wurster coating, the pellets would have taken a straight path through the spray zone, resulting in unidirectional exposure of the pellet surface to the spray zone, with more depositing on the surface facing the direction of the spray material.

The difference in coat qualities could also be explained by differences in pellet movement in the product staging bed during coating. In Precision coating, the pellets in the peripheral product staging bed were observed to be less fluidized and descended gradually before being drawn in and up the partition column. This shows that a non-turbulent queue system was present in the product staging bed in Precision coating. As such, pellets would have an equal chance of passing through the spray zone. For Wurster coating, pellets appeared to be in constant low amplitude flux caused by the peripheral fluidizing air at the product staging bed before being moved into and up the partition column. Freshly coated pellets were seen to be mixed with uncoated pellets before entering the spray zone in the partition column again. This contributed to the lower coating uniformity observed with Wurster coating (Table 7).

A drug release study was carried out to determine if such differences in uniformity of coat could contribute to changes in drug release profiles. Chlorpheniramine maleate was incorporated because of its high solubility in water and hence, its release would be solely dependent on the sustained release action of the applied ethylcellulose coat and not affected by ease of drug solubility. From Fig. 29, it could be concluded that the better formed coats by Precision coating caused the drug to be released at a slower rate than those pellets coated using the same conditions by Wurster coating. The dissolution medium for pellets coated by Wurster coating also turned turbid at the end

of the run, indicating that the sugar pellet cores and coats had partially disintegrated. The dissolution medium which contained pellets coated by Precision coating appeared much clearer, with core pellets still intact. This again was indicative of the superior encapsulation efficiency of the ethylcellulose coat deposited by Precision coating. The coating was possibly better formed, more uniform and less easily damaged.

From this study, the influence of swirl accelerated airflow evidently improved the product characteristics of bottom-spray air suspension coating. The Precision coater had enabled more uniform coating with less agglomeration and gross defects than the Wurster coater. As such, flow, packing, coat uniformity and sustained release profile of the coated pellets were enhanced. The adaptation of the bottom-spray air suspension coater with a swirl accelerator will provide more advantageous conditions for pellet coating.

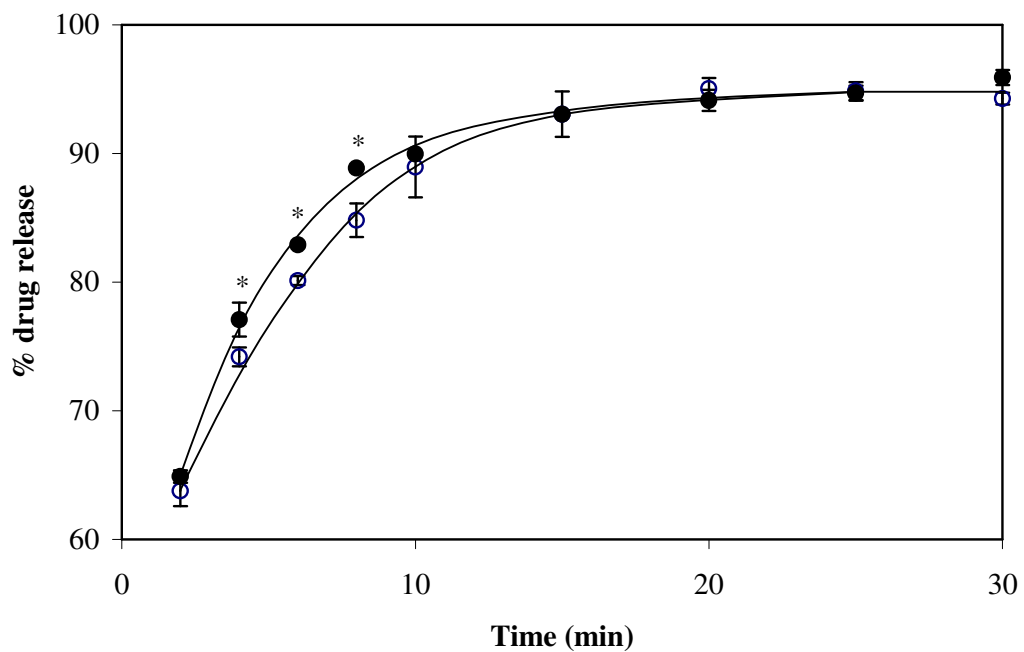


Fig. 29. Drug release profile of drug-loaded pellets coated by Wurster coating (●) and Precision coating (○). \* significant difference in means ( $p < 0.05$ )

## **A.2 Influence of processing conditions for Precision coating**

From the previous section, it was established that the Precision coater had superior coating performance as compared to the Wurster coater. Hence, subsequent studies were carried out using only the Precision coater.

It was found that the drying efficiency and particle movement were important determinants of product characteristics. This led to the next hypothesis that optimal drying efficiency and particle movement would be necessary for desirable product characteristics. Hence, the processing conditions affecting the drying efficiency and particle movement of the particles were varied and their effects on the coated products were determined. The processing conditions studied included temperature, airflow rate, partition gap and accelerator insert diameters. The influence of pellet size on drying efficiency and agglomeration was also studied to better understand the conditions favorable for coating smaller particulates.

### **A.2.1 Effects of inlet air temperature and airflow rate**

Inlet air temperature ( $T_p$ ) and AF can contribute to the overall drying capacity of the inlet air. By varying these factors, the relationship between DE and product characteristics could be determined. Changes in  $T_p$  would affect only the thermodynamics of the process whereas changes in AF would affect both the thermodynamics and fluid dynamics of the particles during coating.

#### **A.2.1.1 Effects of change in inlet air temperature**

Drying efficiency increased at a decreasing rate with increasing  $T_p$  (Fig. 30a). At the lowest  $T_p$  of 60 °C, the DE was low as the drying air could not remove very efficiently the moisture deposited onto the pellets.

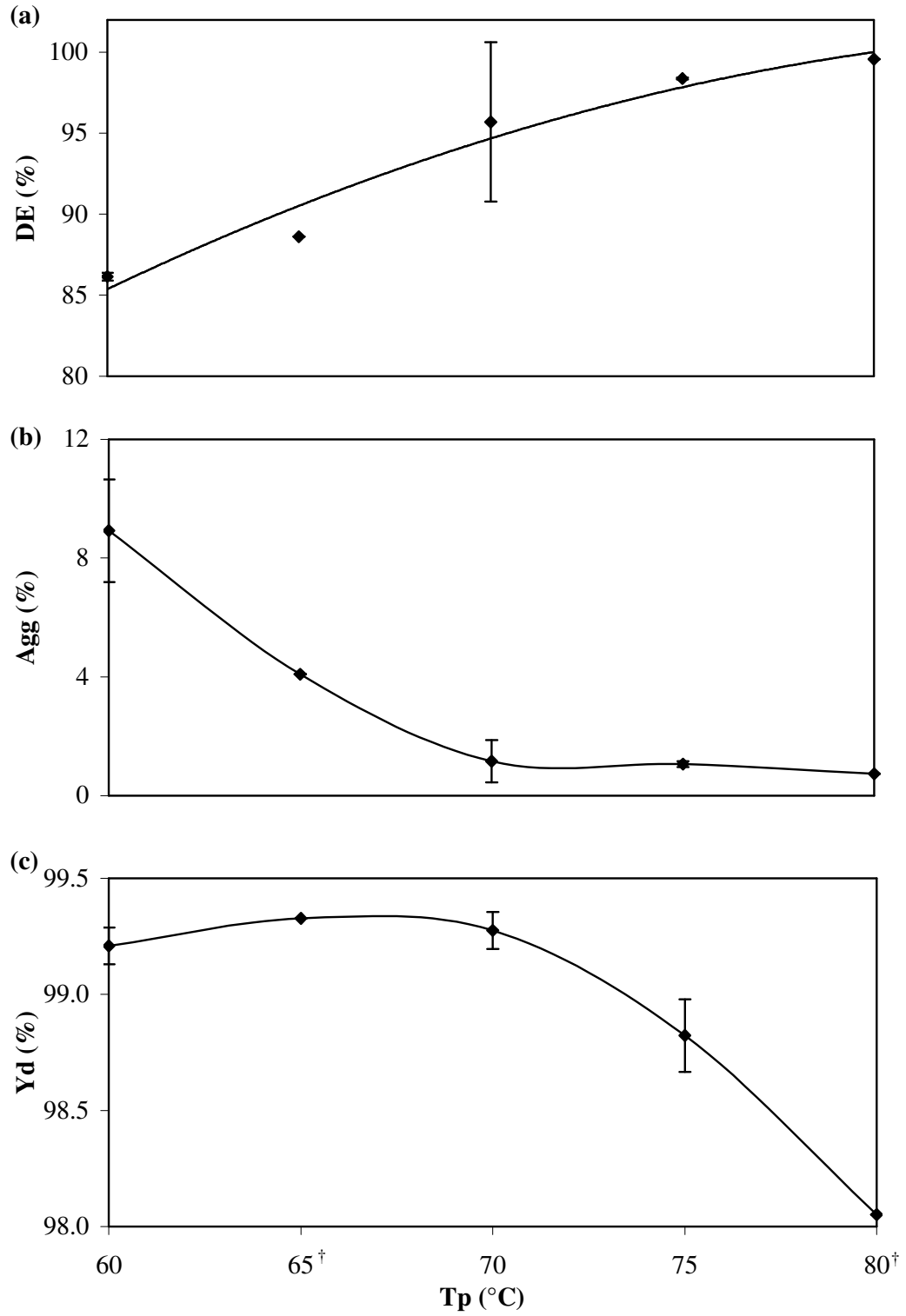


Fig. 30. Influence of  $T_p$  on (a) DE, (b) Agg and (c) Yd in Precision coating.  
 ( $^{\dagger}$  :  $n = 2$ )

As the temperature increased to 70 °C, the air relative humidity was lowered and had greater capacity for moisture uptake by the higher vapor pressure difference. Beyond 70 °C, the DE leveled off close to 100 % and Agg reached a minimum (Fig. 30b) but the Yd started to decrease (Fig. 30c). This indicates that as almost all the moisture was removed beyond the Tp of 70 °C, the excessively dry condition conferred little additional benefit to reducing agglomeration. Moreover, it caused a decrease in Yd due to spray-drying effect or attrition. This suggests that the optimal thermodynamic condition for coating was when DE approached close to 100 %, whereby the drying conditions were just sufficient to remove all the moisture introduced into the system.

#### **A.2.1.2 Effect of change in airflow rate**

When the AF was increased, the DE increased from 93 % at AF of 60 m<sup>3</sup>/h to 98 % at AF of 90 m<sup>3</sup>/h, reaching a high of 99 % at AF of 100 m<sup>3</sup>/h (Fig. 31a). The DE came close to 100 % beyond the AF of 80 m<sup>3</sup>/h, showing that almost all the moisture introduced had been removed under those conditions. Increasing the AF further caused slight reduction in Agg (Fig. 31b) but marked decrease in Yd (Fig. 31c). The trends were similar to those observed when Tp was increased (Fig. 30) and could be attributed to the same reasons.

Although the DE at AF of 60 m<sup>3</sup>/h with Tp of 70 °C (Fig. 31a) was higher than that of AF of 80 m<sup>3</sup>/h with Tp of 60 °C (Fig 30a), the Agg was similar at about 8.5 % (Fig. 30b, 31b). This shows that in addition to DE, the pellet movement was also important in influencing Agg. The lower AF caused inadequate fluidization of the pellets resulting in the high Agg observed. There was also a slight reduction in Agg beyond the AF of 80 m<sup>3</sup>/h, which could be due to the increased fluidization of the pellets at higher AF.

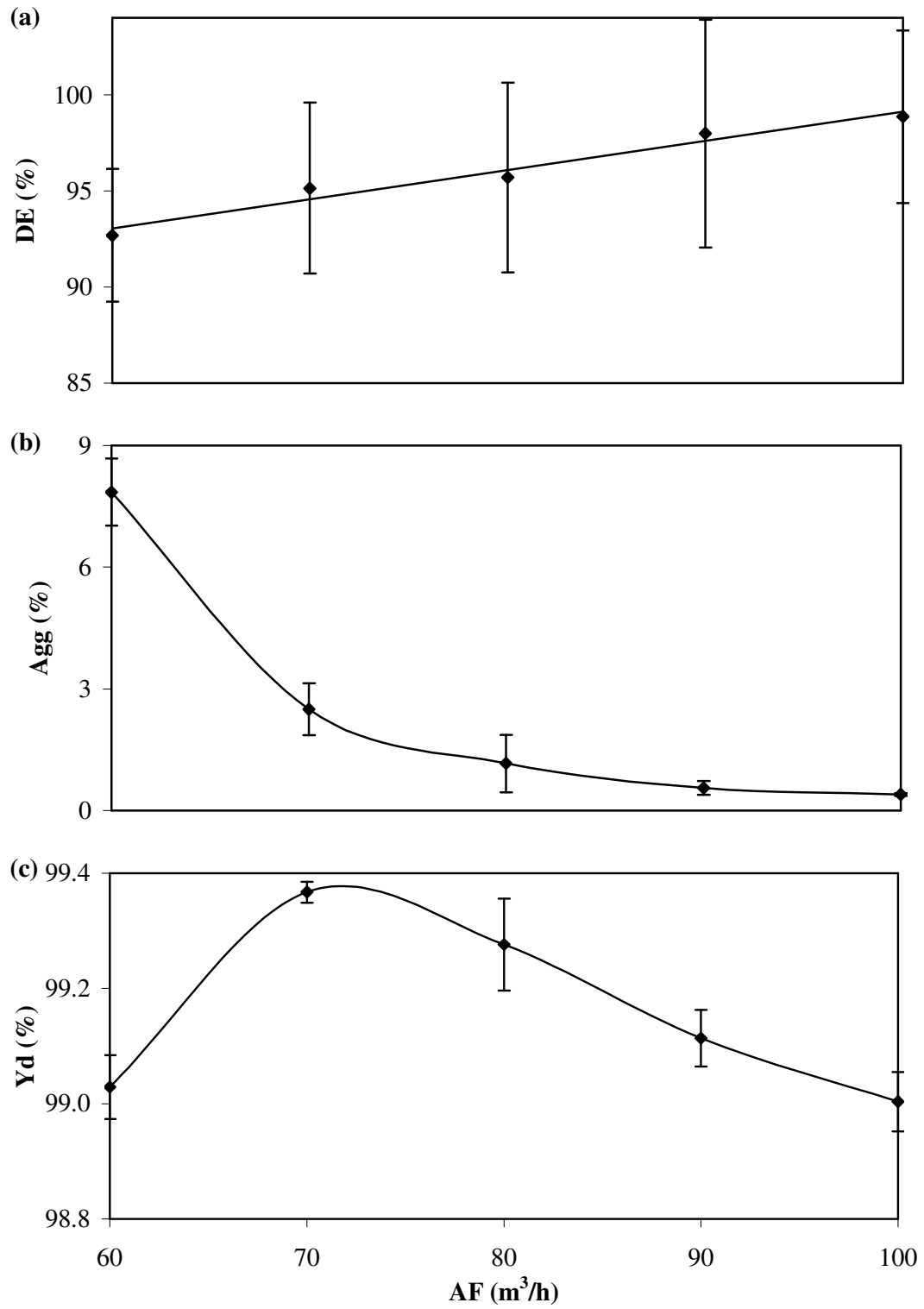


Fig. 31. Influence of AF on (a) DE, (b) Agg and (c) Yd in Precision coating.



The degree of agglomeration was found to be minimized at a DE of ~100 %, whereby all the moisture introduced was removed by the drying air. Once DE approached 100 %, further drying decreased the Yd due to spray drying effect and attrition. Low DE was often associated with high Agg, however, a high DE was not always favourable to produce low Agg. This was attributed to the confounding influence of particle movement on the agglomeration tendency of the pellets.

### **A.2.2 Effect of change in accelerator insert diameter**

In Precision coating, the AI diameter was an important processing variable as it regulated the particle trajectories through the partition column. The AI diameter can be changed to adjust the air velocity within the partition column. A smaller AI diameter generated a higher air velocity (Fig. 19), in accordance with the law of conservation of mass. This increased the pressure differential across the PG, thus encouraging pellet entry, and imparting greater acceleration to pellets as they passed through the spray zone. Hence, the effects of AI diameters on particle velocity, DE, Agg and Yd were studied to identify their impact on the coating process.

The air velocities generated by the different AI diameters brought about unexpected changes in PV. Despite the higher air velocities generated by smaller AI diameters, PV values for the 20 and 24 mm AI diameters were rather close ( $p > 0.05$ ) (Fig. 32b). This could be due to the concentration of air movement as a central jet in the partition column with the 20 mm AI diameter such that the particle velocities were higher only in the middle but compromised further out from the center, making the mean PV similar to that of the 24 mm AI diameter.

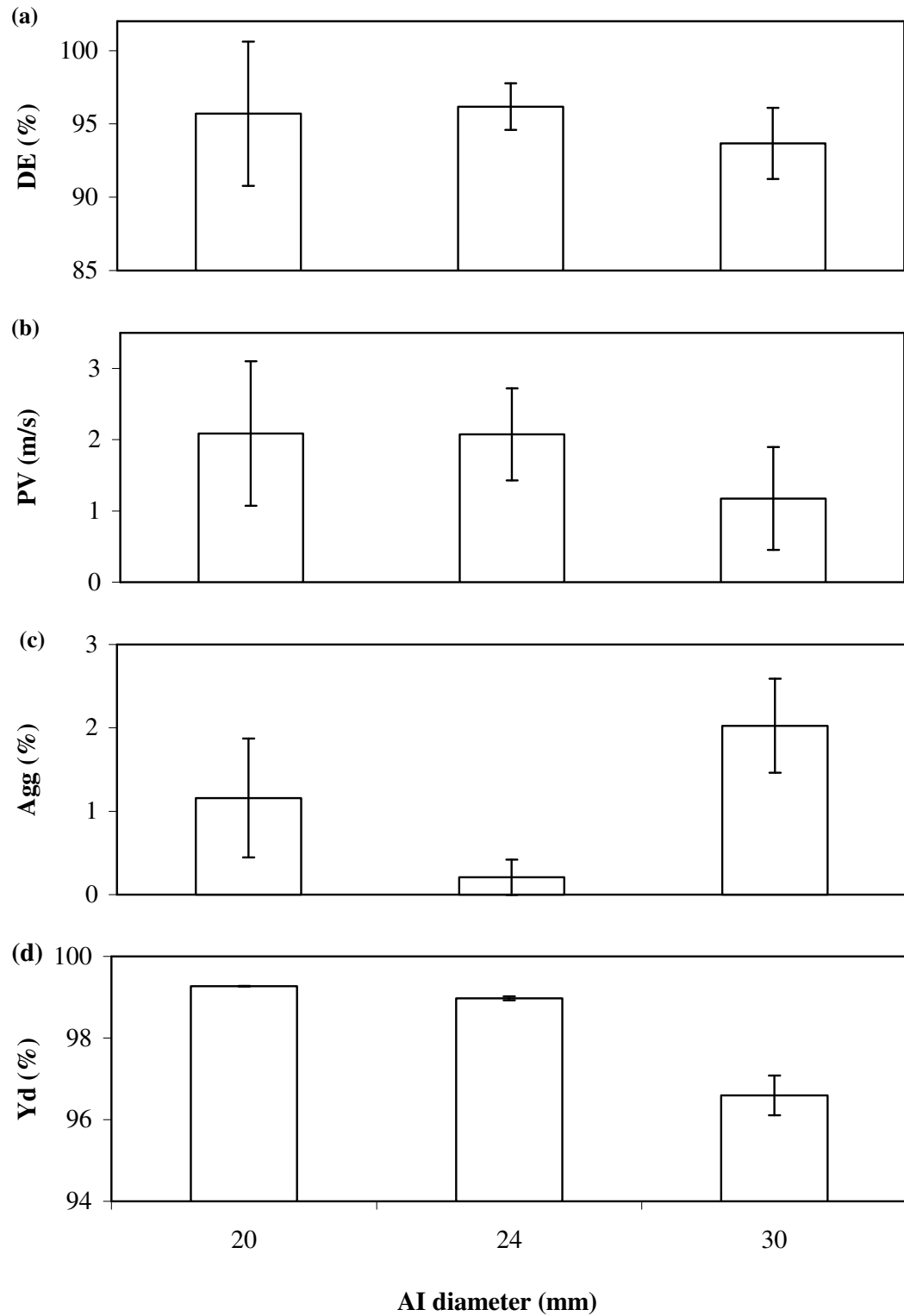


Fig. 32. Influence of AI diameter on (a) DE, (b) PV, (c) Agg and (d) Yd in Precision coating.

The PV decreased significantly only for the 30 mm AI diameter where the air velocity was generally lower, resulting in a reduction of PV within the partition column. This was substantiated by air velocity measurements using a micromanometer at the peripheral and central parts of the partition column, which show that air velocity was significantly higher in the center than periphery of the partition column, and that the smallest AI diameter had the highest air velocity at the center and the lowest air velocity at the periphery of the partition column ( $p < 0.05$ ) (Fig. 33).

The largest AI diameter of 30 mm had the lowest DE (Fig. 32a), showing that low PV compromised the drying of the pellets. However, despite similar PV and DE values for AI diameters of 20 and 24 mm, the Agg obtained with the 20 mm AI diameter was unexpectedly larger than that of the 24 mm AI diameter (Fig. 32c). For the 20 mm AI diameter, faster moving air concentrated in the center of the partition column left the periphery of the partition column with much lower air velocity (Fig. 33). This could have compromised the overall particle movement through the partition column, resulting in a greater tendency for agglomeration. It was observed under high speed playback that there were more pellets descending at the peripheral region within the partition column with the use of a larger AI diameter. This shows that the direction of pellet trajectories within the partition column also had a great impact on Agg.

Thus, a balanced air distribution within the partition column, as seen in the 24 mm AI diameter, was necessary to ensure optimal particle movement up the partition column and minimize Agg.

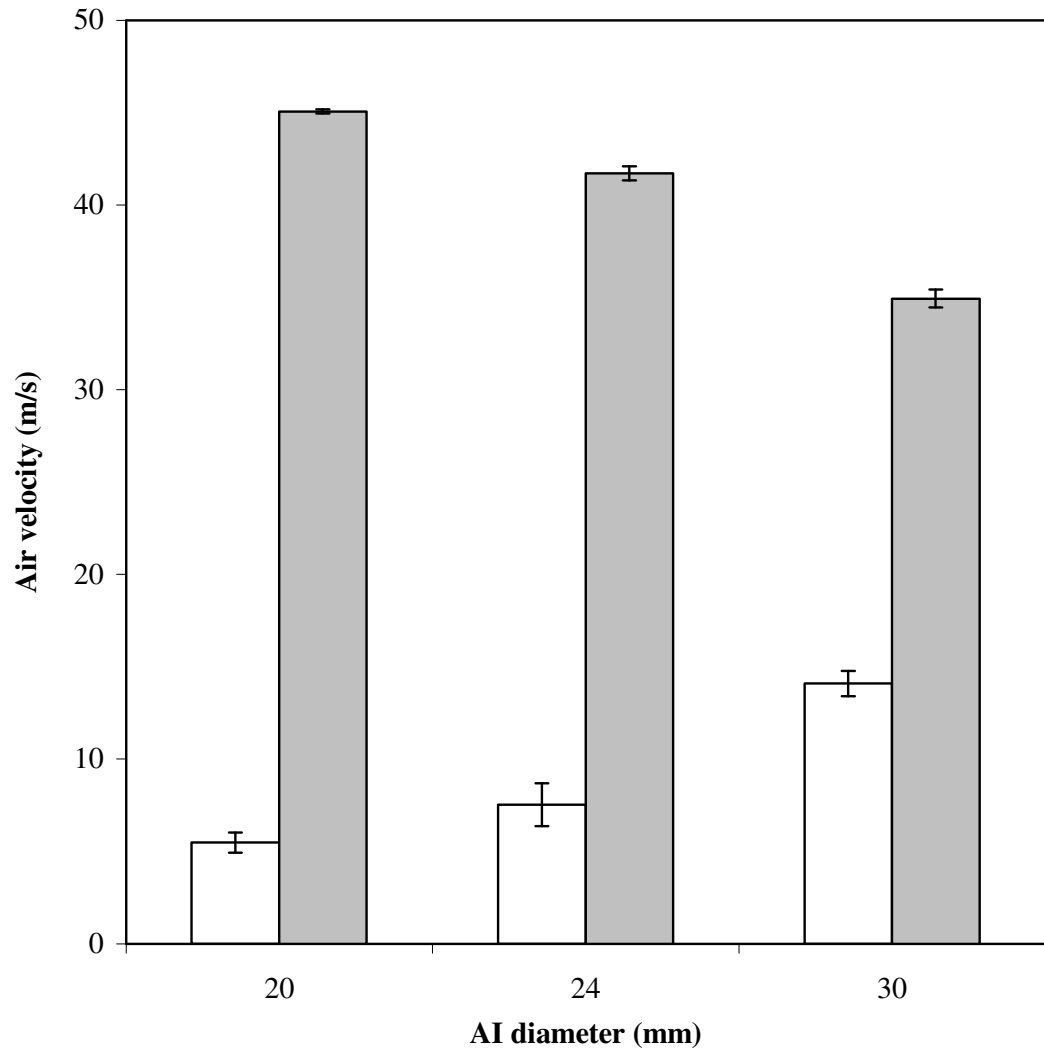


Fig. 33. Influence of AI diameter on the air velocities at the peripheral (clear) and central (shaded) positions within the partition column in Precision coating.

Closeness of pellet packing with the AI diameter of 30 mm also brought about higher Agg. From high speed images, more pellets were present in the partition column when AI diameter of 30 mm was used as compared to that of the 20 and 24 mm AI diameters (Fig. 34). Moreover, it was observed that the MFR of pellets decreased with larger AI diameter. This indicates that the movement of pellets up the partition column was slower and closer together when larger AI diameters were used. The slower moving pellets could have received comparatively more coating material while passing through the spray zone and took a longer time to dry. Coupled with the closer proximity of pellets, the conditions favoured the formation of liquid bridges between pellets.

The slower drying with the use of the 30 mm AI diameter could have led to loss of deposited coating material to the surrounding as the pellets brushed against the walls of the coating chamber and partition column, resulting in a lower  $Y_d$  (Fig. 32d).

For all AI diameters, higher speed in the centre and lower speed in the periphery was observed. The distribution of air velocity within the partition column had a strong impact on the agglomeration as it affected the pellet velocities, inter-pellet distances and pellet trajectories within the partition column. Poor pellet movement also compromised the DE. Overall, pellet movement was enhanced when the air velocities within the partition column were not too concentrated or diffused.

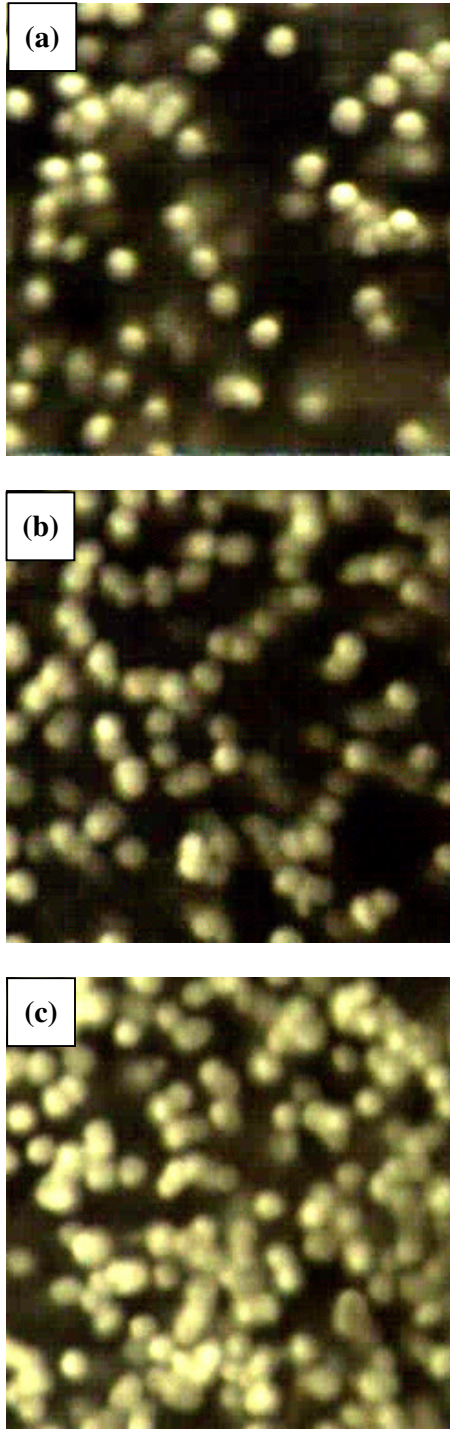


Fig. 34. High speed images of pellets moving in Precision coating using accelerator insert (AI) diameters of (a) 20 mm, (b) 24 mm and (c) 30 mm over an area of 10 mm  $\times$  10 mm. (The images were taken at 4000 frames per second)

### **A.2.3 Effects of airflow rate and partition gap on the coated pellets**

In the previous sections, AF, Tp, PG and AI diameter were found to affect the drying efficiency and product characteristics. Here, their effects on the quality of coated pellets would be further analyzed. However, Tp was not studied as the suitable temperature is partially dependent on the type of coating polymer used. AI diameter was also not studied due to the limited variety available.

The inlet airflow served to provide both the circulation of pellets and drying needs of the coater. The Agg decreased considerably from 7.85 to 2.50 % when the AF was increased from 60 to 70 m<sup>3</sup>/h, and approached a minima at higher AFs (Fig. 35a). The sharp decrease in agglomeration was indicative that there was sufficient drying capacity provided by the inlet drying air. Slight further reduction in Agg beyond the optimal AF of 70 m<sup>3</sup>/h was probably due to increased attritive environment which rapidly broke down any freshly coalesced particle-particle agglomerates.

There was a strong correlation ( $R^2 = 0.95$ ) between Agg and PG (Fig. 35b). When PG was increased, the entry and movement of pellets into the spray zone would be proportionally increased. For a fixed AF, the velocity of pellet movement through the partition column would be expected to decrease proportionally, leading to more sluggish movement of particles in the partition column (Deasy, 1984). This could have resulted in conditions for increased tendency of agglomeration, especially at wider PGs. However, this effect was still very small as the change in the Agg only increased by about 1 %.

There was an optimal AF at which the Yd was maximal (Fig. 36a). With increase in AF, the Yd increased from 99.0 % to 99.4 %, then decreased linearly to 99.0 %. The percent change in Yd seem small due to the high load of pellets used. However, the

amount of fines it represented was substantial, ranging from 6 g for a Yd of 99.4 %, to 10 g for a Yd of 99.0 %. At the lowest AF of 60 m<sup>3</sup>/h, the freshly-coated pellets were probably not dried completely, depositing some coat material onto the wall of the coater as they came into contact with it. At the AF of 70 m<sup>3</sup>/h, the Yd was at a maximum (99.4 %), showing that spray drying effects were probably at the lowest. The above discussion on effect of AF on Agg also suggested that adequate drying capacity was reached at around 70 m<sup>3</sup>/h. With increasing AF, the Yd decreased in a linear pattern ( $R^2 = 0.99$ ) indicating that there was increased amount of spray drying effect and likely, attrition also increased proportionally with the increase in AF.

Partition gap controls the flow of pellets into the partition column. When the PG was narrowest (6 mm), the Yd was the lowest (97.6 %) (Fig. 36b). The narrow PG probably restricted the pellet mass flow into the partition column, causing inadequate density of pellets passing the coating zone. This resulted in loss of coating material by deposition on the surrounding partition column wall and by spray drying effect. Increasing the PG produced an increase in Yd, reaching a peak (99.3 %) at PG of 18 mm. A similar trend was observed for the colour intensity of the pellets, with a clear maximum ( $\delta E$  of 153) at PG of 18 mm (Fig. 37b). The slight decrease in Yd and colour intensity at the larger PG of 22 mm was probably because of the lower air velocity generated with increase in PG (Fig. 17). This resulted in a longer transit time of pellets conveying through the partition column and would have caused increased over-wetting and deposition of wet coats onto the surrounding walls.

Airflow rate had minimal effect on pellet quality over the range studied. It did not affect the colour intensity and uniformity (Fig. 37a & Fig. 38a), and surface roughness (Fig. 39a) of the coated pellets significantly ( $p < 0.05$ ). These findings indicated that



the swirling airflow pattern in Precision coating continued to provide a conducive coating environment even when the AF was increased beyond its optimal value.

Partition gap, on the other hand, seemed to have greater influence on coat quality. Colour uniformity was lowest at PG of 6 mm (RSD of  $\delta E = 24.2\%$ ) and increased (RSD of  $\delta E = 13.2$  to  $12.5\%$ ) with increase in PG, leveling off beyond a gap of 14 mm (Fig. 38b). The narrow PG of 6 mm restricted pellet entry from the product bed into the partition column and this resulted in longer residence time in the product bed as well as reduced cycling rate through the spray zone. The reduced cycling rate did not favour coating uniformity. The small partition gap could also increase the suction of pellets into the partition column due to Venturi effect, causing the pellets to transit through the spray zone faster. This would have diminished the likelihood for a wider circumferential coating in one pass, creating a more unidirectional flow and hence less exposure of the pellet surfaces to the coating material. Thus, the combination of reduced cycling rate and less favourable coat distribution conditions produced an overall poorer coat quality at PG of 6 mm. There was a slight increase in surface roughness (Fig. 39b) with PG, which could be due to increased formation and breakage of liquid bridges. However, this was not found to be significant.

These findings indicate that AF had greater impact on the drying of pellets than on coat quality whereas PG, which controlled the amount of pellets entering and velocity of pellets passing through the partition column, affected the quality of coat formed. Nevertheless, despite the large changes in PG and AF used, the detected changes were rather small in magnitude, largely inconsequential in terms of affecting the various performance parameters studied. These observations demonstrated the robustness of Precision coating with the swirling airflow when employed for pellet coating.

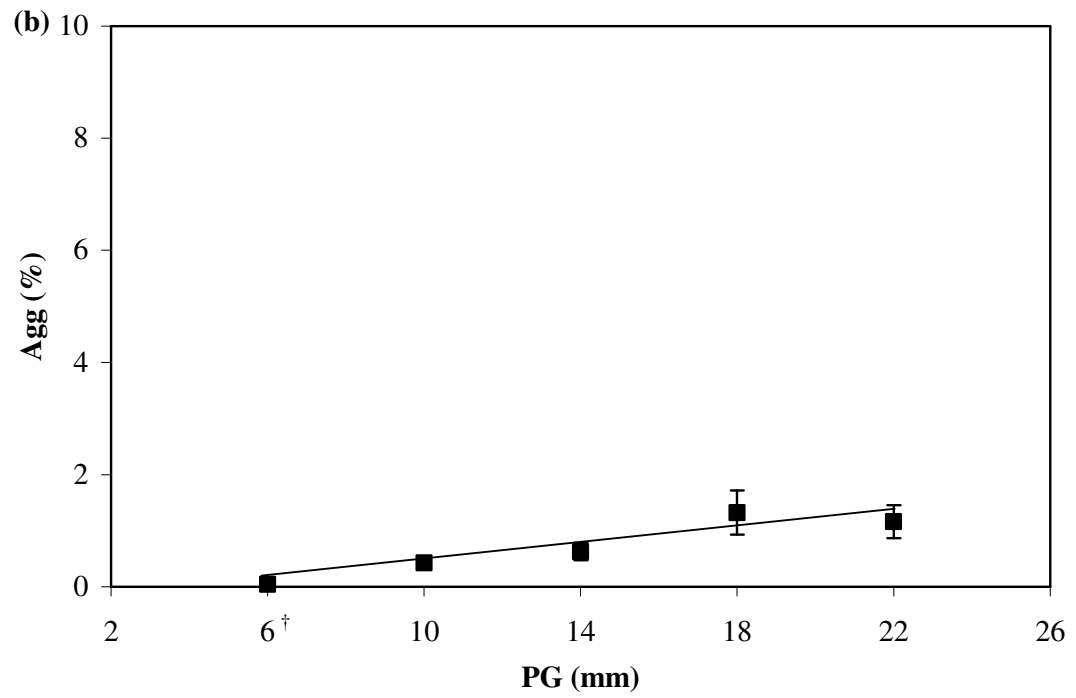
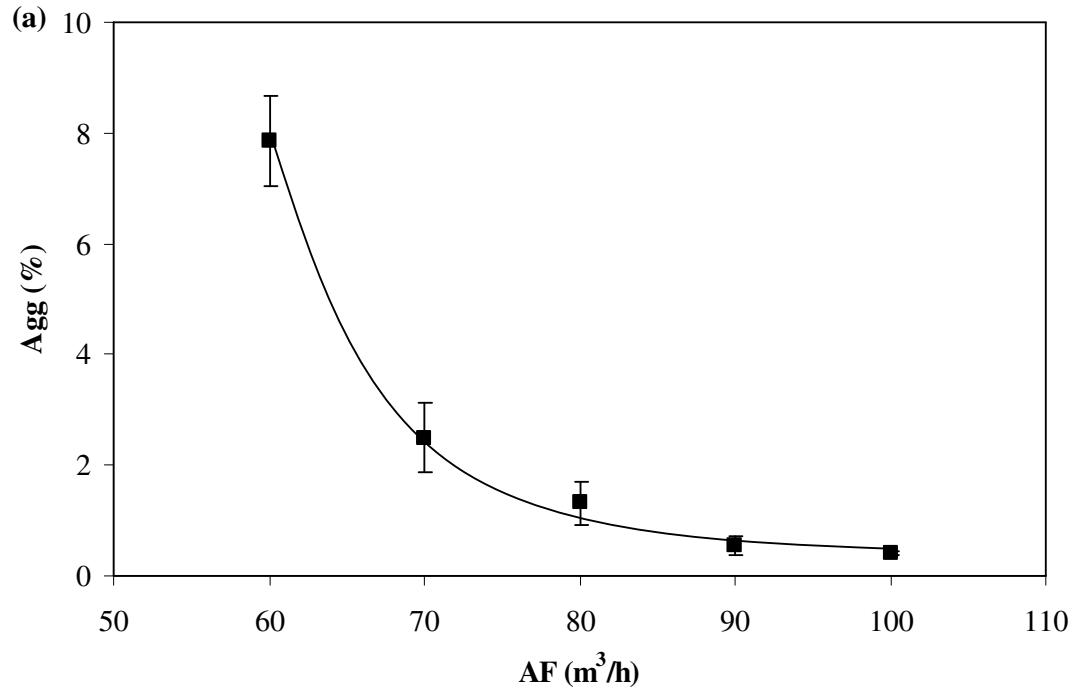


Fig. 35. Influence of (a) AF and (b) PG on the Agg of Precision-coated pellets.  
(<sup>†</sup>: n = 2)

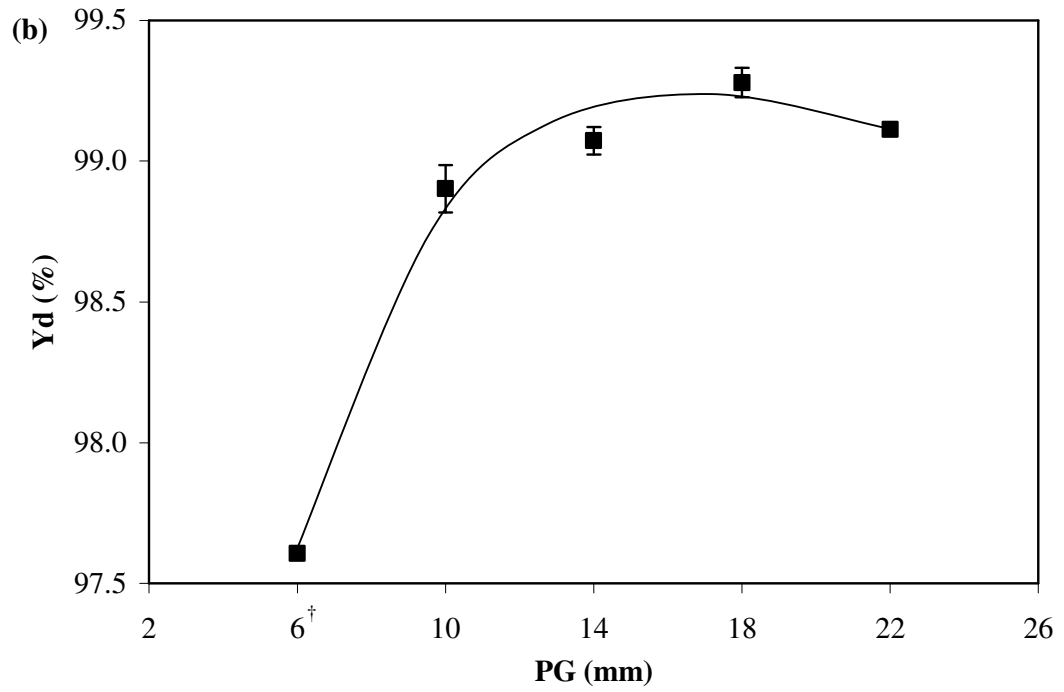
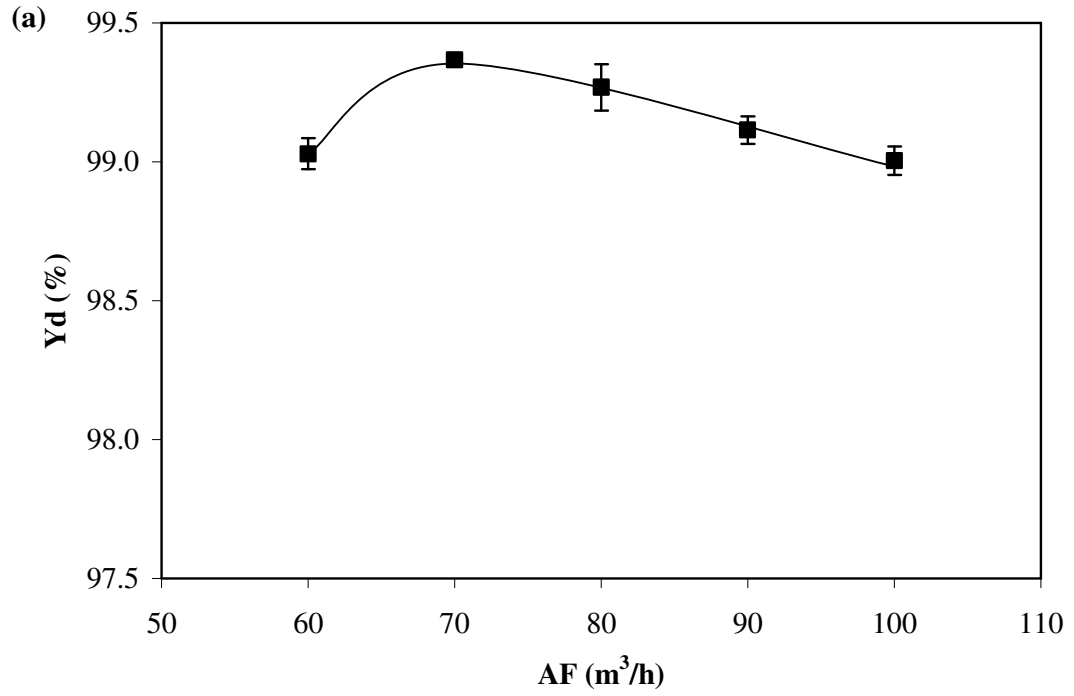


Fig. 36. Influence of (a) AF and (b) PG on the Yd of Precision-coated pellets.  
 (†: n = 2)

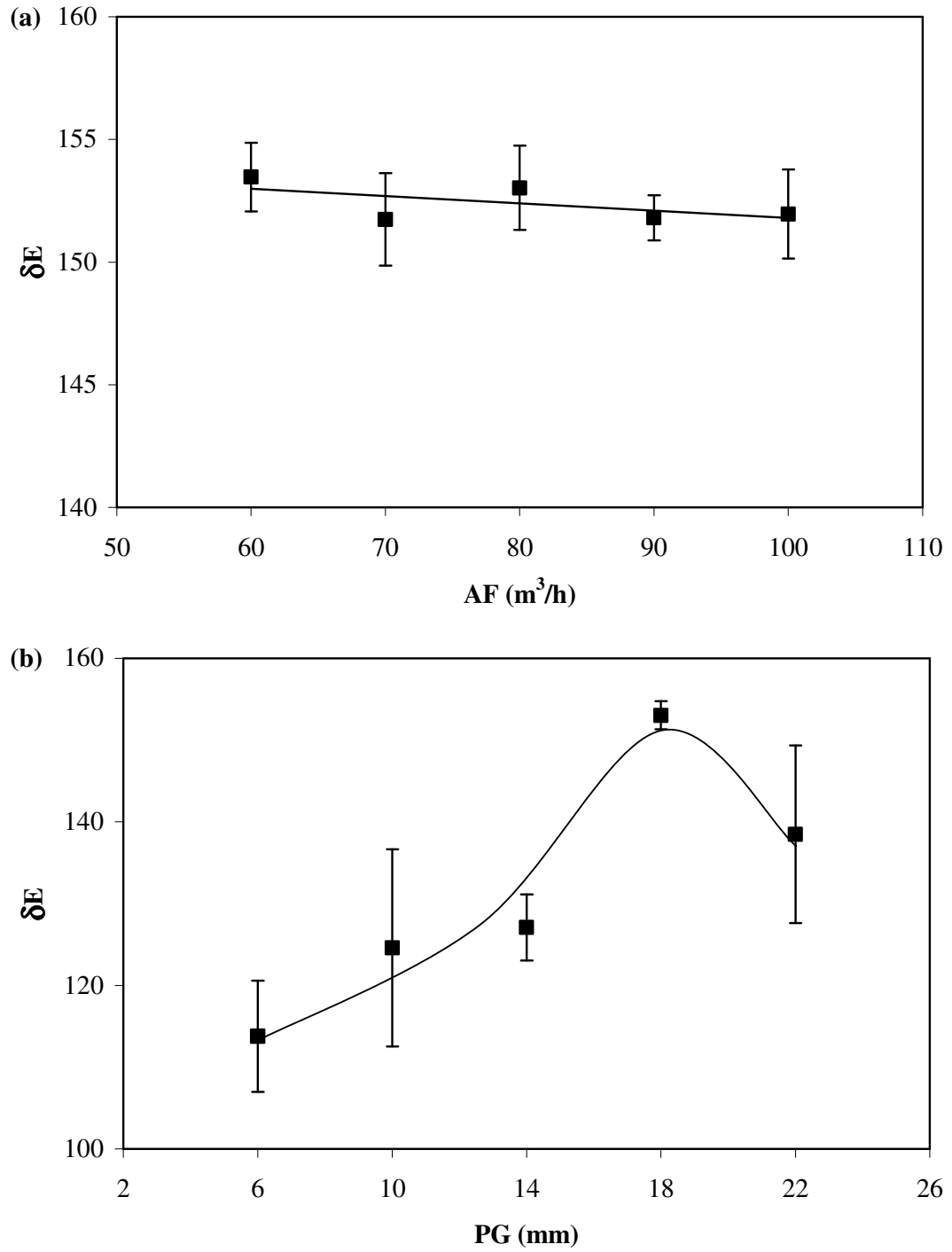


Fig. 37. Influence of (a) AF and (b) PG on the  $\delta E$  of Precision-coated pellets.

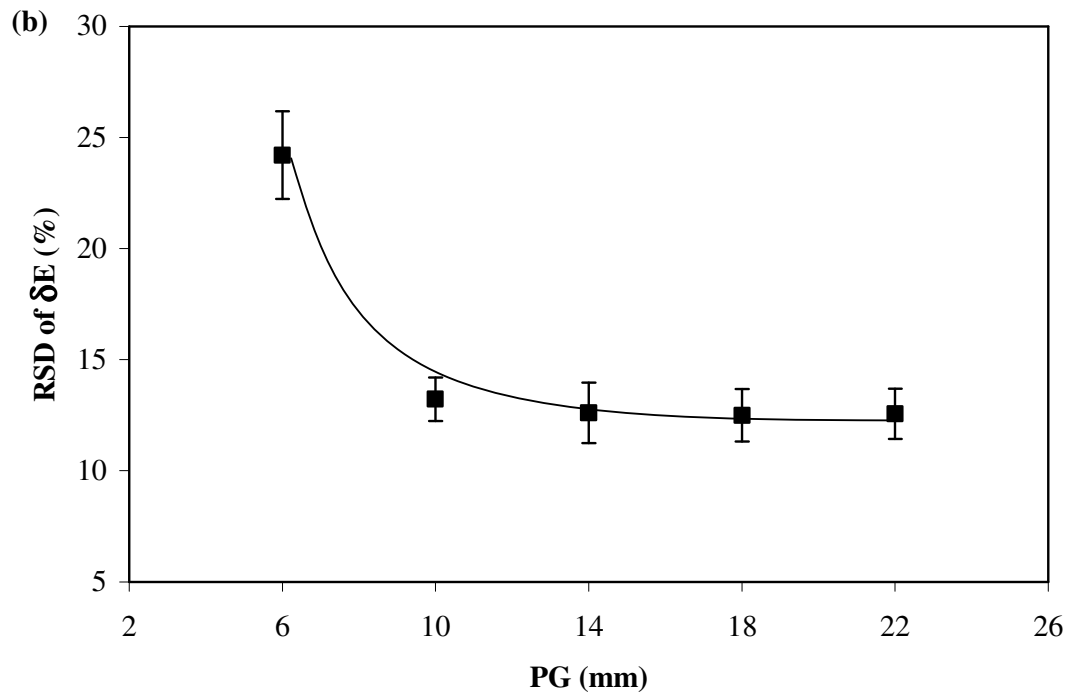
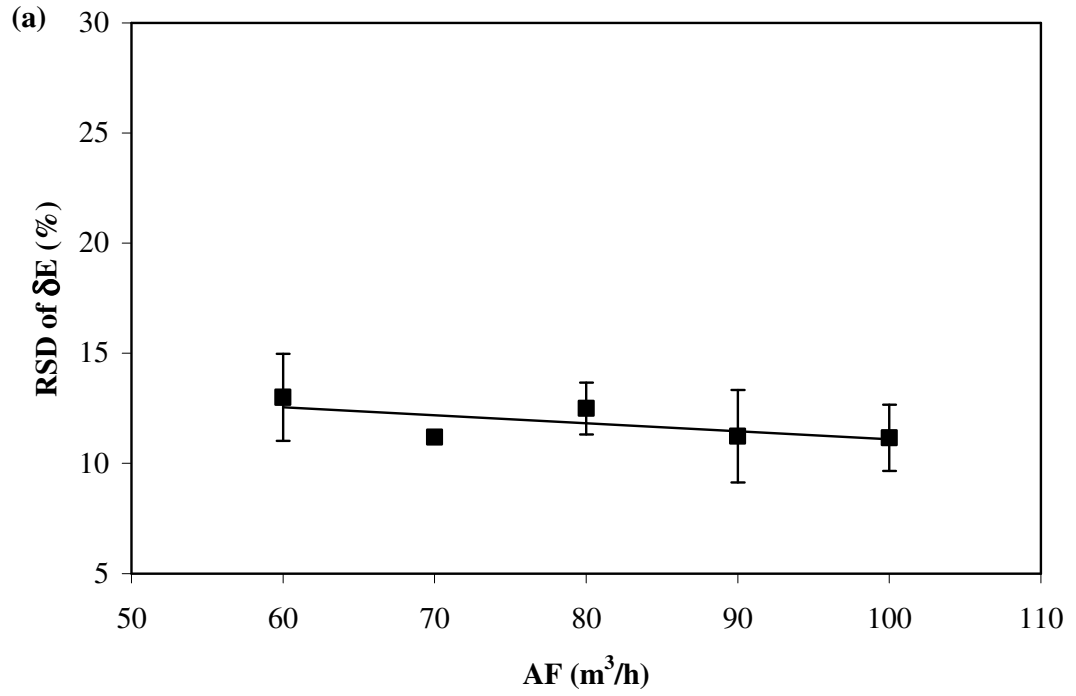


Fig. 38. Influence of (a) AF and (b) PG on the RSD of  $\delta E$  of Precision-coated pellets.

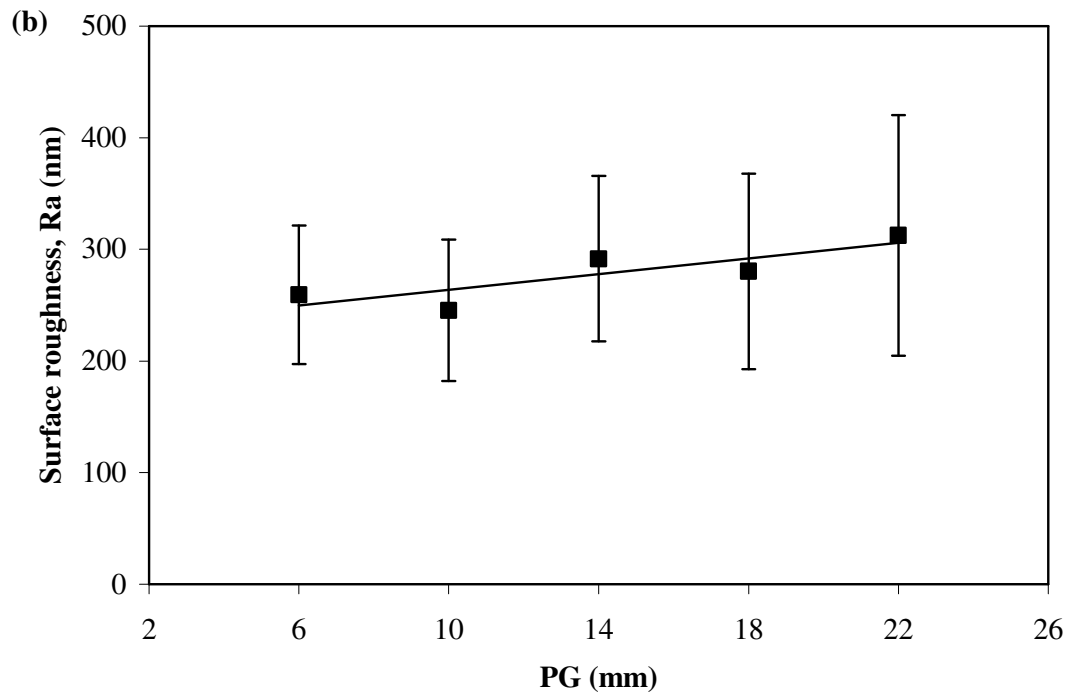
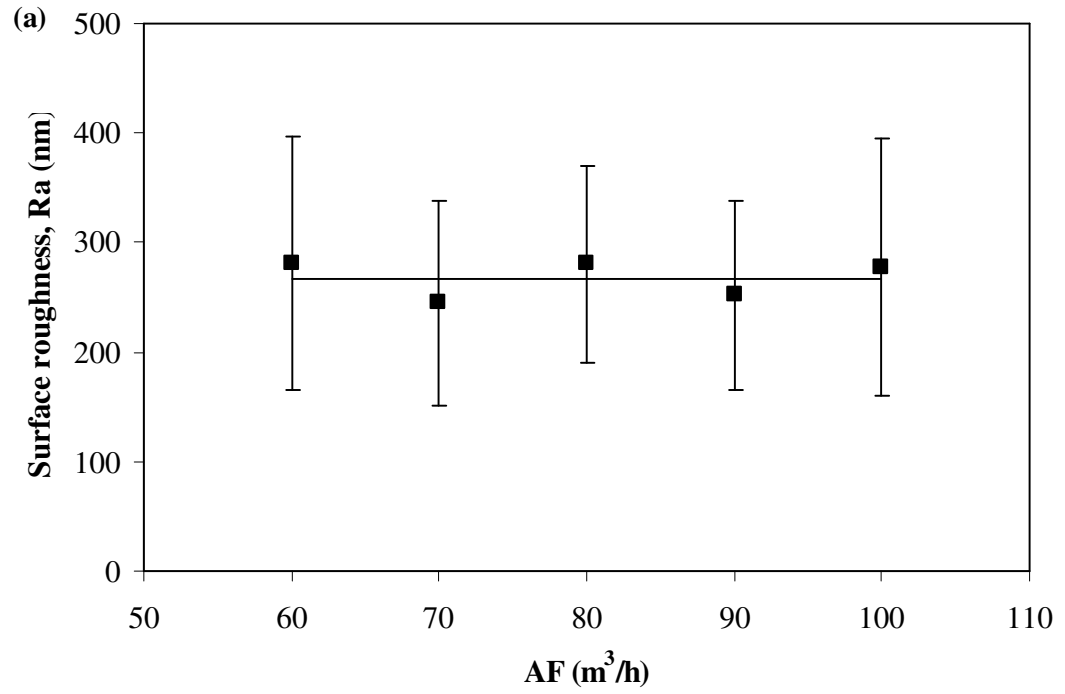


Fig. 39. Influence of (a) AF and (b) PG on the surface roughness of Precision-coated pellets.

#### **A.2.4 Effects of airflow rate and partition gap on pellets of different sizes**

The primary aim of this study was to understand the conditions that were favourable for coating smaller particulates. Hence, the influences of the main processing variables, AF and PG, on the coating of smaller particulates were evaluated.

Generally, smaller pellets had lower DE and higher Agg than larger pellets (Fig. 40 and 41). Similar atomizing pressure was used for coating both sizes of pellets. It was probable that the spray droplets produced were too big for the smaller pellets, causing over-wetting and encouraging the formation of liquid bridges (Hemati *et al.*, 2003). Once coalesced, smaller pellets would become difficult to separate, producing clusters of agglomerates which retained moisture within and further from the surface. In contrast, larger pellets, with lower specific surface area, had a lower propensity to agglomerate by nature (Smith and Nienow, 1983).

##### **A.2.4.1 Effects of change in airflow rate**

There was a greater increase in DE with increase in AF for smaller pellets than for larger pellets (Fig. 40a). The increase in DE was accompanied by marked reduction in the Agg for both pellet sizes, especially for smaller pellets (Fig. 40b), showing that the AF was a major factor affecting DE and agglomeration of particles during coating. Besides the improvement in DE, the increased movement of pellets with increased AF would help to break up liquid bridges. This probably resulted in the greater reduction in Agg of smaller pellets than larger pellets, which would have fewer agglomerates to breakup in the first place.

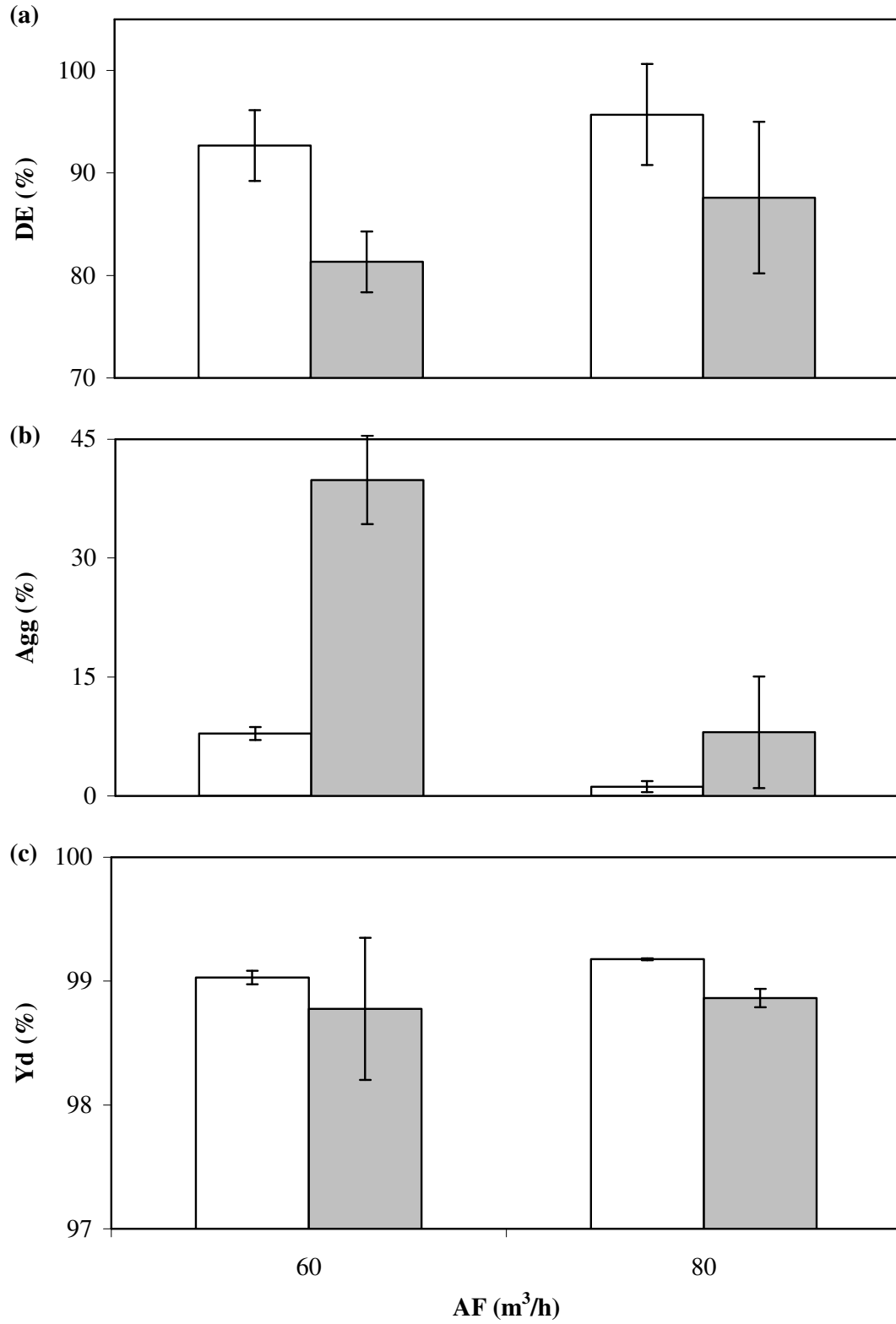


Fig. 40. Influence of AF on (a) DE, (b) Agg and (c) Yd of Precision-coated pellets of sizes 500 to 600 µm (clear) and 355 to 425 µm (shaded).



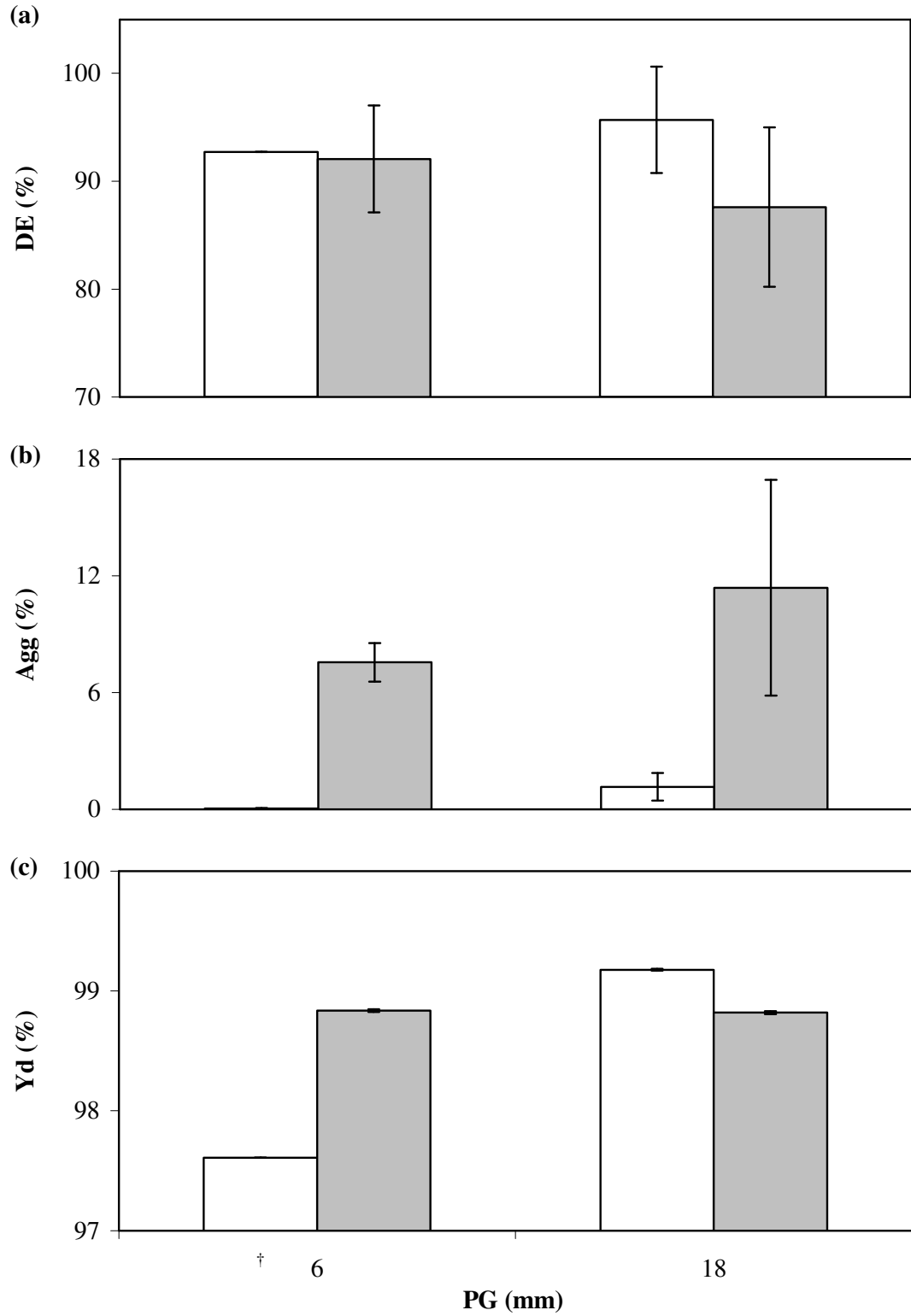


Fig. 41. Influence of PG on (a) DE, (b) Agg and (c) Yd of Precision-coated pellets of sizes 500 to 600  $\mu\text{m}$  (clear) and 355 to 425  $\mu\text{m}$  (shaded). ( $\dagger$ : n = 2)

The Yd of smaller pellets was generally lower than that of larger pellets, being more apparent at the higher AF (Fig. 40c). This shows that the smaller pellets were relatively more difficult to be coated when subjected to harsher conditions brought about by higher AF conditions. Thus, depending on the accepted level of Agg or Yd for the final product, AF should be carefully controlled in the coating of smaller pellets.

#### **A.2.4.2 Effect of change in partition gap**

The greater suction of pellets generated by smaller PGs was favorable in lowering Agg especially for smaller pellets. There was a slight increase in DE with larger PG for larger pellets, however, it did not cause much change to the Agg. For the smaller pellets, DE decreased and Agg increased substantially at a larger PG (Fig. 41a, b). Due to the lower air velocities at larger PG (Fig. 17), there was sluggish movement of pellets into and up the partition column, accompanied by more pellets falling downwards along the periphery of the coating zone. Although this effect would be more pronounced with larger pellets, their increase in Agg was not as much as that of smaller pellets. This indicates that the Agg of smaller pellets was more susceptible to changes in particle movement due to changes in PG than larger pellets.

There was an increase in the Yd with larger PG for the larger pellets (Fig. 41c). A smaller PG served to restrict the amount of pellets that could enter the partition column. While the smaller pellets were not markedly affected by the smaller PG due to their size, the larger pellets were more restricted. This might have caused the pellet mass flow into the partition column to be scarce and the lower pellet proximity resulted in the loss of coating material to the surrounding partition column wall.

Hence, a small PG may be used to achieve a lower Agg but it is important to balance pellet mass flow into the partition column.

Smaller pellets were harder to dry and required a higher AF condition to improve the DE and reduce the Agg level. However, the higher AF caused the Yd to be compromised due to potential increase in attrition for smaller pellets. A smaller PG provided stronger suction of pellets, more vibrant pellet flow and was favorable in reducing Agg especially for smaller pellets. Smaller PG restricted the mass flow of larger pellets into the partition column and resulted in loss of material to spray drying effect or deposition on the wall of the partition column. Hence, careful considerations must be made to ensure adequate drying, low Agg and acceptable Yd for a coating process, especially for more challenging situations like the attempt to coat smaller particulates using bottom-spray air suspension system.

## **B Coating of fine lactose particles**

From the above studies conducted, the suitability of bottom-spray air suspension processes and the influences of various processing variables on the coating conditions and product quality were better understood. This enabled better choice of coating equipment and processing conditions for the following studies.

For the coating of fine particles, lactose was chosen as the core particles as it is an inert and commonly used pharmaceutical excipient. HPMC was used as the film forming polymer as it is widely used as a film coating material for pharmaceuticals. Plasticizer was not used due to possible confounding effects with insoluble additives (Okhamafe and York, 1984b).

Nano-CaCO<sub>3</sub> was evaluated for potential anti-tack property in the prevention of pellet agglomeration. Nano-CaCO<sub>3</sub> has a good safety profile, being able to dissolve in acid and hence less likely to cause toxic accumulation in the body as compared to other hydrophobic nanoparticle counterparts (Jani *et al.*, 1994). Calcium carbonate reacts with the acidic gastric juices to produce carbon dioxide gas, which can prolong residence time of the dosage units in the stomach (Davies *et al.*, 1994). It was also found to be an effective sustained release carrier for a hydrophilic drug and a bioactive protein (Ueno *et al.*, 2005).

The small size and hydrophobic nature of nano-CaCO<sub>3</sub> also renders it possible to be used as a surface modifying agent. Larger hydrophobic particles would not adhere to fine powders without binder and would dislodge easily. It was postulated that due to its small size, the nano-CaCO<sub>3</sub> would adhere onto particles by electrostatic and/or van der Waal's forces. This would allow the nano-CaCO<sub>3</sub> to be adhered onto the lactose surfaces loosely, forming a dry lubricating layer around each particle. In addition to

the lubricating effect, the surface layer also imparts greater hydrophobicity to the surface of the particles.

Hence, in the following experiments, two modes of application of nano-CaCO<sub>3</sub> were evaluated for its anti-tack effects. Nano-CaCO<sub>3</sub> were sprayed onto core lactose particles as a surface modifying agent prior to film coating, or incorporated into the coating formulation as an additive. The amounts of nano-CaCO<sub>3</sub> used for surface modification and as additive were similar in the two studies to enable meaningful comparison of the two modes of application of nano-CaCO<sub>3</sub>. However, they were expressed in different percentages according to the conventional method of expressing additives as a percentage of the film coating polymer and the surface agents as a percentage of the core particles.

The experimental designs did not include the comparison of nano-CaCO<sub>3</sub> with micron sized CaCO<sub>3</sub>, which would be crucial for the assessment of the benefits of using nano-sized particles over more commonly encountered micron-size particles. This was because preliminary studies carried out using micron-size particles incorporated into the HPMC coating formulations resulted in nozzle clogs which disrupted the runs. Neat suspensions of micron-size CaCO<sub>3</sub> could not be kept suspended during the run, hence making the surface modification study impractical to carry out. The use of strong suspending agents to prepare micronized CaCO<sub>3</sub> suspension was not carried out as this would not be quite comparable as the nano-CaCO<sub>3</sub> formulations used. Henceforth, the studies were only carried out using nano-CaCO<sub>3</sub>.

## **B.1 Influence of calcium carbonate nanoparticles as a surface modifying agent on Precision coating of lactose particles**

### **B.1.1 Effects of nano-CaCO<sub>3</sub> concentrations on the coated lactose particles**

Water, when used alone in the surface modification step, served as the control group which the other treatment groups were compared against. When used as a surface modifying agent, nano-CaCO<sub>3</sub> only affected the sizes of smaller particles amongst the HPMC coated particles and did not significantly affect the sizes of the larger particles when compared to the control group (Fig. 42). There were no significant changes in the D<sub>90</sub> values for all the concentrations of nano-CaCO<sub>3</sub> and only a significant reduction in the D<sub>50</sub> value at 0.3 % w/w. However, the D<sub>10</sub> values were significantly reduced to varying extents, depending on nano-CaCO<sub>3</sub> concentrations. In the control group, the D<sub>10</sub> of coated lactose particles was significantly larger than those of nano-CaCO<sub>3</sub> treated particles. This suggested that nano-CaCO<sub>3</sub> exhibited anti-tack behaviour only for particles which were very small (< 100 μm) and this effect was dependent on the concentration of nano-CaCO<sub>3</sub> used. As a result, the spans were higher when nano-CaCO<sub>3</sub> was used because there were little changes to D<sub>50</sub> and D<sub>90</sub> while D<sub>10</sub> was decreased (Fig. 43).

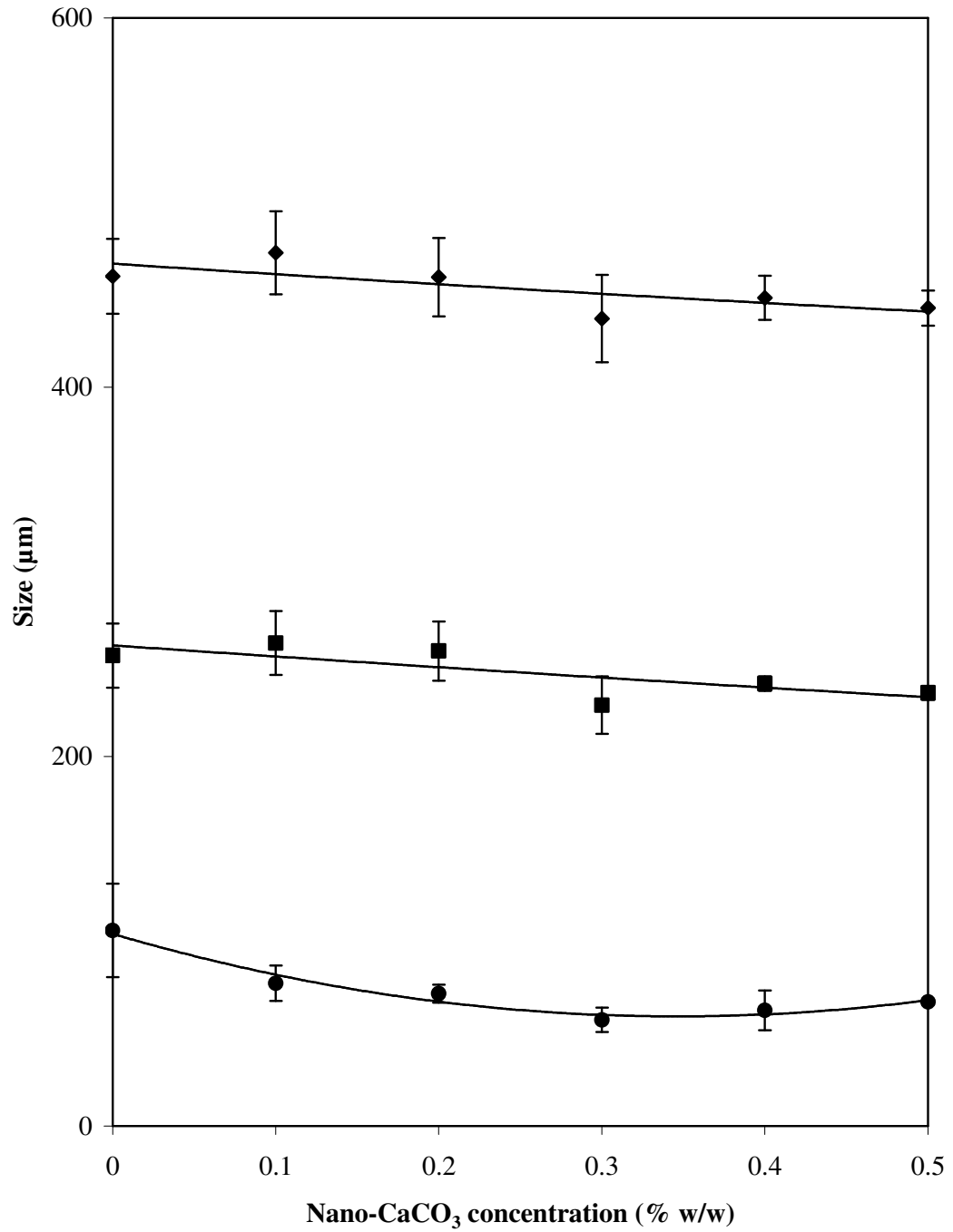


Fig. 42. Effect of nano-CaCO<sub>3</sub> concentration on the D<sub>10</sub> (●), D<sub>50</sub> (■) and D<sub>90</sub> (◆) values of HPMC-coated lactose particles.

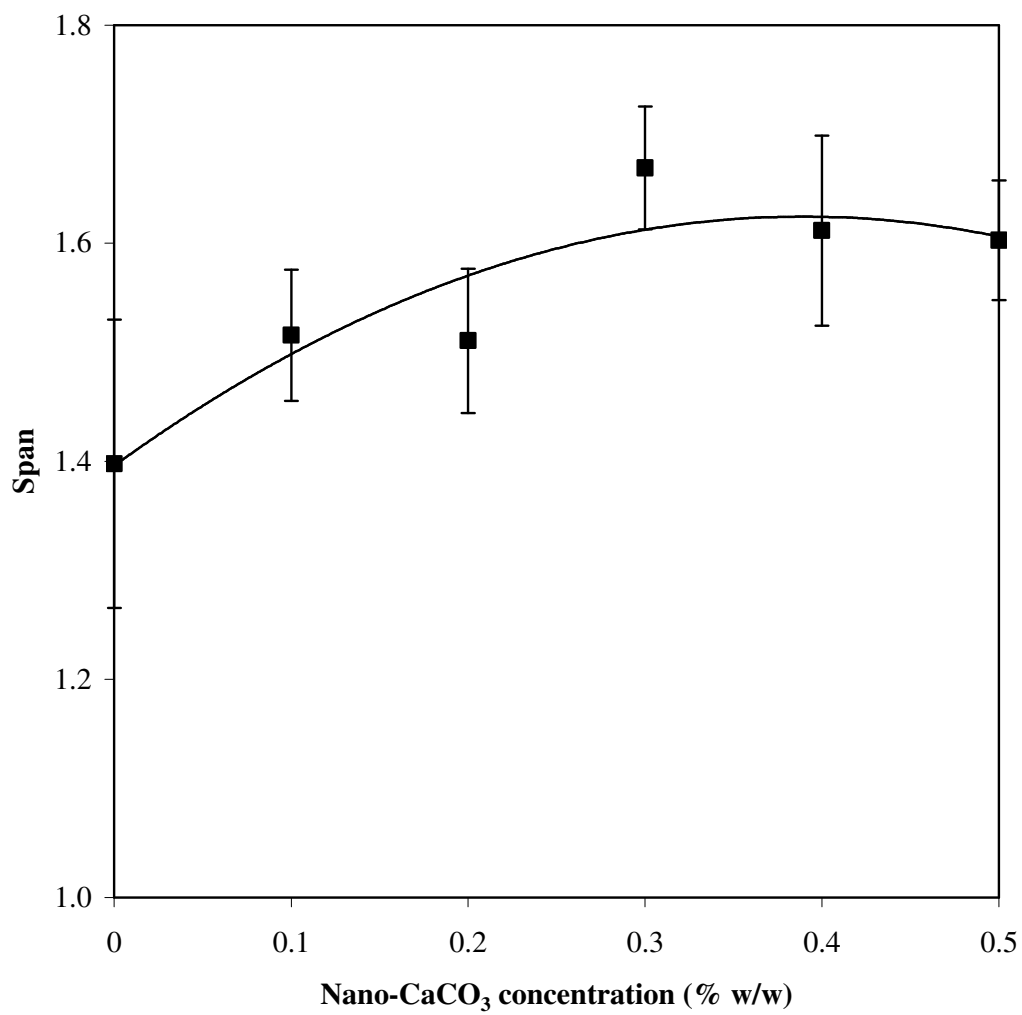


Fig. 43. Effect of nano-CaCO<sub>3</sub> concentrations on the span of HPMC-coated lactose particles.



### **B.1.2 Effects of nano-CaCO<sub>3</sub> concentration on core lactose particles**

The ability of nano-CaCO<sub>3</sub> in preventing the agglomeration of core particles during subsequent coating with HPMC solution shows that the properties of the lactose particles were changed. Hence, the surface modified core particles were characterized to identify the properties that could have brought about the decreased tendency of agglomeration. Scanning electron micrographs of individual core lactose particles which were surface-modified with various amounts of nano-CaCO<sub>3</sub> did not show any apparent differences between the core particles (Fig. 44).

A higher magnification enabled the nano-CaCO<sub>3</sub> to be seen on the surfaces of the lactose particles (Fig. 45). This shows that the nano-CaCO<sub>3</sub> had indeed been deposited onto the surface of the lactose particles. This was most apparent for cores with the highest concentration of nano-CaCO<sub>3</sub> (0.5 % w/w) as illustrated in Fig. 45. Calculations show that surface coverage of lactose with nano-CaCO<sub>3</sub> reached approximately 100 % at nano-CaCO<sub>3</sub> concentration of 0.4 % w/w (Table 8).

The size of surface coated lactose particles increased significantly when the concentration of nano-CaCO<sub>3</sub> was increased to 0.2 and 0.3 % w/w, and decreased significantly when the concentration of nano-CaCO<sub>3</sub> was further increased to 0.4 and 0.5 % w/w (Fig. 46). With increasing concentration of nano-CaCO<sub>3</sub>, there was initially a decrease in span at concentrations of 0.2 to 0.3 % w/w, followed by an increase in span at higher concentrations (Fig. 47). In order to understand the changes in physical dimension, the aspect ratio and sphericity of the particles were determined.

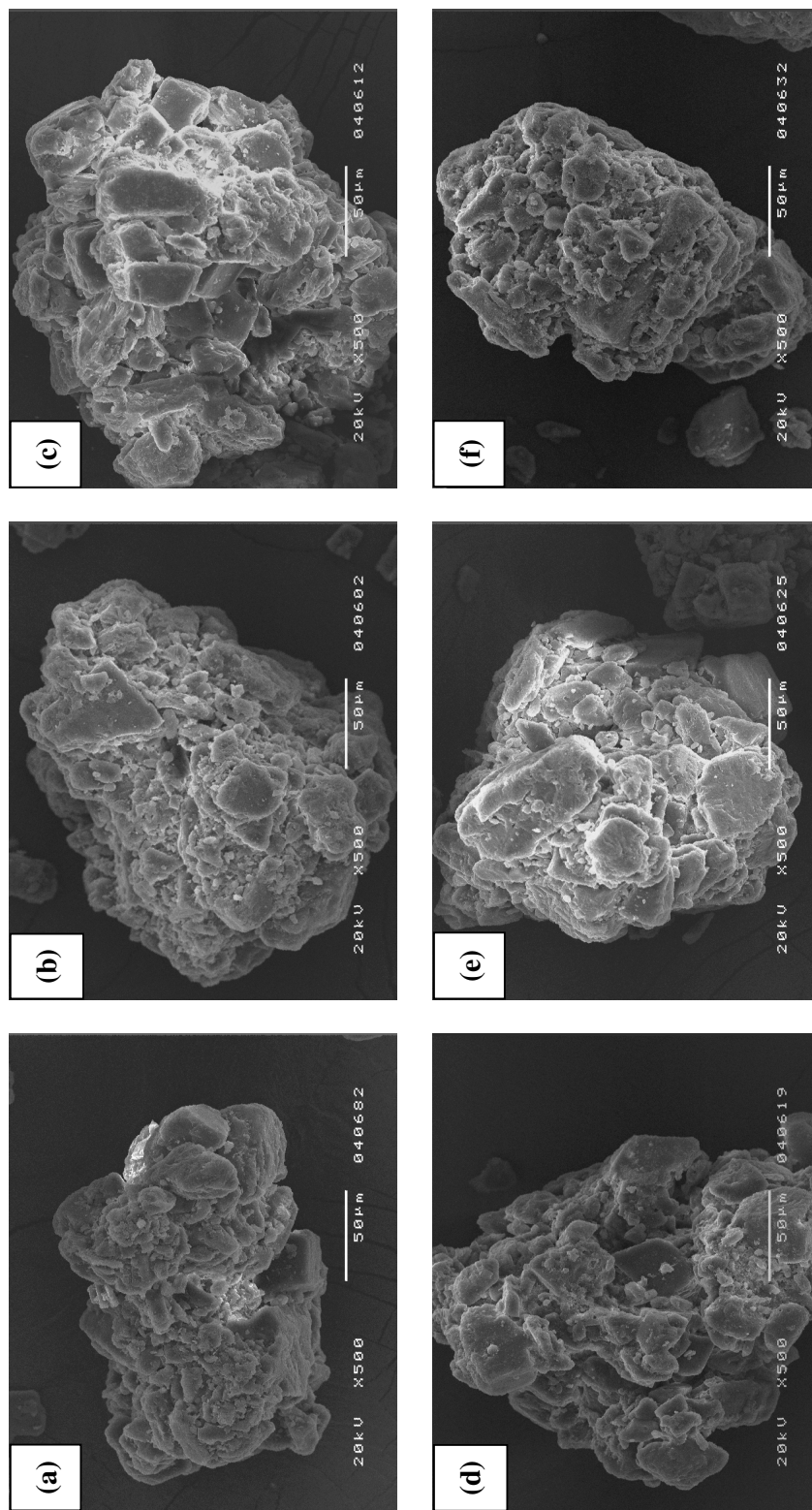


Fig. 44. Scanning electron photomicrographs of core lactose particles sprayed with (a) water and nano-CaCO<sub>3</sub> suspensions to a nano-CaCO<sub>3</sub> concentration of (b) 0.1 % w/w, (c) 0.2 % w/w, (d) 0.3 % w/w, (e) 0.4 % w/w and (f) 0.5 % w/w. (× 500 magnification)

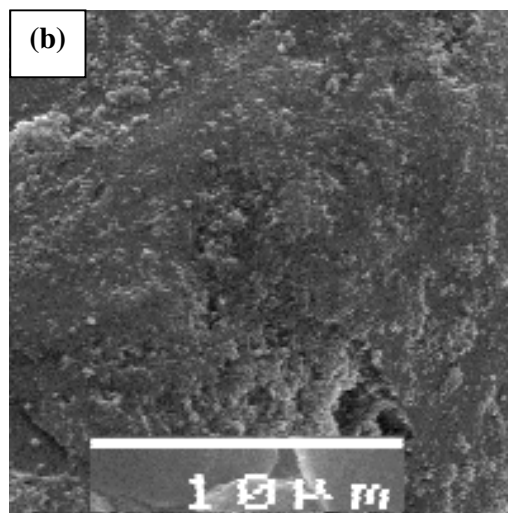
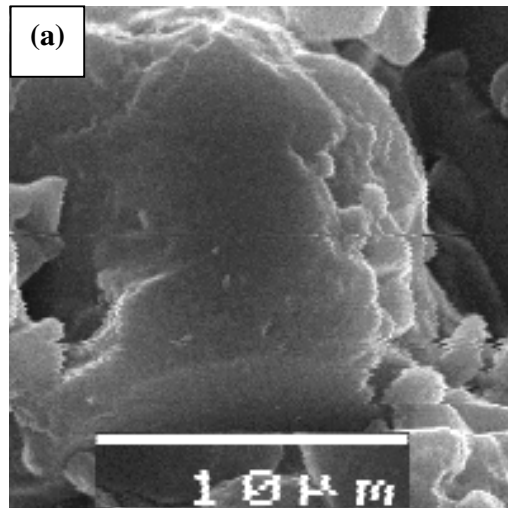


Fig. 45. Scanning electron photomicrographs of core lactose particles sprayed with (a) water and (b) nano-CaCO<sub>3</sub> suspension to a nano-CaCO<sub>3</sub> concentration of 0.5 % w/w. (× 2000 magnification)

Table 8. Surface coverage of lactose with nano-CaCO<sub>3</sub>

<b>Concentration of nano-CaCO<sub>3</sub> (% w/w)</b>	<b>Coverage (%)</b>
0	0
0.1	24.0
0.2	47.9
0.3	71.9
0.4	95.8
0.5	120

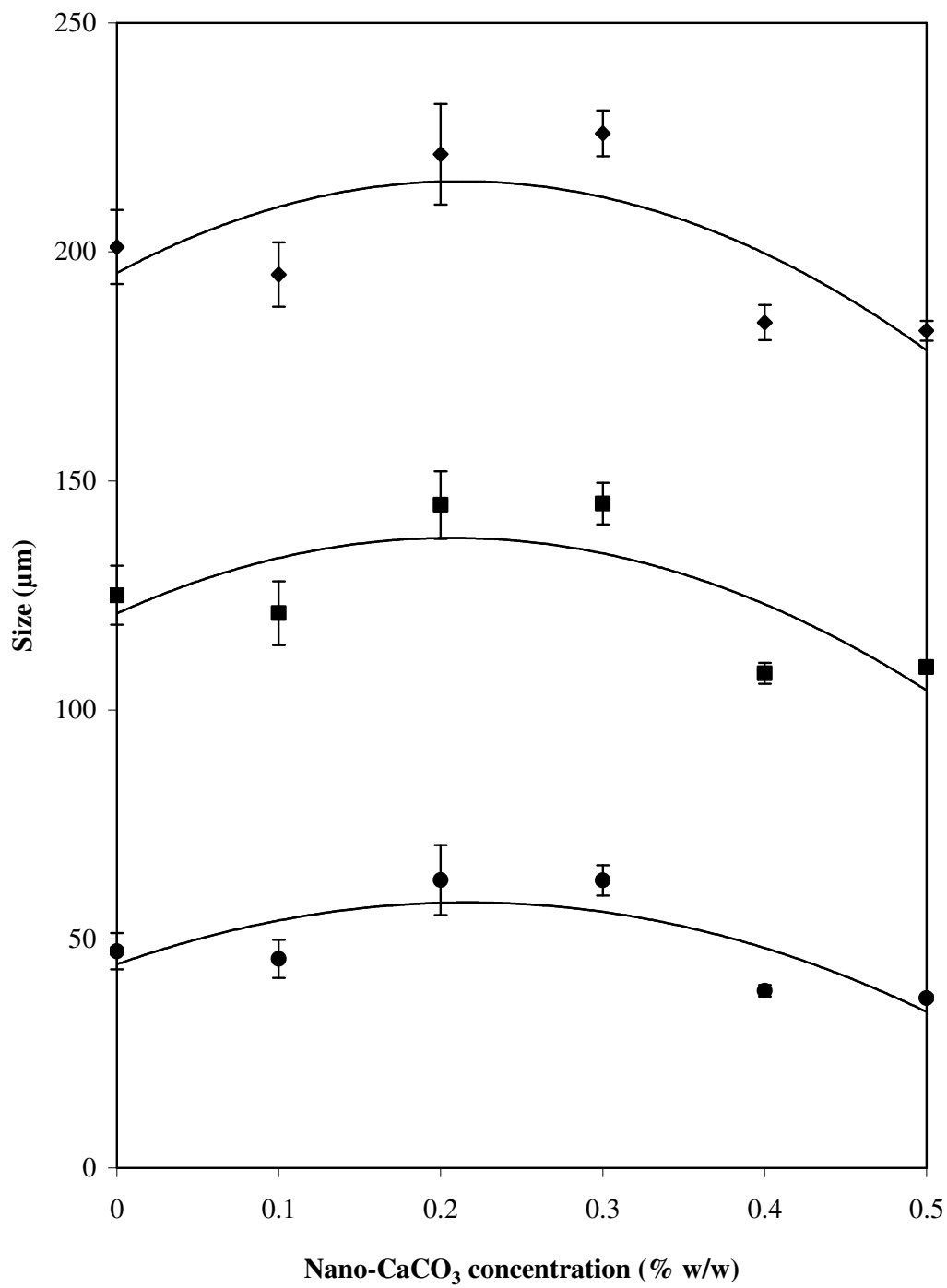


Fig. 46. Effect of nano-CaCO<sub>3</sub> concentrations on the D<sub>10</sub> (●), D<sub>50</sub> (■) and D<sub>90</sub> (◆) values of core lactose particles.

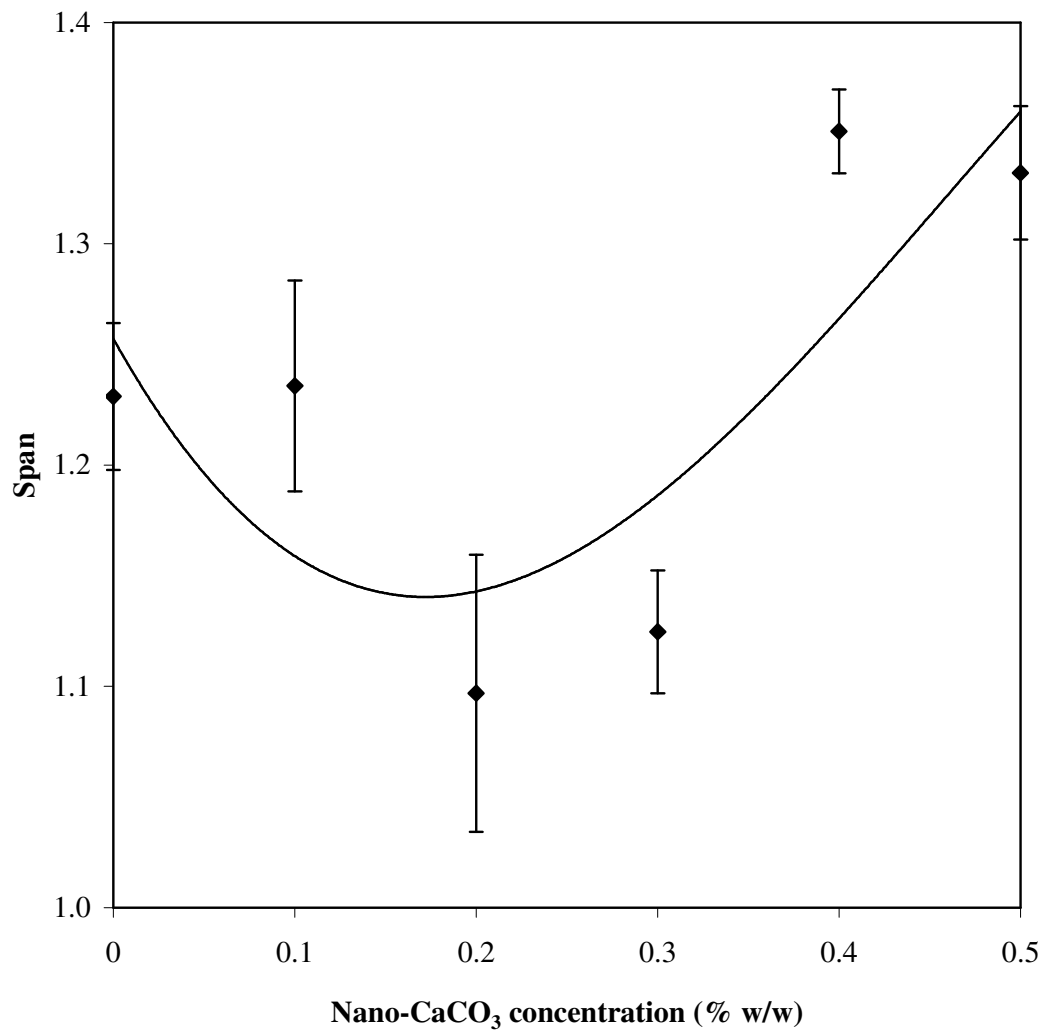


Fig. 47. Effect of nano-CaCO<sub>3</sub> concentrations on the span of core lactose particles.

There were no significant changes in aspect ratio as the concentration of nano-CaCO<sub>3</sub> increased, indicating that there were no major breakdown or aggregation of particles (Fig. 48a). However, the particles became more spherical with increasing concentration of nano-CaCO<sub>3</sub> (Fig. 48b). There was a significant increase in the sphericity of the particles modified with 0.4 and 0.5 % w/w nano-CaCO<sub>3</sub> concentration compared to the particles of the control group ( $p < 0.05$ ).

Surface roughness, Ra, show smoothening of particle surfaces with increase in nano-CaCO<sub>3</sub> concentration (Fig. 49a). The roughness seemed to plateau beyond 0.4 % w/w of nano-CaCO<sub>3</sub>. As the nano-CaCO<sub>3</sub> applied was a small percentage of the lactose load, it was unlikely that the smoothening was due to the filling up of crevices by the nano-CaCO<sub>3</sub>. Lactose surfaces were more likely to be smoothened by filling of the surface crevices by lactose fines or by attrition of fine protuberances from the surface.

The coated lactose shows improved flow with increase in nano-CaCO<sub>3</sub> concentration as seen in the smaller angle of repose (Fig. 49b). The improved flow could be due to the coating of nano-CaCO<sub>3</sub> on the surfaces of lactose particles, creating a physical barrier between lactose particles. As the cohesion between nano-CaCO<sub>3</sub> particles would be expected to be lower than that of lactose particles, the nano-CaCO<sub>3</sub> prevented the lactose particles from sticking together, consequently improving their flow. This effect reached a plateau at around 0.4 to 0.5 % w/w of nano-CaCO<sub>3</sub> concentration, probably due to saturation of the lactose surfaces with nano-CaCO<sub>3</sub> (Table 8). Beyond the saturation point, all the surfaces of lactose would have been covered with nano-CaCO<sub>3</sub>, and any extra addition of nano-CaCO<sub>3</sub> would not change the surface properties of lactose. In addition to acting as a physical barrier between lactose particles, the nano-CaCO<sub>3</sub> helped to lubricate the lactose particles as shown by

the improvement of flow with higher concentrations of nano-CaCO<sub>3</sub> (Fig. 49b). As the nano-CaCO<sub>3</sub> were small in size, it was postulated that their adhesion to the lactose was by electrostatic and/or van der Waal's forces. Hence, nano-CaCO<sub>3</sub> could have acted as nano-sized ball bearings, providing dry lubrication to the particles and enhancing the flow of particles.

At low concentrations, the improved flow and increased collision between particles caused fines to be compacted into the crevices of the lactose particles increasing the size of lactose particles (Fig. 46), reducing the sphericity (Fig. 48b) and decreasing the roughness (Fig. 49a). At higher nano-CaCO<sub>3</sub> concentrations, there was no further decrease in the roughness while the size of core lactose particles decreased. This suggested that surface remodeling of lactose particles took place, resulting in smaller and more spherical lactose particles.

The effects of surface modification by nano-CaCO<sub>3</sub> coating of lactose particles were initially favourable, as improved flow and smoother surfaces reduced agglomeration propensity of particles. However, as the improvement in flow properties lessened beyond 0.3 % w/w nano-CaCO<sub>3</sub> concentration (Fig. 49b), there was no further reduction in D<sub>10</sub> of coated lactose particles (Fig. 42). Angle of repose correlated significantly ( $p = 0.005$ ) with the D<sub>10</sub> of the corresponding HPMC-coated particles as indicated by an R<sup>2</sup> value of 0.86. This shows that flow property of core particles was a major factor affecting their agglomeration tendency during subsequent HPMC coating. Possibly, the surface modification benefited the smaller size fractions of lactose particles more as they would have poorer flow properties. Hence, surface modification of lactose particles with nano-CaCO<sub>3</sub> would potentially be advantageous for fine particles with poor flow properties.



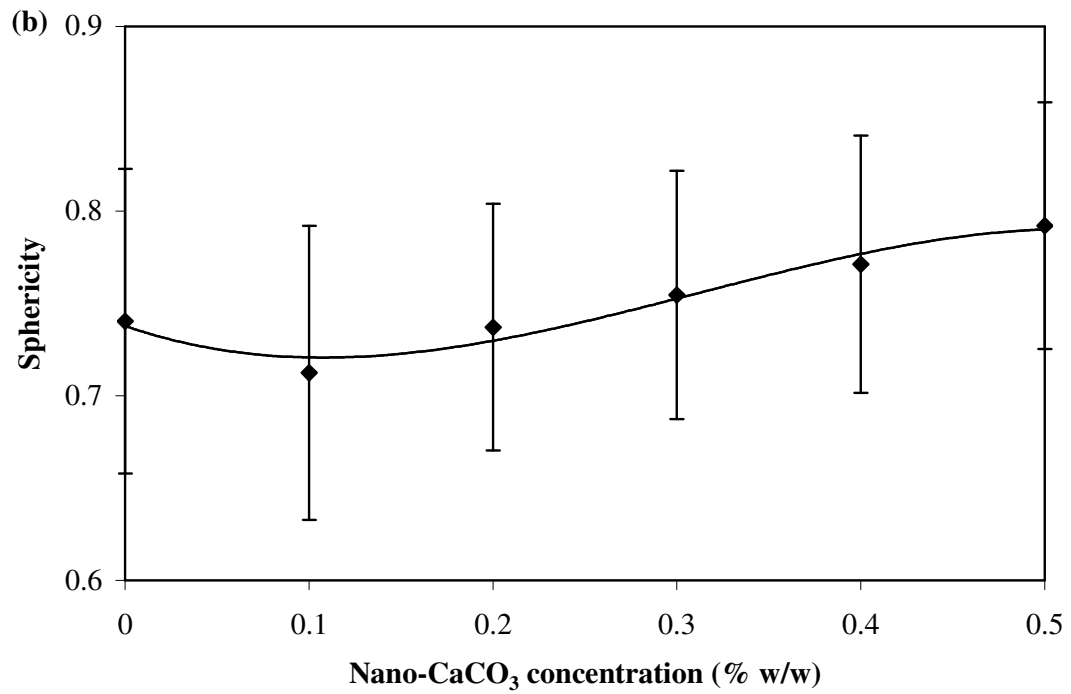
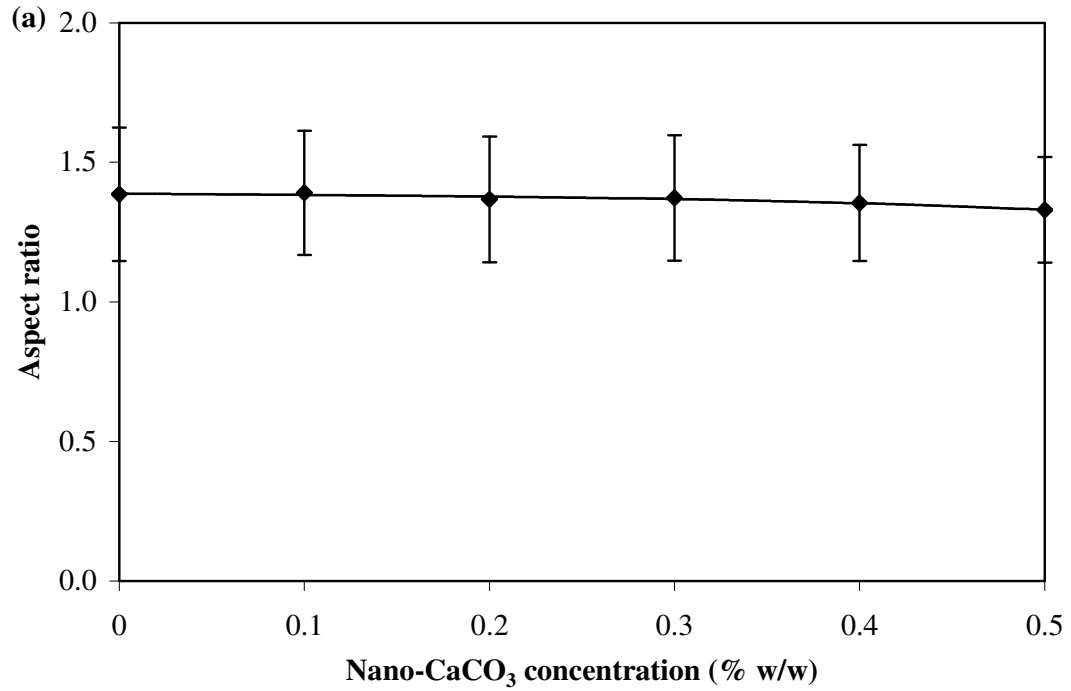


Fig. 48. Effect of nano-CaCO<sub>3</sub> concentration on the (a) aspect ratio and (b) sphericity of core lactose particles.

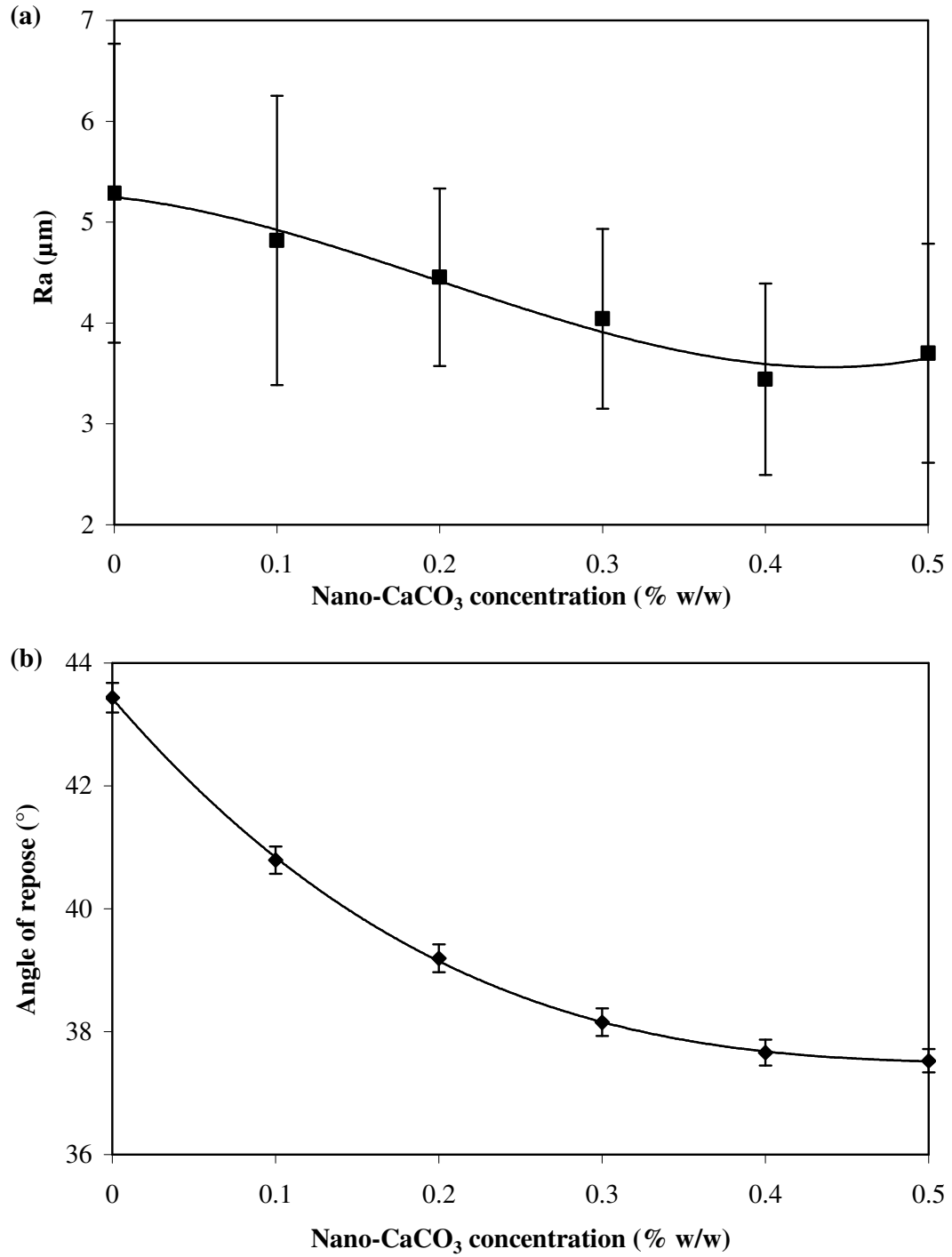


Fig. 49. Effect of nano-CaCO<sub>3</sub> concentration on the (a) Ra and (b) angle of repose of core lactose particles.

## **B.2 Influence of calcium carbonate nanoparticles as an anti-tack additive on Precision coating of lactose particles**

### **B.2.1 Effects of nano-CaCO<sub>3</sub> concentration on coated lactose particles**

Lactose particles coated with HPMC solution was used as the control group. Upon coating, the size of lactose particles changed to different extents with different concentrations of nano-CaCO<sub>3</sub> used (Fig. 50). Coating formulations containing nano-CaCO<sub>3</sub> resulted in significant decrease of D<sub>10</sub>, D<sub>50</sub> and D<sub>90</sub> of coated lactose as compared to those coated by HPMC alone. Increasing concentrations of nano-CaCO<sub>3</sub> caused a decrease in D<sub>10</sub>, D<sub>50</sub> and D<sub>90</sub>, reaching a minima at around the concentration of 6 % w/w. This shows that the concentration of nano-CaCO<sub>3</sub> in the coating formulation was important in influencing the anti-tack effect of the coating formulation.

However, the span values of coated particles obtained over the nano-CaCO<sub>3</sub> concentrations of 2 % w/w to 10 % w/w were similar (Fig. 51), showing that there was overall suppression of agglomeration of all the size fractions of particles when the additive was used. The span was larger than that of particles coated in the control group. This could be attributed to the greater degree of reduction in the D<sub>10</sub> values of the particles coated with nano-CaCO<sub>3</sub> additive as compared to the D<sub>10</sub> of particles coated without nano-CaCO<sub>3</sub>.

### **B.2.2 Effects of nano-CaCO<sub>3</sub> concentration on the coating formulations**

The agglomeration observed in coated lactose particles could be attributed to the tackiness of the HPMC coating formulations as the size changes of the coated lactose particles corresponded to the tack values of the HPMC coating formulations (Fig. 52).

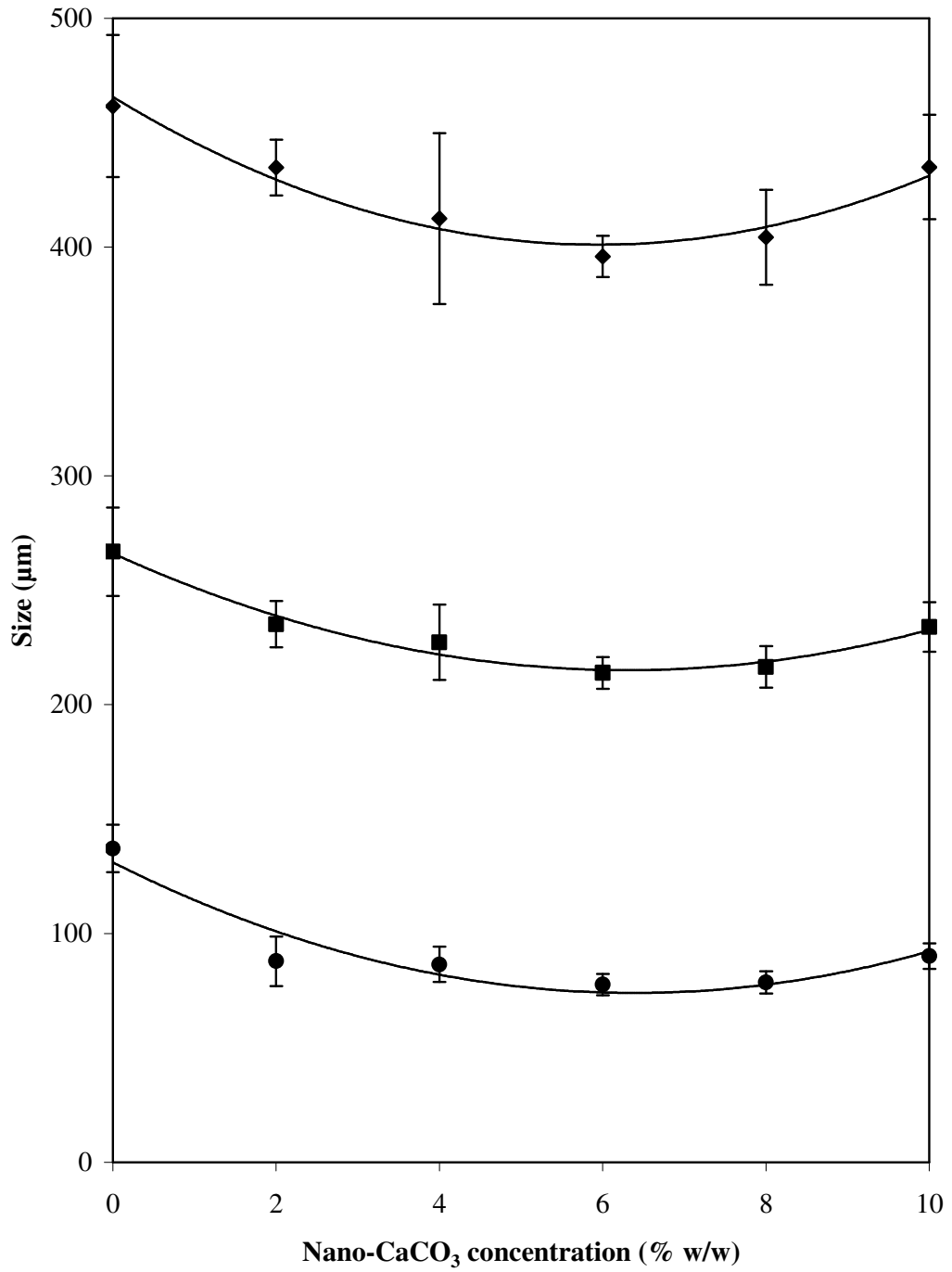


Fig. 50. Effect of nano-CaCO<sub>3</sub> concentration on the D<sub>10</sub> (●), D<sub>50</sub> (■) and D<sub>90</sub> (◆) of HPMC-coated lactose particles.

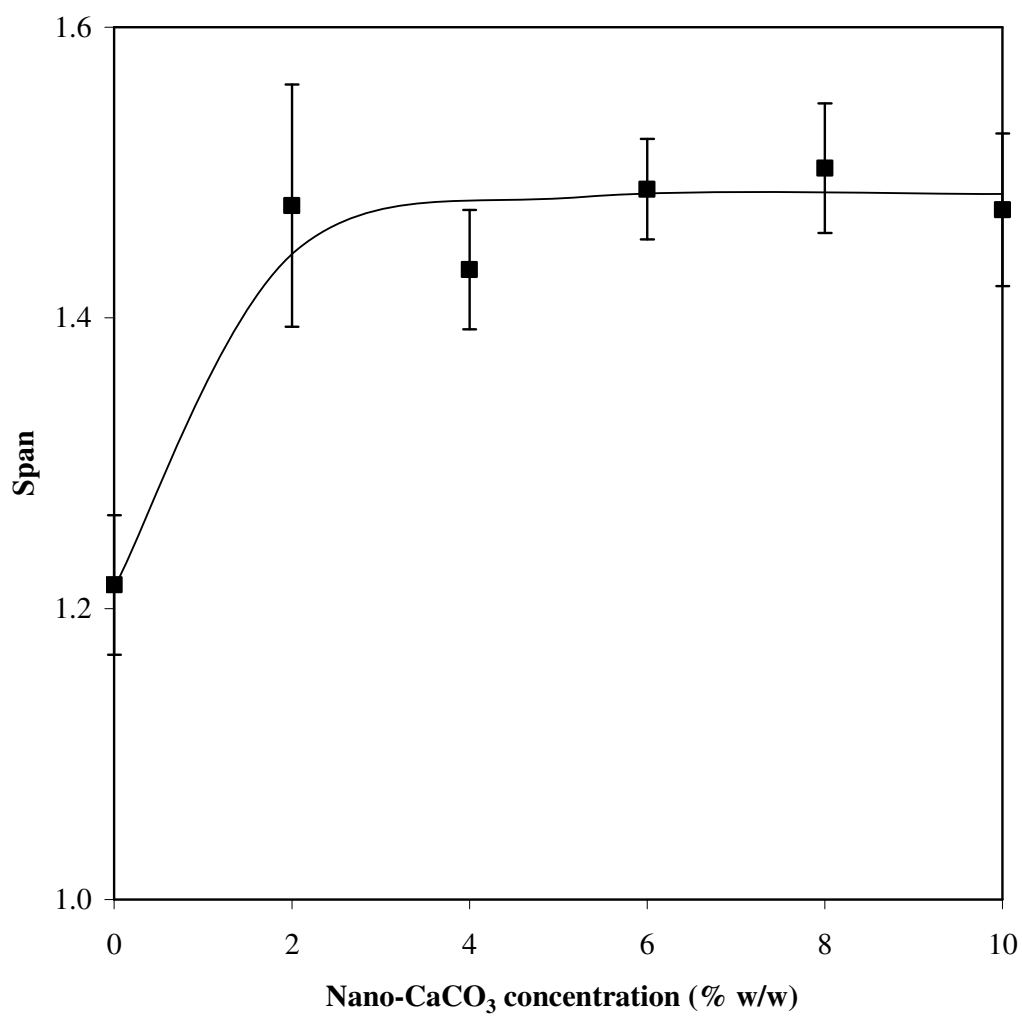


Fig. 51. Effect of nano-CaCO<sub>3</sub> concentration on the span of HPMC-coated lactose particles.

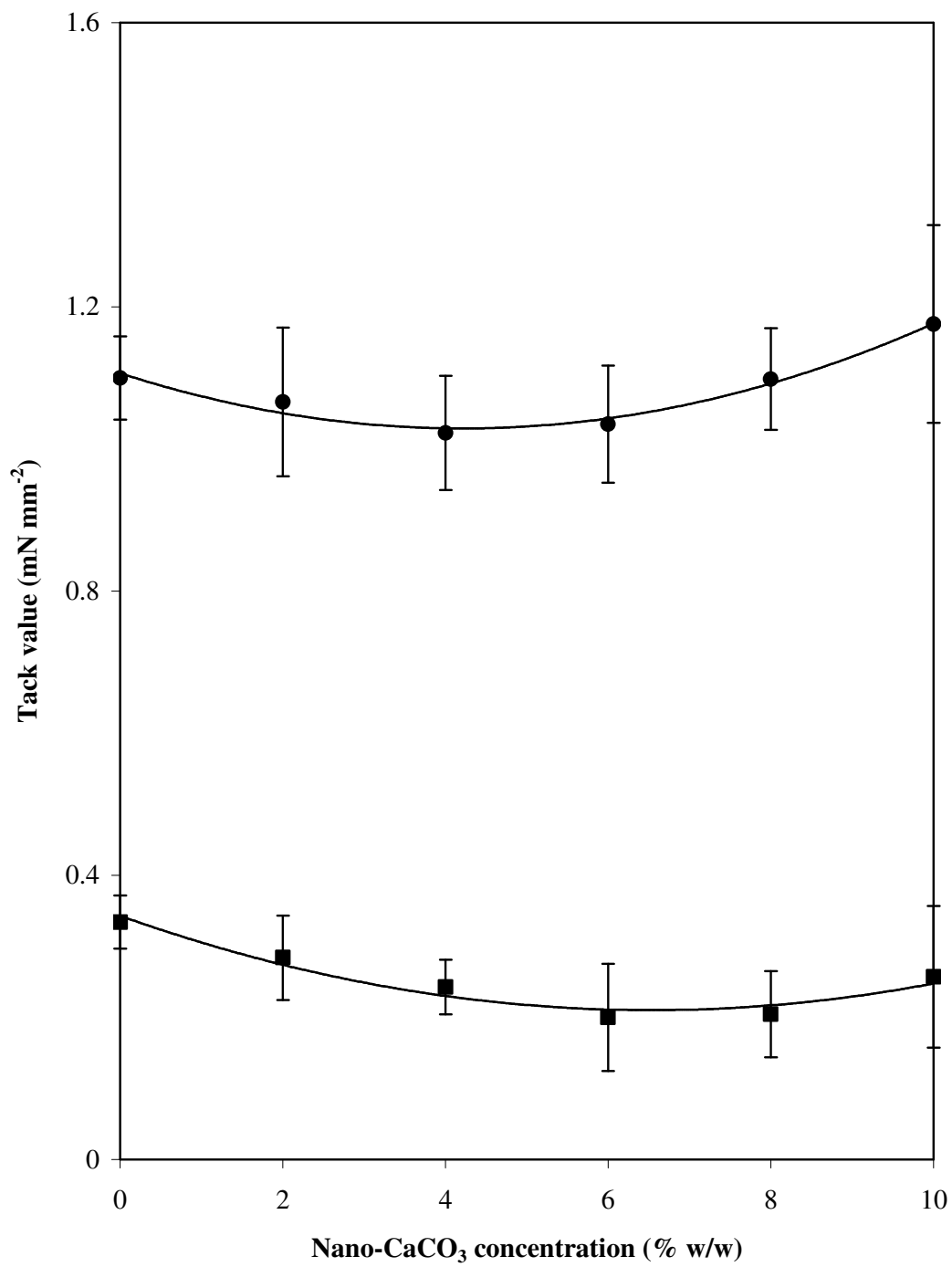


Fig. 52. Effect of nano-CaCO<sub>3</sub> concentration on the tack values of neat suspensions (■) and HPMC suspensions (●).

A reduction in tackiness of the media was observed when nano-CaCO<sub>3</sub> was suspended in both water and HPMC solution (Fig. 52). Tack values of the HPMC coating formulations decreased with increasing nano-CaCO<sub>3</sub> concentrations, reaching a minimal at the concentration of 4 to 6 % w/w, then increased at higher concentrations. For neat suspensions, the tack values were much lower than those of HPMC formulations due to the comparatively lower tack of water. Increasing concentrations of nano-CaCO<sub>3</sub> reduced the tack value of water, with the minima observed at the concentrations of 6 to 8 % w/w. This indicates that the physical presence of nano-CaCO<sub>3</sub> in suspension, whether in water or HPMC solution, was able to bring about small reductions in tackiness. The nano-CaCO<sub>3</sub> disrupted the continuity of the liquid media, thereby decreasing their adhesion to surfaces.

Further increase in the nano-CaCO<sub>3</sub> concentration, from 6 to 10 % w/w, led to a greater increase in tack value of HPMC coating formulations than the neat suspensions. Being a dispersed system of insoluble particles in aqueous media, physical or chemical changes could occur. Depending on the nano-CaCO<sub>3</sub> concentration, the changes in properties of the coating formulation could differ. Hence, further tests were done to investigate the factors affecting the anti-tack effect.

Viscosity of the coating material has been found to be one of the causes of agglomeration in coating (Wong *et al.*, 2002). Coating formulations with higher viscosities face greater resistance to flow and may form larger spray droplets upon atomization, both hindering the spread and drying of sprayed droplets over the core particle surfaces.

Increasing concentrations of nano-CaCO<sub>3</sub> increased the viscosity of the HPMC coating formulations and neat suspensions (Fig. 53).

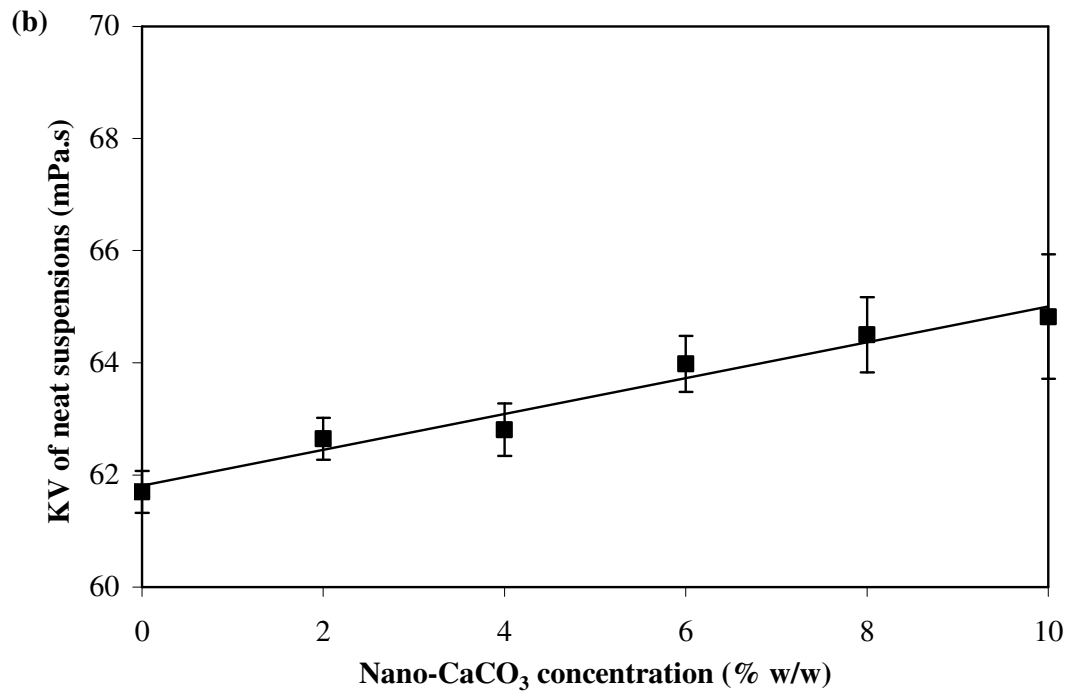
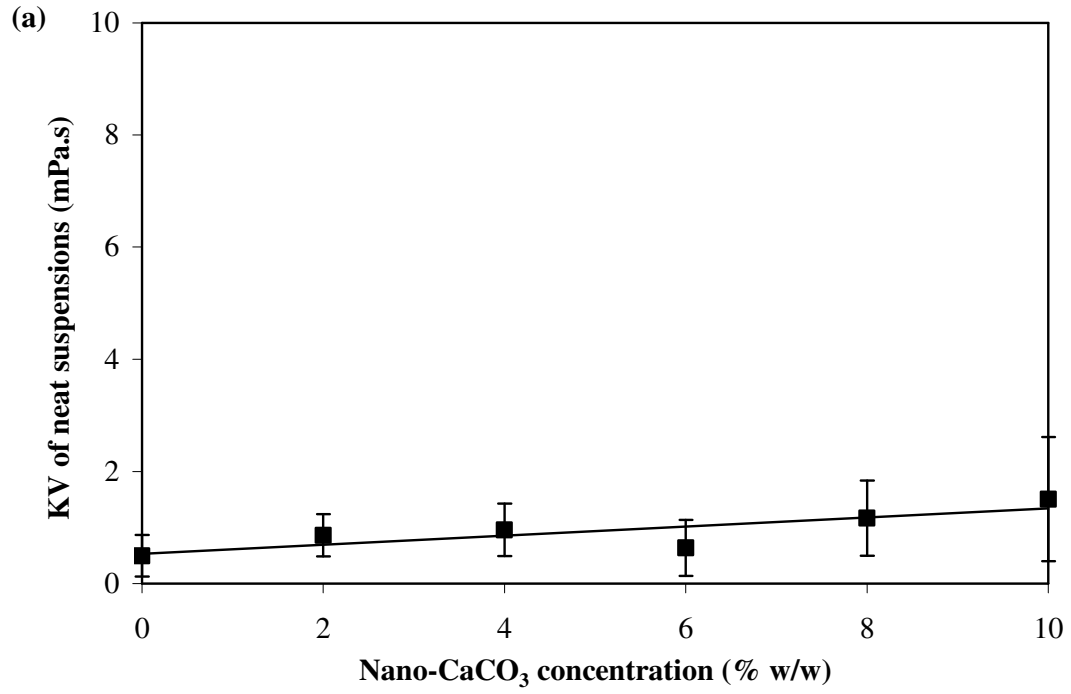


Fig. 53. Effect of nano-CaCO<sub>3</sub> concentration on the kinematic viscosity, KV, of (a) neat suspensions and (b) HPMC suspensions.



Being suspended in the liquid media, increasing concentrations of nano-CaCO<sub>3</sub> would reduce interparticulate distances between the nano-CaCO<sub>3</sub> and increased the tendency to aggregate. The larger the extent of aggregation, the higher will be the resistance to liquid flow and this contributed to an increase in the viscosity of the suspension as seen in Fig. 53. At very high nano-CaCO<sub>3</sub> concentrations, flocculation occurred by the formation of an interlinking network of nano-CaCO<sub>3</sub>. The network of floccules may entrap and disrupt the continuous phase, further increasing suspension viscosity.

Although changes in viscosity helped in the understanding of how the structure of the suspension changed with different concentrations of nano-CaCO<sub>3</sub>, it did not account for the size changes of the coated lactose particles. In contrast to the general observation that higher viscosity can contribute to higher agglomeration tendency, the viscosity correlated inversely with the size of coated lactose particles from 0 to 6 % w/w of nano-CaCO<sub>3</sub> (Fig. 50 and 53). Moreover, neat suspensions of nano-CaCO<sub>3</sub> altered the tack values without reflecting the trend of the viscosity values. Hence, the rather small viscosity changes of the coating formulations was not of any critical attribute affecting the anti-tack activity. Instead, it was some other factor(s) which influenced tack properties of the suspensions.

Surface tension of the coating media is known to affect the spreading and adhesion of the coat over the substrate surface during coating (Machiste and Buckton, 1996). HPMC, being a macromolecule with hydrophobic cellulose chains and hydrophilic hydroxypropyl groups, preferentially adsorbs at the liquid-air interface, reducing the surface tension of water from 72 dynes cm<sup>-1</sup> to 48 dynes cm<sup>-1</sup> (Fig. 54). Nano-CaCO<sub>3</sub> itself did not exhibit any appreciable surface activity when dispersed in water. However, when increasing concentrations of nano-CaCO<sub>3</sub> were added to the HPMC

solution, the surface tension increased steadily. This indicates that nano-CaCO<sub>3</sub> caused reduced HPMC presence at the liquid interface probably due to adsorption.

Calcium carbonate was found to be an adsorbent for various polymers (El-Sherbiny and Xiao, 2004). Nano-CaCO<sub>3</sub>, being hydrophobic, would have served as a good adsorbent in the HPMC solution, binding with the non-polar carbon chains of HPMC. The resultant increase in surface tension was small and unlikely to have any appreciable effect on the tackiness of the coating formulations. Instead, the loss of free HPMC strands in solution due to the adsorption onto nano-CaCO<sub>3</sub> was more likely to cause the decrease in tackiness of the HPMC coating formulations.

The adsorption of polymer chains by nano-CaCO<sub>3</sub> would have decreased the tackiness of the coating formulations when higher concentrations of nano-CaCO<sub>3</sub> were used. However, the tack values decreased to a minimum at about 6 to 8 % w/w and then increased with increasing concentration of nano-CaCO<sub>3</sub> (Fig. 52). The reason for the rise in tack activity was probably due to the greater impact of high viscosity. Hence, it could be concluded that tackiness of the coating formulation was affected by both adsorption of the polymer as well as dispersion viscosity and an optimal concentration of nano-CaCO<sub>3</sub> brought balance between these two conflicting effects leading to optimal anti-tack effect.

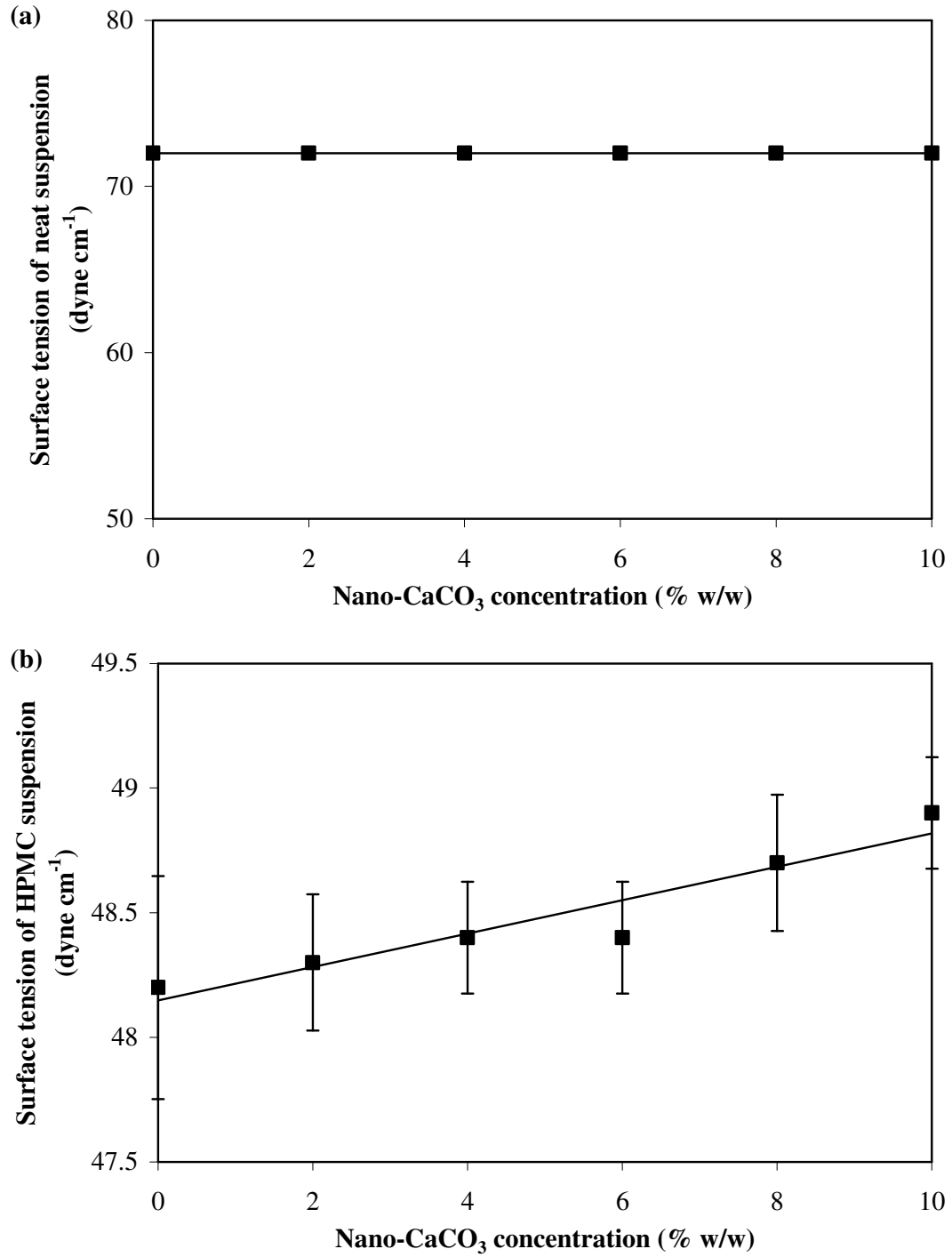


Fig. 54. Effect of nano-CaCO<sub>3</sub> concentration on the surface tension of (a) neat suspensions and (b) HPMC suspensions.

### B.2.3 Effects of nano-CaCO<sub>3</sub> concentration on the cast films

The influence of nano-CaCO<sub>3</sub> on the properties of film coat is important as it may adversely affect the quality of the coating besides influencing the coating process. Film coat strength can be affected by the insoluble additives as they can physically disrupt bonds between polymer chains leading to decreased film strength and elongation properties. When there is good chemical or physical interaction between additive and polymer, the resultant film can show increased tensile strength and decreased plastic elongation (Okhamafe and York, 1984b).

Although insoluble, nano-CaCO<sub>3</sub> may interact with HPMC. Evidence of any chemical interactions were sought by studying the FTIR spectra of the films prepared from coating formulations with different amounts of nano-CaCO<sub>3</sub> (Fig. 55). All spectra of the film samples show peaks at 3456 cm<sup>-1</sup> (O-H stretch), 2931 and 1464 cm<sup>-1</sup> (C-H stretch), and 1071 cm<sup>-1</sup> (C-O stretch) of the HPMC. The increase in prominence of the peak at 1464 cm<sup>-1</sup> with increasing nano-CaCO<sub>3</sub> content was probably contributed by the nano-CaCO<sub>3</sub> absorption band at 1440 cm<sup>-1</sup> (Fig. 55a) and no other significant spectra changes were detectable.

This was indicative that there were no marked chemical interaction between HPMC and nano-CaCO<sub>3</sub>. Sakata *et al.* (2006) proposed that Ca<sup>2+</sup> ions, an electron acceptor, interacted with HPMC, an electron donor, by forming hydrogen bonds. However, Dorozhkin (2000) found no evidence of interactions between the insoluble calcium phosphate and HPMC. Hence, the lack of interaction between HPMC and nano-CaCO<sub>3</sub> could be attributed to the lack of soluble Ca<sup>2+</sup> ions to react with HPMC due to the insolubility of nano-CaCO<sub>3</sub>. Thus, any effects of nano-CaCO<sub>3</sub> on HPMC films could be attributed to the physical presence of the nanoparticles.

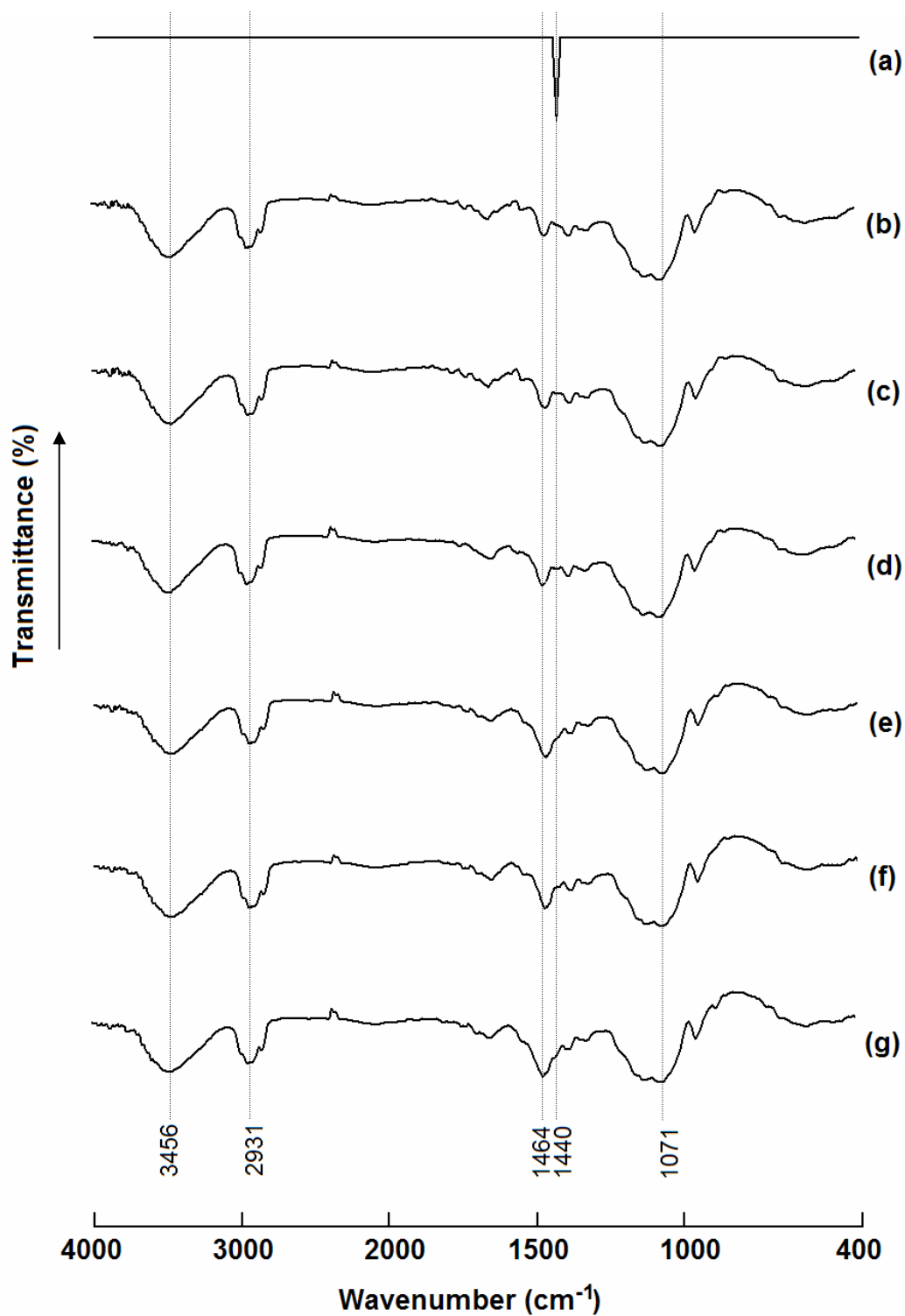


Fig. 55. FTIR spectra of (a) nano-CaCO<sub>3</sub>, and HPMC films with (b) 0 % w/w (c) 2 % w/w, (d) 4 % w/w (e) 6 % w/w, (f) 8 % w/w and (g) 10 % w/w nano-CaCO<sub>3</sub>.

Increasing amounts of nano-CaCO<sub>3</sub> in HPMC films decreased the mechanical strength of the films to a small extent, where the mechanical strength was defined by the maximum stress of the film at break point (Fig. 56a). This indicates that nano-CaCO<sub>3</sub> caused minor physical disruptions in the polymer film. These physical disruptions caused points of weaknesses or flaws in the film, causing the film to break easier when stretched. However, elasticity of the films did not change with increasing nano-CaCO<sub>3</sub> concentrations (Fig. 56b), showing that nano-CaCO<sub>3</sub> did not affect interaction between the polymer chains. Although there was a decrease in mechanical strength of the films with increasing concentrations of nano-CaCO<sub>3</sub>, all the films studied were not brittle and had good integrity.

The film surface roughness increased with increasing nano-CaCO<sub>3</sub> concentration (Fig. 57a), reaching a plateau at nano-CaCO<sub>3</sub> concentration of 6 to 10 % w/w. As the concentration of insoluble additive was increased, the critical pigment volume concentration (CPVC) was reached when there was insufficient polymer to surround all the insoluble particles (Gibson *et al.*, 1988). Glossiness would decrease with increasing pigment volume concentration and tend to remain constant once the CPVC was reached (Gibson *et al.*, 1988). Since glossiness could be directly related to surface roughness, the plateau in surface roughness indicates that the CPVC was reached at around 6 to 8 % w/w nano-CaCO<sub>3</sub>. However, film integrity remained good even after the CPVC was reached (Fig. 56). This was probably because nano-CaCO<sub>3</sub> was sufficiently small dimensionally to cause any major disruptions in polymer chains cross-linking. Thus, although the CPVC was reached, the mechanical properties were not adversely affected.

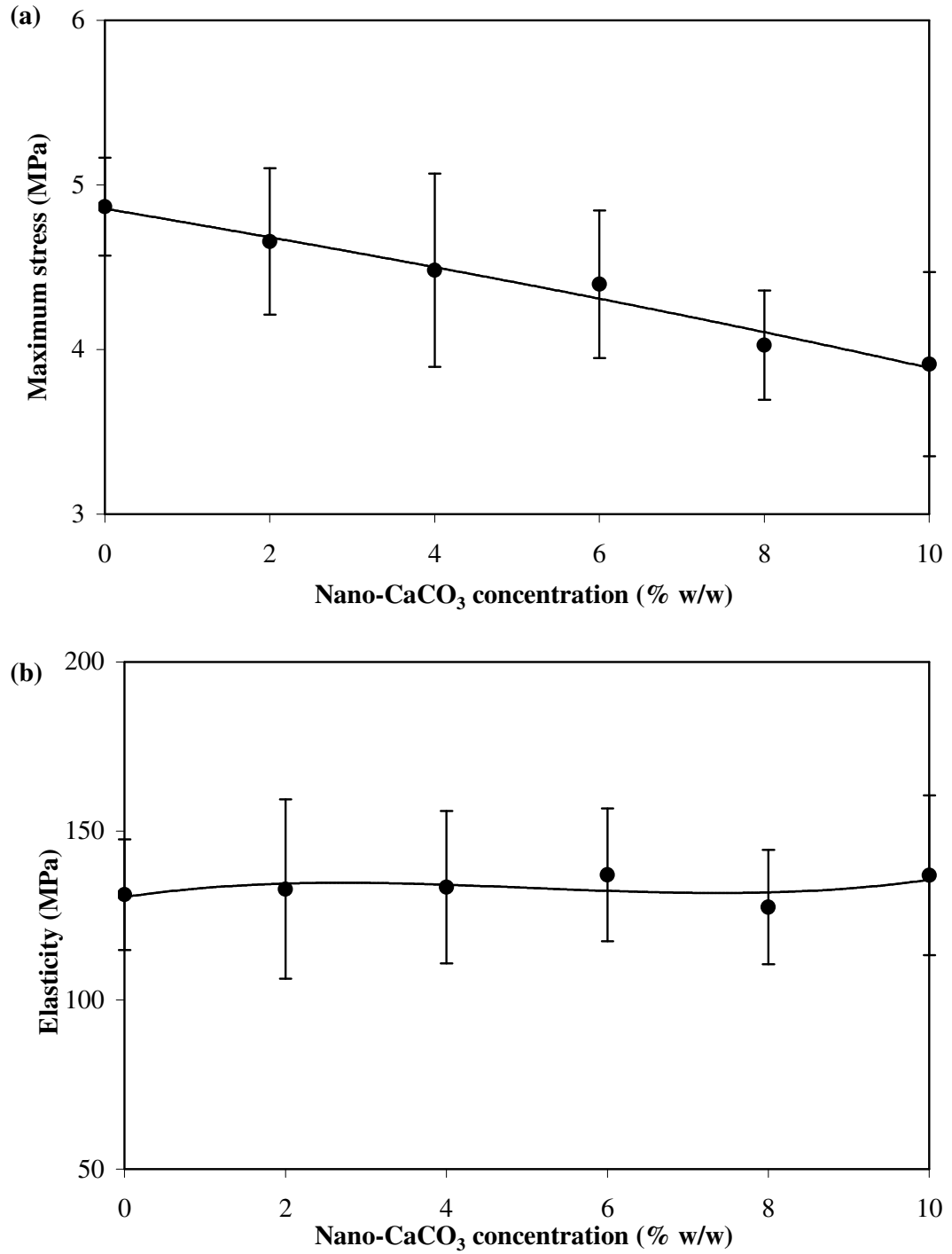


Fig. 56. Effect of nano-CaCO<sub>3</sub> concentration on the (a) maximum stress and (b) elasticity of the cast HPMC films.

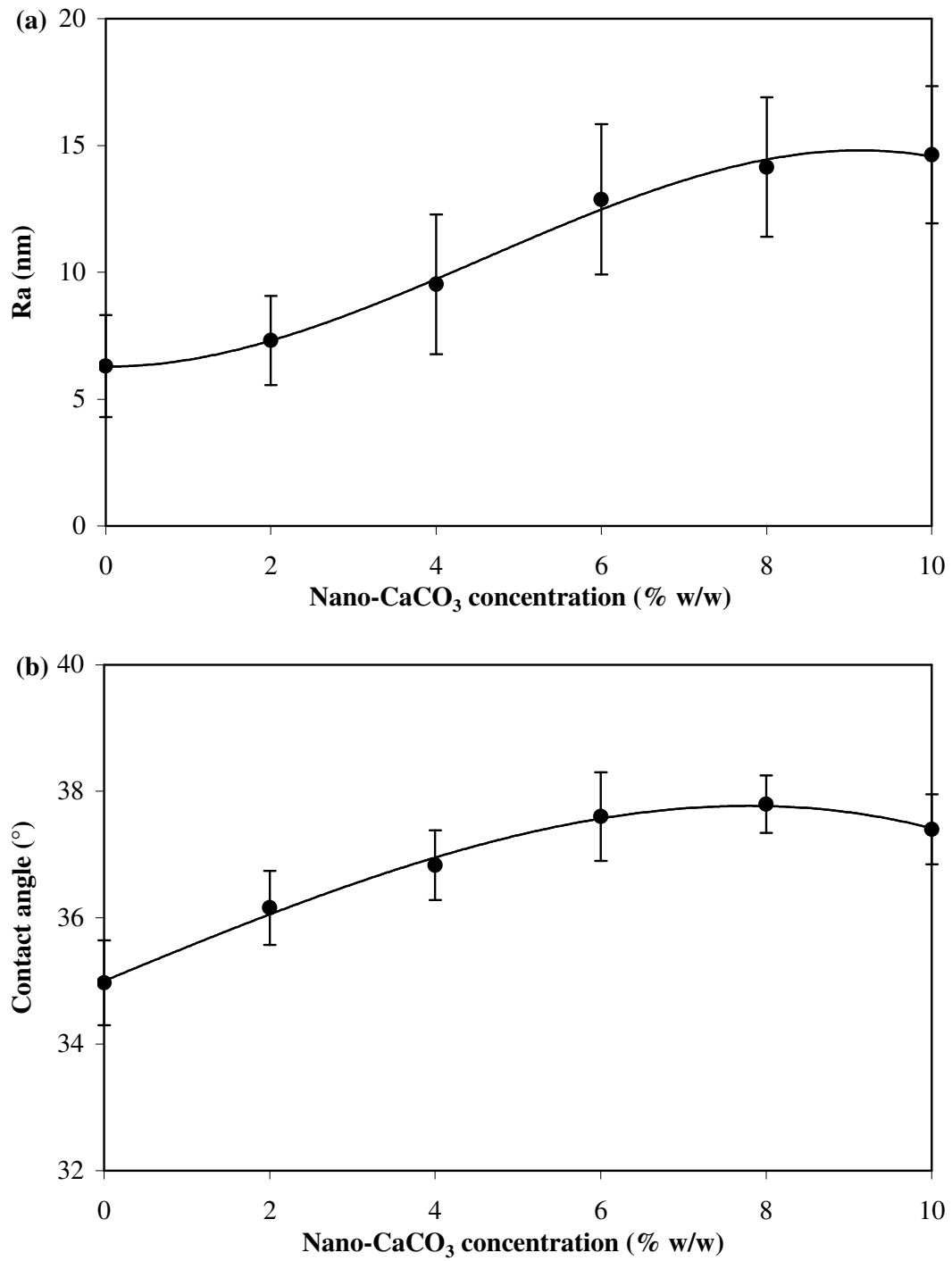


Fig. 57. Effect of nano-CaCO<sub>3</sub> concentration on the (a) Ra and (b) contact angle of cast films.



The increased film roughness also affected its wettability. A rougher surface would impede the spreading of spray droplets over the substrate surfaces. A more wettable surface would enhance the drying of deposited coating material as the coating material would spread better to form thinner layers. The contact angles of films increased up to 8 % w/w and decreased slightly beyond that. Closer examination showed that the change in contact angle when the nano-CaCO<sub>3</sub> concentration was varied from 6 to 10 % w/w was slight (Fig. 57b). The increased surface concentration of nano-CaCO<sub>3</sub> could decrease film wettability and hence, had contributed to more agglomeration when higher concentrations of nano-CaCO<sub>3</sub> were used for coating.

This study shows that nano-CaCO<sub>3</sub> was an effective anti-tack additive for HPMC coating formulations over the concentrations of 2 to 10 % w/w with respect to the amount of HPMC used. It was found that a balance between the adsorption of polymer chains and the increase in viscosity by the nano-CaCO<sub>3</sub> incorporated was necessary to bring about the highest anti-tack effect. Therefore, the concentration of nano-CaCO<sub>3</sub> used in the polymer solution was important. Over the concentrations of nano-CaCO<sub>3</sub> used, there were no changes in the brittleness of cast films and only a slight decrease in tensile strength. However, the increase in surface roughness and the decrease in wettability of films with nano-CaCO<sub>3</sub> concentration could have contributed to the increased agglomeration of lactose particles during coating.

**PART V:**  
**CONCLUSION**

## V CONCLUSION

Compared to Wurster coater, Precision coater was superior for coating fine particles due to the better performance in coating, especially in lowering the degree of agglomeration. This was primarily attributed to the fluid dynamics of the process whereby the Precision Coater had precise control of the particle movement through the spray zone. In addition, the swirl accelerator generated better airflow conditions, accelerated particle movement and caused better separation of particles within the spray zone. These accounted for the improvements in coat quality, as well as better coating reproducibility and shorter coating time.

The methods developed in this study to determine the mass flow rate and the drying efficiency were found to be useful for the study of process characteristics although there were certain limitations identified with their use. They were sensitive in differentiating the fluid dynamics and thermodynamics between Wurster and Precision coating.

Accelerator insert diameter, partition gap and airflow rate were some of the process variables that were studied in view of their importance in affecting the MFR. These variables were found to affect the drying efficiency and particle movement to different extents. Accelerator insert diameter and partition gap controlled the particle movement through the partition column and unlike airflow rate had no control over the drying capacity of the coater. However, inadequate particle movement due to inappropriate choice of accelerator insert diameter and partition gap affected the drying efficiency of Precision coating. Hence, it is important to ensure adequate particle movement for optimal drying efficiency.

Partition gap affected the quality of coated pellets but had little effect on the agglomeration. On the other hand, airflow rate had little influence on coat quality but affected the agglomeration markedly. This indicates that despite having adequate drying of particles and minimal agglomeration, adequate particle movement was also necessary to ensure that products formed were of good quality. The influence of partition gap and airflow rate was different for pellets of different sizes. Adequate airflow rate was more important for smaller pellets whereas adequate partition gap was more important for larger pellets. Hence, although the study of processing variables helped in the understanding of Precision coating, the results obtained could not be directly extrapolated to core particles with different characteristics such as size, hardness and shape as core particles with different characteristics would exhibit different behaviour when subjected to air suspension coating.

In the second part of this project, methods to enhance the coating of fine lactose particles were explored with the use of nano-CaCO<sub>3</sub>. The application of nano-CaCO<sub>3</sub> as a surface modifying agent and as an additive in coating formulations resulted in significant decrease in the agglomeration tendency of core lactose particles during film coating with HPMC. The reduction was due to different mechanisms as explained in the respective studies and led to a reduction of agglomeration to varying degrees. Nano-CaCO<sub>3</sub> as an additive in the film coating material was able to reduce the agglomeration of all size fractions of particles coated whereas nano-CaCO<sub>3</sub> as a surface modifying agent only reduced the agglomeration of the smallest size fraction of particles coated. Overall, the additive was more beneficial in preventing agglomeration during fine particle coating.

**PART VI:**  
**REFERENCES**

## VI REFERENCES

Abletshauser, C.B., Schneider, R., Rupprecht, H., 1993. Film coating of pellets with insoluble polymers obtained in situ crosslinking in the fluidized bed. *J. Control. Rel.*, 27, 149-156.

Abrahamsson, B., Alpsten, M., Jonsson, U.E., 1996. Gastro-intestinal transit of a multiple-unit formulation (metoprolol CR/ZOK) and a non-disintegrating tablet with the emphasis on colon. *Int. J. Pharm.*, 140, 229-35.

Alden, M., Torkington, P., Strutt, A.C.R., 1988. Control and Instrumentation of a Fluidized-Bed Drier Using the Temperature-Difference Technique. I. Development of a Working Model. *Pow. Tech.*, 54, 15-25.

Alderborn, G., 2007. Tablets and compaction. In: M.E. Aulton (Ed.), *Pharmaceutics: The design and manufacture of medicines* (pp. 441-482). New York: Churchill Livingstone.

Algifri, A.H., Bhardwaj, R.K., Rao, Y.V.N., 1988. Heat transfer in turbulent decaying swirl flow in a circular pipe. *Int. J. Heat Mass Transfer*, 31(8), 1563-1568.

Aulton, M.E., Hogan, J.E., Twitchell, A.M., 1997. Physical properties of HPMC solutions and their role in the film coating process and the quality of the coated product. In: J.W. McGinity (Ed.), *Aqueous polymeric coatings for pharmaceutical dosage forms* (pp. 227-266). New York: Marcel Dekker.

Bader, R., Findlay, J., Knowlton, T.M., 1988. Gas/solids flow patterns in a 30.5 cm diameter circulating fluidized bed. In: P. Basu, J.F. Lange (Ed.), *Circulating fluidized bed technology II* (pp. 123-137). London: Pergamon Press.

Barthelemy, P., Laforet, J.P., Farah, N., 1999. Compritol ® 888 ATO: an innovative hot-melt coating agent for prolonged release drug formulations. *Eur. J. Pharm. Biopharm.*, 47, 87-90.

Berggren, J., Frenning, G., Alderborn, G., 2004. Compression behaviour and tablet-forming ability of spray-dried amorphous composite particles. *Eur. J. Pharm. Sc.*, 22, 191-200.

Bechgaard, H., Nielsen, G.H., 1978. Controlled-release multiple-units and single-unit doses. *Drug Dev. Ind. Pharm.*, 4, 53-67.

Beckert, T., Petereit, H., Dressman, J., Rudolph, M., 2005. Multi-particulate form of medicament, comprising at least two differently coated forms of pellet. United States Patent, 6,897,205.

Bertelsen, P., Christensen, F.N., Holm, P., 1994. Comparison of organic solvent-based ethylcellulose coating on KCl crystals applied by top and bottom spraying in fluidized-bed equipment. *Int. J. Pharm.*, 111, 117-125.

Bodmeier, R., 1997. Tableting of coated pellets. *Eur. J. Pharm. Biopharm.*, 43, 1-8.

Cassanello, M., Larachi, F., Legros, R., Chaouki, J., 1999. Solids dynamics from experimental trajectory time-series of a single particle motion in gas-spouted beds. *Chem. Eng. Sci.*, 54, 2545-2554.

Chan, L.W., Chan, W.Y., Heng, P.W.S., 2001. An improved method for the measurement of colour uniformity in pellet coating. *Int. J. Pharm.*, 213(1-2), 63-74.

Chang, R.K., Iturrioz, G., Luo, C.W., 1990. Preparation and evaluation of shellac pseudolatex as an aqueous enteric coating system for pellets. *Int. J. Pharm.*, 60, 171-173.

Chang, R.K., Robinson, J.R., 1990. Sustained drug release from tablets and particles through coating. In: H.A. Lieberman, L. Lachman, J.B. Schwartz (Ed.), *Pharmaceutical dosage forms, tablets* (pp. 199-287). New York: Marcel Dekker.

Chopra, S.K., Tawashi, R., 1985. Tack behavior of coating solutions III. *J. Pharm. Sc.*, 74, 746-749.

Chopra, R., Alderborn, G., Podczek, F., Newton, J.M., 2002. The influence of pellet shape and surface properties on the drug release from uncoated and coated pellets. *Int. J. Pharm.*, 239, 171-178.

Christensen, F.N., Bertelson, P., 1997. Qualitative description of the Wurster-based fluid-bed coating process. *Drug Dev. Ind. Pharm.*, 23, 451-463.

Cole, G.C., 1995a. Introduction and overview of pharmaceutical coating. In: G.C. Cole (Ed.), *Pharmaceutical Coating Technology* (pp. 1-5). London: Taylor and Francis.

Cole, G.C., 1995b. Coating pans and coating columns. In: G.C. Cole (Ed.), *Pharmaceutical Coating Technology* (pp. 205-239). London: Taylor and Francis.

Collett, J., Moreton, C., 2001. Modified-release peroral dosage forms. In: M.E. Aulton (Ed.), *Pharmaceutics - the science of dosage form design* (pp. 289-305). New York: Churchill Livingstone.



Dannelly, C.C. and Leonard, C.R., 1978. Apparatus for spray coating discrete particles. United States Patent, 4,117,801.

Davies, N.M., Farr, S.J., Kellaway, I.W., Taylor, G., Thomas, M., 1994. A comparison of the gastric retention of alginate containing tablet formulations with and without the inclusion of excipient calcium ions. *Int. J. Pharm.*, 105, 97-101.

Deasy, P.B., 1984. Interfacial polycondensation. In: P.B. Deasy (Ed.), *Microencapsulation and related drug processes* (pp. 119-144). New York: Marcel Dekker.

Dechesne, J.P., Delattre, L., 1987. A new enteric tablet of acetylsalicylic acid. II. Biopharmaceutical aspects. *Int. J. Pharm.*, 34, 259-262.

Dorozhkin, S.V., 2001. Is there a chemical interaction between calcium phosphates and hydroxypropylmethylcellulose (HPMC) in organic/inorganic composites? *J. Biomed. Mater. Res.*, 54, 247-255.

Eerikainen, S., Lindqvist, A.S., 1991. The behaviour of various fillers in spheronized uncoated and film coats granules containing slightly water-soluble indomethacin. *Int. J. Pharm.*, 75, 181-192.

El-Sherbiny, S., Xiao, H., 2004. Effect of polymeric thickeners on pigment coatings: adsorption, rheological behaviour and surface structures. *J. Mater. Sci.*, 39, 4487-4493.

Emås, M., Nyqvist, H., 2002. Methods of studying aging and stabilization of spray-congealed solid dispersions with carnauba wax. 1. Microcalorimetric investigation. *Int. J. Pharm.*, 197, 117-127.

Faroongsarng, D., Peck, G.E., 1991. The swelling of core tablets during aqueous coating I. A simple model describing extent of swelling and water penetration for insoluble tablets containing a superdisintegrant. *Drug Dev. Ind. Pharm.*, 17, 2439-2455.

Faroongsarng, D., Peck, G.E., 1992. The swelling of core tablets during aqueous coating. II An application of the model describing extent of swelling and water penetration for insoluble tablets. *Drug Dev. Ind. Pharm.*, 18, 1527-1534.

Felton, L.A., McGinity, J.W., 2002. Influence of insoluble excipients on film coating systems. *Drug Dev. Ind. Pharm.*, 28(3), 225-243.

Fini, A., Rodriguez, L., Cavallari, C., 2002. Ultrasound-compacted and spray-congealed indomethacin/polyethyleneglycol systems. *Int. J. Pharm.*, 247, 11-22.

Fitzpatrick, S., Ding, Y., Seiler, C., Lovegrove, C., Booth, S., Forster, R., Parker, D., Seville, J., 2003. Positron emission particle tracking studies of a Wurster process for coating applications. *Pharm. Tech.*, 27(9), 70-78.

Fukumori, Y., 1994. Coating of multiparticulates using polymeric dispersions. In: I. Ghebre-Sellassie (Ed.), *Multiparticulate Oral Drug Delivery* (pp. 79-112). New York: Marcel Dekker.

Fulzele, S.V., Satturwar, P.M., Dorle, A.K., 2002. Polymerized rosin: novel film forming polymer for drug delivery. *Int. J. Pharm.*, 249, 175-184.

Ghebre-Sellassie, I., Gordon, R.H., Middleton, D.L., Nesbitt, R.U., Fawzi, M.B., 1986. A unique application and characterization of Eudragit E 30 D film coatings in sustained release formulations. *Int. J. Pharm.*, 31, 43-54.

Ghebre-Sellassie, I., Gordon, R.H., Nesbitt, R.U., Fawzi, M.B., 1987. Evaluation of acrylic-based modified-release film coatings. *Int. J. Pharm.*, 31, 211-218.

Gibson, S.H.M., Rowe, R.C., White, E.F.T., 1988. Determination of the critical pigment volume concentrations of pigmented film coating formulations using gloss measurement. *Int. J. Pharm.*, 45, 245-248.

Gupta, V.K., Beckert, T.E., Price, J.C., 2001. A novel pH- and time-based multi-unit potential colonic drug delivery system. I. Development. *Int. J. Pharm.*, 213(1-2), 83-91.

Gutierrez-Rocca, J.C., McGinity, J.W., 1994. Influence of water soluble and insoluble plasticizers on the physical and mechanical properties of acrylic resin copolymers. *Int. J. Pharm.*, 103, 293-301.

Heinamaki, J.T., Lehtola, V.M., Nikupaavo, P., Yliruusi, J.K., 1994. The mechanical and moisture permeability properties of aqueous-based hydroxypropyl methylcellulose coating systems plasticized with polyethylene glycol. *Int. J. Pharm.*, 112, 191-196.

Hemati, M., Cherif. R., Saleh. K., Pont, V., 2003. Fluidized bed coating and granulation: influence of process-related variables and physicochemical properties on the growth kinetics. *Pow. Tech.*, 130, 18– 34.

Heng, P.W.S., Chan, L.W., Chan, W.Y., 1999. Application of spot colour measurement for the optimization of colour coating. *S.T.P. Pharm. Sc.*, 9, 539-544.

Heng, P.W.S., Wan, L.S.C., Tan, Y.T.F., 1996. Relationship between aggregation of HPMC coated spheroids and tackiness/viscosity/additives of the coating formulations. *Int. J. Pharm.*, 138, 57-66.

Hogan, J.E. 1995a. Modified release coatings. In: G. Cole (Ed.), *Pharmaceutical Coating Technology* (pp. 407-437). London: Taylor and Francis.

Hogan, J.E., 1995b. Film-coating materials and their properties. In: G. Cole (Ed.), *Pharmaceutical Coating Technology* (pp. 6-52). London: Taylor and Francis.

Hogan, J.E., 2001. Coating of tablets and multiparticulates. In M.E. Aulton (Ed.), *Pharmaceutics - the science of dosage form design* (pp. 441-448). New York: Churchill Livingstone.

Horvath, E., Ormos, Z., 1989. Film coating of dragee seeds by fluidized bed spraying methods. *Acta Pharm. Tech.*, 35(2), 90-96.

Husson, I., Leclere, B., Spenlehauer, G., Veillard, M., Couarraze, G., 1991. Modeling of drug release from pellets coated with an insoluble polymeric membrane. *J. Control. Rel.*, 17, 163-174.

Huyghebaert, N., Snoeck, V., Vermeire, A., Cox, E., Goddeeris, B.M., Remon, J.P., 2005. Development of an enteric-coated pellet formulation of F4 fimbriae for oral vaccination of suckling piglets against enterotoxigenic *Escherichia coli* infections. *Eur. J. Pharm. Biopharm.*, 59(2), 273-281.

Ichikawa, H., Fujioka, K., Christianah, A., 2001. Use of ion-exchange resins to prepare 100  $\mu\text{m}$ -sized microcapsules with prolonged drug-release by the Wurster process. *Int. J. Pharm.*, 216, 67-76.

Iida, K., Todo, H., Okamoto, H., Danjo, K., Leuenberger, H., 2005. Preparation of dry powder inhalation with lactose carrier particles surface-coated using a Wurster fluidized bed. *Chem. Pharm. Bull.*, 53(4), 431-434.

Jani, P.U., McCarthy, D.E., Florence, A.T., 1994. Titanium dioxide (rutile) particle uptake from the rat GI tract and translocation to systemic organs after oral administration. *Int. J. Pharm.*, 105, 157-168.

Jiménez, T., Turchiuli, C., Dumoulin, E., 2006. Particles agglomeration in a conical fluidized bed in relation with air temperature profiles. *Chem. Eng. Sc.*, 61, 5954-5961.

Johansson, B., Alderborn, G., 1996. Degree of pellet deformation during compaction and its relationship to the tensile strength of tablets formed of microcrystalline cellulose pellets. *Int. J. Pharm.*, 132, 207-220.

Johansson, B., Nicklasson, F., Alderborn, G., 1998. Effect of pellet size on degree of deformation and densification during compression and on compactability of microcrystalline cellulose pellets. *Int. J. Pharm.*, 163, 35-48.

Jones, B.E., 2007. Hard gelatin capsules. In M.E. Aulton (Ed.), *Pharmaceutics: The design and manufacture of medicines* (pp. 515-526). New York: Churchill Livingstone.

Jones, D.M., Percel, P.J., 1994. Coating of multiparticulates using molten materials: Formulation and process considerations. In: I. Ghebre-Sellassie (Ed.), *Multiparticulate Oral Drug Delivery* (pp. 113-142). New York: Marcel Dekker.

Jono, K., Ichikawa, H., Miyamoto, M., Fukumori, Y., 2000. A review of particulate design for pharmaceutical powders and their production by spouted bed coating. *Pow. Tech.*, 113, 269-277.

Jose, M.J.S., Olazar, M., Alvarez, S., Izquierdo, M.A., Bilbao, J., 1998. Solid cross-flow into the spout and particle trajectories in conical spouted beds. *Chem. Eng. Sci.*, 53, 3561-3570.

Keary, C.M., 2001. Characterization of methocel cellulose ethers by aqueous SEC with multiple detectors. *Carb. Polymers*, 45, 293-303.

Kevat, M.D., Patel, A.R., Prabhakaran, P., 2005. Heat transfer augmentation in airflow passing through a swirl path over a combustion chamber. *App. Thermal Eng.*, 25, 2591-2603.

Kim, T.H., Park, Y.H., Kim, K.J., Cho, C.S, 2003. Release of albumin from chitosan-coated pectin beads in vitro. *Int. J. Pharm.*, 250, 371-383.

Kristmundsdottir, T., Gudmundsson, O.S., Ingvarsdottir, K., 1996. Release of diltiazem from Eudragit microparticles prepared by spray-drying. *Int. J. Pharm.*, 137, 159-65.

Larsen, C.C., Sonnergaard, J.M., Bertelsen, P., Holm, P., 2003. A new process control strategy for aqueous film coating of pellets in fluidised bed. *Eur. J. Pharm. Sc.*, 20, 273-283.

Lehmann, K., 1994. Coating of multiparticulates using polymeric solutions: Formulation and process considerations. In: I. Ghebre-Sellassie (Ed.), *Multiparticulate Oral Drug Delivery* (pp. 51-78). New York: Marcel Dekker.

Lehmann, K., 1997. Chemistry and application properties of polymethacrylate coating systems. In: J.W. McGinity (Ed.), *Aqueous polymeric coatings for pharmaceutical dosage forms* (pp. 101-176). New York: Marcel Dekker.

Leszek, K., 1987. Excipients used in the formulation of extended-release dosage forms. In: K. Leszek (Ed.), *Extended release dosage forms* (pp. 171-188). Florida: CRC press.

Maa, Y., Ameri, M., Rigney, R., Payne, L. G., Chen, D., 2004. Spray-coating for Biopharmaceutical powder formulations: Beyond the conventional scale and its application. *Pharm. Res.*, 21(3), 515-523.

Machiste, E.O., Buckton, G., 1996. Dynamic surface tension studies of hydroxypropylmethylcellulose film-coating solutions. *Int. J. Pharm.*, 145, 197-201.

Maronga, S.J., Wnukowski, P., 1997. Establishing temperature and humidity profiles in fluidized bed particulate coating. *Pow. Tech.*, 94, 181-185.

Maronga, S.J., Wnukowski, P., 1998. The use of humidity and temperature profiles in optimizing the size of fluidized bed in a coating process. *Chem. Eng. Process.*, 37, 423-432.

Mazzone, D.N., Tardos, G.I., Pfeffer, R., 1987. The behaviour of liquid bridges between two relatively moving particles. *Pow. Tech.*, 51, 71-83.

Mehta, A.M., 1997. Processing and equipment considerations for aqueous coatings. In: J.W. McGinity (Ed.), *Aqueous Polymeric coatings for pharmaceutical dosage forms*, 2<sup>nd</sup> Ed (pp. 287-326). New York: Marcel Dekker.

Munday, D.L., Fassihi, A.R., 1989. Controlled release delivery: Effect of coating composition on release characteristics of mini-tablets. *Int. J. Pharm.*, 52, 109-114.

Musko, Z., Hodi, P., Gaspar, R., Pintye, J., Revesz, S., Eros, I., Falkay, G., 2001. Study of in vitro and in vivo dissolution of theophylline from film-coated pellets. *Eur. J. Pharm. Biopharm.*, 51, 143-146.

Nagai, T., Obara, S., Kokubo, H., Hoshi, N., 1997. Application of HPMC and HPMCAS to aqueous film coating of pharmaceutical dosage forms. In: J.W. McGinity (Ed.), *Aqueous polymeric coatings for pharmaceutical dosage forms* (pp. 117-226). New York: Marcel Dekker.

Nakano, T., Yuasa, H., 2001. Suppression of agglomeration in fluidized bed coating. IV. Effects of sodium citrate concentration on the suppression of particle agglomeration and the physical properties of HPMC film. *Int. J. Pharm.*, 215, 3-12.

Nyamweya, N., Mehta, K., Hoag, S.W., 2001. Characterization of the interactions between polymethacrylate-based aqueous polymeric dispersions and aluminium lakes. *J. Pharm. Sc.*, 90, 1937-1947.

O'Donnell, P.B., Wu, C., Wang, J., Wang, L., Oshlack, B., Chasin, M., Bodmeier, R., McGinity, W., 1997. Aqueous pseudolatex of zein for film coating of solid dosage forms. *Eur. J. Pharm. Biopharm.*, 43, 83-89.

Obara, S., Maruyama, N., Nishiyama, Y., 1999. Dry coating: an innovative enteric coating method using a cellulose derivative. *Eur. J. Pharm. Biopharm.*, 47, 51-59.



Okhamafe, A.O., York, P., 1984a. Effect of solids-polymer interactions on the properties of some aqueous-based tablet film coating formulations. I. Moisture permeability. *Int. J. Pharm.*, 22, 265-272.

Okhamafe, A.O., York, P., 1984b. Effect of solids-polymer interactions on the properties of some aqueous-based tablet film coating formulations. II. Mechanical characteristics. *Int. J. Pharm.*, 22, 273-281.

Oliveira, W.P., Freire, J.T., Coury, J.R., 1997. Analysis of particle coating by spouted bed process. *Int. J. Pharm.*, 158, 1-9.

Ouriemchi, E.M., Bouzon, J., Vergnaud, J.M., 1994. Oral dosage forms with a core and shell with the same polymer containing different drug concentrations. *Int. J. Pharm.*, 102, 47-54.

Ozbey, M., Soylemez, M.S., 2005. Effect of swirling flow on fluidized bed drying of wheat grains. *Energy Conver. Manage.*, 46, 1495–1512.

Parker, D.J., Dijkstra, A.E., Martin, I.T.W., Seville, J.P.K., 1997. Positron emission particle tracking studies of spherical particle motion in rotating drums. *Chem. Eng. Sc.*, 52(13), 2011-2022.

Passerini, N., Perissutti, B., Albertini, B., 2003. Controlled release of verapamil hydrochloride from waxy microparticles prepared by spray congealing. *J. Control. Rel.*, 88, 263-75.

Pearnchob, N., Bodmeier, R., 2003a. Coating of pellets with micronized ethycellulose particles by a dry powder coating technique. *Int. J. Pharm.*, 268, 1-11.

Pearnchob, N., Bodmeier, R., 2003b. Dry polymer powder coating and comparison with conventional liquid-based coatings for Eudragit<sup>®</sup> RS, ethylcellulose and shellac. *Eur. J. Pharm. Biopharm.*, 56, 363-369.

Pillay, V., Fassihi, R., 1999. In vitro release modulation from crosslinked pellets for site-specific drug delivery to the gastrointestinal tract: I. Comparison of pH-responsive drug release and associated kinetics. *J. Control. Rel.*, 59, 229-242.

Porter, S.C, 1989. Controlled-release film coatings based on ethylcellulose. *Drug Dev. Ind. Pharm.*, 15, 1495-1521.

Porter, S.C., Bruno, C.H., 1990. Coating of Pharmaceutical Solid-Dosage forms. In: H.A. Lieberman, L. Lachman, J.B. Schwartz (Ed.), *Pharmaceutical dosage forms, tablets* (pp. 77-159). New York: Marcel Dekker.

Porter, S.C., Ghebre-Sellassie, I., 1994. Key factors in the development of modified-release pellets. In: I. Ghebre-Sellassie (Ed.), *Multiparticulate Oral Drug Delivery* (pp. 159-180). New York: Marcel Dekker.

Radebaugh, G.W., 1992. Film coatings and film forming materials: evaluation. In: J. Swarbrick, J.C. Boylan (Ed.), *Encyclopedia of pharmaceutical technology, Volume 6* (pp. 1-28). New York: Marcel Dekker.

Ragnarsson, G., Johansson, M.O., 1988. Coated drug cores in multiple unit preparations: influence of particle size. *Drug Dev. Ind. Pharm.*, 14, 734-739.

Ragnarsson, G., Sandberg, A., Jonsson, U.E., Sjiigren, J., 1987. Development of a new controlled release metoprolol product. *Drug Dev. Ind. Pharm.*, 13, 1495-1509.

Ronsse, F., Pieters, J.G., Dewettinck, K., 2007. Combined population balance and thermodynamic modeling of the batch top-spray fluidised bed coating process. Part I- Model development and validation. *J. Food Eng.*, 78, 296-307.

Rowe, R.C., 1986. The effect of the molecular weight of ethylcellulose on the drug release properties of mixed films of ethylcellulose and hydroxypropyl methylcellulose. *Int. J. Pharm.*, 29, 37-41.

Rowe, R.C., 1997. Defects in aqueous film coated tablets. In: J.W. McGinity (Ed.), *Aqueous Polymeric coatings for pharmaceutical dosage forms 2<sup>nd</sup> Ed.* (pp. 419-440). New York: Marcel Dekker.

Sadeghi, F., Ford, J.L., Rajabi-Siahboomi, A., 2003. The influence of drug type on the release profile from Surelease-coated pellets. *Int. J. Pharm.*, 254, 123-135.

Sakata, Y., Shiraishi, S., Otsuka, M., 2006. A novel white film for pharmaceutical coating formed by interaction of calcium lactate pentahydrate with hydroxypropyl methylcellulose. *Int. J. Pharm.*, 317, 120-126.

Savage, G.V., Rhodes, C.T., 1995. The sustained release coating of solid dosage forms: A historical review. *Drug Dev. Ind. Pharm.*, 21, 93-118.

Shallcross, D.C., 1997. Psychrometric charts. In: D.C. Shallcross (Ed.), *Handbook of psychrometric charts: humidity diagrams for engineers* (pp. 44-45). London: Blackie Academic and Professional.

Shelukar, S., Ho, J., Zega, J., Roland, E., Yeh, N., Quiram, D., Nole, A., Katdare, A., Reynolds, S., 2000. Identification and characterization of factors controlling tablet coating uniformity in a Wurster coating process. *Pow. Tech.*, 110, 29-36.

Shi, X.Y., Tan, T.W., 2002. Preparation of chitosan/ethylcellulose complex microcapsule and its application in controlled release of Vitamin D<sub>2</sub>. *Biomaterials*, 23, 4469-4473.

Shivanand, P., Sprockel, O.L., 1998. A controlled porosity drug delivery system. *Int. J. Pharm.*, 167, 83-96.

Shtern, V., Borissov, A., Hussain, F., 1998. Temperature distribution in swirling jets. *Int. J. Heat Mass Transfer*, 41(16), 2455-2467.

Singh, S.K., Reddy, I.K., Khan, M.A., 1996. Optimization and characterization of controlled release pellets coated with an experimental latex: II. Cationic drug. *Int. J. Pharm.*, 141, 179-95.

Smith, P.G., Nienow, A.W., 1983. Particle growth mechanisms in fluidized bed granulation-I: The effect of process variables. *Chem. Eng. Sc.*, 38(8), 1223-1231.

Sousa, J.J., Sousa, A., Moura, M.J., Podczek, F., Newton, J.M., 2002. The influence of core materials and film coating on the drug release from coated pellets. *Int. J. Pharm.*, 233, 111-122.

Sriamornsak, P., Puttipatkhachorn, S., Prakongpan, S., 1997. Calcium pectinate gel coated pellets as an alternative carrier to calcium pectinate beads. *Int. J. Pharm.*, 156, 189-194.

Stein, M., Ding, Y.L., Seville, J.P.K., Parker, D.J., 2000. Solids motion in bubbling gas fluidized beds. *Chem. Eng. Sci.*, 55, 5291-5300.

Sudsakorn, K., Turton, R., 2000. Non-uniformity of particle coating on a size distribution of particles in a fluidized bed coater. *Pow. Tech.*, 110, 37-43.

Sugito, K., Ogata, H., Goto, H., Noguchi, M., Kogure, T., Takano, M., Maruyama, Y., Sasaki, Y., 1990. Gastrointestinal transit of non-disintegrating solid formulations in humans. *Int. J. Pharm.*, 60, 89-97.

Sun, Y.M., Chang, C.C., Huang, W.F., Liang, H.C., 1997. Fluidized-bed spray coated porous hydrogel beads for sustained release of diclofenac sodium. *J. Control. Rel.*, 47, 247-260.

Tarvainen, M., Sutinen, R., Peltonen, S., Mikkonen, H., Maunus, J., Vaha-Heikkila, K., Lehto, V.P., Paronen, P., 2003. Enhanced film-forming properties for ethylcellulose and starch acetate using n-alkenyl succinic anhydrides as novel plasticizers. *Eur. J. Pharm. Sc.*, 19, 363-371.

Thies, C., 1996. A survey of microencapsulation processes. In: S. Benita (Ed.), *Microencapsulation methods and industrial applications* (pp 1-20). New York: Marcel Dekker.

Thoma, K., Bechtold, K., 1999. Influence of aqueous coatings on the stability of enteric coated pellets and tablets. *Eur. J. Pharm. Biopharm.*, 47, 39-50.

Tobio, M., Schwendeman, S.P., Guo, Y., 2000. Improved immunogenicity of a core-coated tetanus toxoid delivery system. *Vaccine*, 18, 618-22.

Tsuchida, K., Aoki, S., 2003. Multiple-unit sustained release tablets. *United States Patent*, 6,558,700.

Tuleu, C., Andrieux, C., Boy, P., Chaumeil, J.C., 1999. Gastrointestinal transit of pellets in rats: effect of size and density. *Int. J. Pharm.*, 180, 123-131.

Tunon, A., Grasjo, J., Alderborn, G., 2003. Effect of intragranular porosity on compression behaviour of and drug release from reservoir pellets. *Eur. J. Pharm. Sc.*, 19, 333-344.

Ueno, Y., Futagawa, H., Takagi, Y., Ueno, A., Mizushima, Y., 2005. Drug-incorporating calcium carbonate nanoparticles for a new delivery system. *J. Cont. Rel.*, 103, 93-98.

Walter, K., 1998. Apparatus for coating solid particles. United States Patent, 5,718,764.

Wan, L.S.C., Heng, P.W.S., Liew, C.V., 1995. The influence of liquid spray rate and atomizing pressure on the size of spray droplets and spheroids. *Int. J. Pharm.*, 118, 213-219.

Wan, L.S.C., Lai, W.F., 1991. Factors affecting drug release from drug-coated granules prepared by fluidized-bed coating. *Int. J. Pharm.*, 72, 163-174.

Wan, L.C.S., Lai, W.F., 1992. A simple method to assess the tack of coating formulations. *STP Pharma Sci.*, 2(2), 174-180.

Wan, L.S.C., Lai, W.F., 1993. The influence of antitack additives on drug release from film-coated granules. *Int. J. Pharm.*, 94, 39-47.

Wang, L., Chaw, C.S., Yang, Y.Y., 2004. Preparation, characterization, and in vitro evaluation of physostigmine-loaded poly(ortho ester) and poly(ortho ester)/poly(D,L-lactide-co-glycolide) blend microspheres fabricated by spray drying. *Biomaterials*, 25, 3275-3282.

Wesdyk, R., Joshi, Y.M., Vincentis, J.D., 1993. Factors affecting differences in film thickness of beads coated in fluidized bed units. *Int. J. Pharm.* 93, 101-109.

Wesseling, M., Kuppler, F., Bodmeier, R., 1999. Tackiness of acrylic and cellulosic polymer films used in the coating of solid dosage forms. *Eur. J. Pharm. Biopharm.*, 47, 73-78.

Wieland-Berghausen, S., Schote, U., Frey, M., 2002. Comparison of microencapsulation techniques for the water-soluble drugs nitenpyram and clomipramine HCl. *J. Control. Rel.*, 85, 35-43.

Wong, T.W., Heng, P.W.S., Yeo, T.N., Chan, L.W., 2002. Influence of polyvinylpyrrolidone on aggregation propensity of coated spheroids. *Int. J. Pharm.*, 242, 357-360.

Wurster, D.E., 1953. Method of applying coating onto edible tablets or the like. U.S. Patent, 2,648,609.

Xu, M., Turton, R., 1997. A new data processing technique for noisy signals: application to measuring particle circulation times in a draft tube equipped fluidized bed. *Pow. Tech.*, 92, 111-117.

Yang, S.T., Ghebre-Sellassie, I., 1990. The effect of product bed temperature on the microstructure of Aquacoat-based controlled-release coatings. *Int. J. Pharm.*, 60, 109-124.

Yang, S.T., Savage, G.V., Weiss, J., Ghebre-Sellassie, I., 1992. The effect of spray mode and chamber geometry of fluid-bed coating equipment and other parameters on an aqueous-based ethylcellulose coating. *Int. J. Pharm.*, 86, 247-257.

Yilmaz, M., Comakli, O., Yapici, S., 1999. Enhancement of heat transfer by turbulent decaying swirl flow. *Energy Conver. Manage.*, 40, 1365-1376.

Yilmaz, M., Comakli, O., Yapici, S., Sara, N., 2003. Heat transfer and friction characteristics in decaying swirl flow generated by different radial guide vane swirl generators. *Energy Conver. Manage.*, 44, 283-300.

Yuasa, H., Nakano, T., Kanaya, Y., 1997. Suppression of agglomeration in fluidized bed coating I. Suppression of agglomeration by adding NaCl. *Int. J. Pharm.*, 158, 195-201.



**PART VII:**  
**LIST OF PUBLICATIONS**

## **VII LIST OF PUBLICATIONS**

### **Journal publications**

Tang, E.S.K, Wang, L., Liew, C.V., Chan, L.W., Heng, P.W.S, 2008. Drying efficiency and particle movement in coating - impact on particle agglomeration and yield. *Int. J. Pharm.*, 350, 172-180.

Heng, P.W.S., Chan, L.W., Tang, E.S.K., 2006. Use of swirling airflow to enhance coating performance of bottom spray air suspension coaters. *Int. J. Pharm.*, 327, 26-35.

Chan, L.W., Tang, E.S.K., Heng, P.W.S., 2006. Comparative study of the fluid dynamics of bottom spray air suspension coaters. *AAPS PharmSciTech.*, 7(2), Article 37.

Tang, E.S.K., Chan, L.W., Heng, P.W.S., 2005. Coating of multiparticulates for sustained release. *Am. J. Drug Del.*, 3(1), 17-28.

### **Conference presentations**

Chan, L.W., Heng, P.W.S., Tang, E.S.K. Drying efficiency and pellet movement in Wurster coating and Precision coating. Inaugural AASP Conference. Makati City, Philippines, 25-28 Oct, 2007.

Tang, E.S.K. Calcium carbonate nanoparticles as an anti-tack agent in fine particle coating (Oral presentation). AAPS-NUS Symposium. Singapore, 5 Mar, 2007.

Tang, E.S.K. Approaches to develop fine particle coating by bottom spray air suspension processing (Oral presentation). Asian Pharmaceuticals Graduate Congress. Singapore, 25-27 Sep, 2006.

Heng, P.W.S., Chan, L.W., Tang, E.S.K. Comparison of air dominated pellet flow rates between the Precision and Wurster coaters. AAPS Annual Meeting and Poster Exposition. Baltimore, Maryland, USA, 7 – 11 Nov, 2004.

Tang, E.S.K. Comparison of the coating of pellets between the Wurster coater and Precision coater (Oral Presentation). Shenyang Pharmaceutical University Graduate Seminar. Shenyang, China, 8 Jun, 2004.

Tang, E.S.K., Heng, P.W.S., Chan, L.W. Comparative study of pellet mass flow in the Precision coater and Wurster coater. Inaugural AASP Conference. Beijing, China, 4 – 6 Jun, 2004.